

## MASTER

### Opening neonatal incubators impact on the incubator's climate and the neonate

Brooimans, Roel J.C.

*Award date:*  
2016

[Link to publication](#)

#### **Disclaimer**

This document contains a student thesis (bachelor's or master's), as authored by a student at Eindhoven University of Technology. Student theses are made available in the TU/e repository upon obtaining the required degree. The grade received is not published on the document as presented in the repository. The required complexity or quality of research of student theses may vary by program, and the required minimum study period may vary in duration.

#### **General rights**

Copyright and moral rights for the publications made accessible in the public portal are retained by the authors and/or other copyright owners and it is a condition of accessing publications that users recognise and abide by the legal requirements associated with these rights.

- Users may download and print one copy of any publication from the public portal for the purpose of private study or research.
- You may not further distribute the material or use it for any profit-making activity or commercial gain



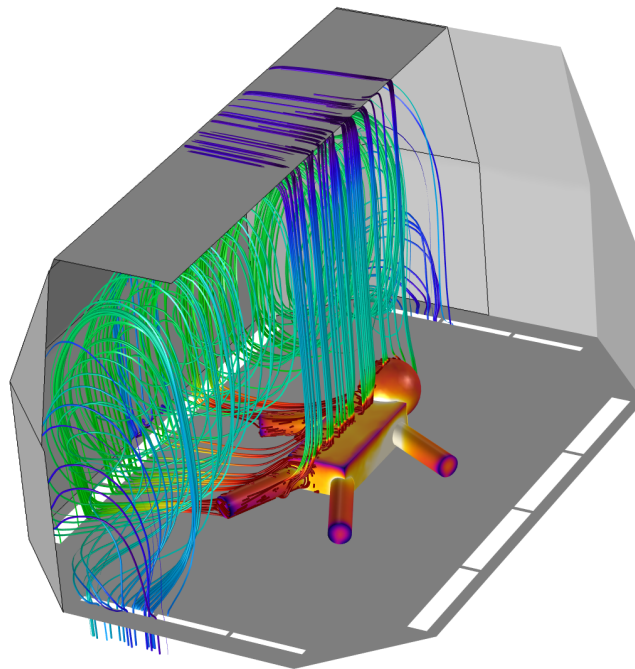
máxima  
medisch centrum

TU/e

Technische Universiteit  
Eindhoven  
University of Technology

# Opening neonatal incubators: Impact on the incubator's climate and the neonate

R.J.C. Brooimans, BSc  
November 24, 2016



*Supervisors:*

dr. ir. C. van Pul

prof. dr. ir. E.J.E. Cottaar



# Abstract

**Purpose:** Preterm infants have trouble maintaining their core body temperature. Therefore, they are often nursed in neonatal incubators. Incubators are closed environments in which the air temperature and relative humidity (RH) are controlled to maintain thermal stability in the infant. Occasionally, due to several clinical reasons, an incubator needs to be opened. An opened incubator is in direct contact with ambient air. The impact of opening an incubator on the thermal stability of the infant is not exactly known. Therefore, in this research, the impact of opening an incubator on its climate and the resulting effect on the neonate are investigated.

**Methods:** In order to investigate the effects of opening an incubator, both measurements and simulations are used. In the simulations, a Computational Fluid Dynamics (CFD) model is developed to compute the climate effects for the incubator. First, CFD is used to model a closed incubator. The impact of the incubator's climate settings on the neonate's body temperature is calculated for six typical infants. The infants range from 28 weeks gestational age (GA) - 1 day postnatal age (PA) to 32 weeks GA - 5 days PA. Next, to model the effects of opening an incubator, a different CFD model is developed. Furthermore, a setup was built to measure the climate effects of opening a real incubator. Incubator climate settings were varied, and the effect of opening on the air temperature, surface temperature and RH was measured at multiple locations inside two incubators. Finally, the effect of the climate changes on the neonates' body temperatures were calculated.

**Results:** The simulations show that, in case the incubator is closed and set to 33°C-45%RH, all six infants lost heat. The body temperature changes range from -2.7 °C/h to -4.2 °C/h. Setting the incubator to 36°C-70%RH resulted in warming up of all infants. The body temperature changes range from +0.1°C/h to +0.8°C/h. Unfortunately, the effects of opening could not be modelled due to convergence errors in the simulation model. The measurements showed that the effect of incubator opening strongly correlates to the incubator's climate and the ambient climate. Air temperature drops ranging from 0.4-2.6°C were observed, surface temperature drops varied from 0.0-2.5 °C and the RH decreases ranged from 10-55%. Opening the access door has more impact on the climate than opening the portholes. Opening an incubator induced different body temperature drops, depending on the opening scenario and the infant. The body temperature drops range from -0.1 °C/h to -3.1 °C/h.

**Conclusion:** Correctly setting up the incubator's climate is of critical importance for the neonate. Incorrect incubator settings will induce a risk for hypo-or hyperthermia in the neonate. Though many studies do not include effects of change in RH, we found that the RH drops are significantly higher compared to the temperature drops. Because evaporative heat loss has the biggest impact on the total heat loss, the effect of a drop in RH is significant on the infant. Therefore, monitoring and maintaining a constant RH is necessary. Finally, CFD has proven to be a useful tool to compute the climate inside an incubator. It allows for parametric testing to determine the optimal climate settings for the desired neonate. On top of that, CFD can be helpful to save money and time in the design of new products.

# Acknowledgements

Hereby I present my thesis: "Opening neonatal incubators: Impact on the incubator's climate and the neonate". The thesis represents the end product of my graduation project executed at the Maxima Medisch Centrum Veldhoven, The Netherlands.

Several people have guided me during the project and contributed to this work. Therefore I would like to use this preface to thank multiple people for their support during the project.

First of all I would like to thank my two supervisors Carola van Pul and Ward Cottaar for their help and feedback. They were not only available during our productive and fruitful meetings, but always provided me a hand when I asked for it.

Secondly, I would like to thank the people at the Department of Neonatology from the Maxima Medisch Centrum Veldhoven. Special thanks to Peter Andriessen (Neonatologist) and Astrid Osagiator (Senior Nurse NICU), for always providing me with useful clinical data and information.

During my project, several external partners have helped me out. I would like to thank the people at the Building Physics Laboratory at the Eindhoven University of Technology for allowing me to make use of their climate chamber. Also, I am grateful that I could make use of an external computer to run my simulations. Leon Kamp, thank you for allowing me to make use of your computer. Moreover I would like to mention my appreciation for the employees at COMSOL Multiphysics. They provided me with an own license and allowed me to make use of their support center. Special thanks to Ruud Börger, for having insightful phone calls with me on how to set up my simulation models.

Additionally, I would like to thank Twan van Hooff, Leon Kamp and Peter Andriessen for participating as external members in my graduation committee.

Furthermore, I would like to express my gratitude to my direct colleagues at the Maxima Medisch Centrum Veldhoven for all the interesting discussions and nice conversations. Teun Minkels, Daniël den Boer, Robert Hommes, Thomas van Dijk, Rohan Joshi and Eduard Meijer: my thanks to you.

Finally, I would like to say how grateful I am to my family and friends from Bacchus and the study association for keeping me motivated throughout the project.

Enjoy reading the thesis.

Roel Brooimans  
Eindhoven, November 24, 2016

# List of Abbreviations

CFD	Computational Fluid Dynamics
GA	Gestational Age
MMC	Maxima Medisch Centrum
NICU	Neonatal Intensive Care Unit
PA	Postnatal Age
RH	Relative Humidity
TEWL	Transepidermal Water Loss

# Contents

<b>1</b>	<b>Introduction</b>	<b>1</b>
1.1	Preterm birth and maintaining body temperature . . . . .	1
1.2	Neonatal incubators and nursing procedures . . . . .	2
1.3	Computational Fluid Dynamics in incubators . . . . .	3
1.4	Maxima Medisch Centrum Veldhoven . . . . .	4
1.5	Goal of this research . . . . .	4
1.6	Structure of this thesis . . . . .	4
<b>2</b>	<b>Theory</b>	<b>5</b>
2.1	Heat transfer in neonates . . . . .	5
2.1.1	Conduction . . . . .	6
2.1.2	Convection . . . . .	7
2.1.3	Radiation . . . . .	8
2.1.4	Evaporation . . . . .	9
2.1.5	Heat transfer through respiration . . . . .	10
2.1.6	Metabolic heat production of the infant . . . . .	11
2.1.7	Significance of heat transfer mechanisms on the neonate . . . . .	11
2.1.8	Impact heat transfer on neonate's body temperature . . . . .	13
2.1.9	Changes in climate and the effect on the neonate . . . . .	13
2.2	Computational Fluid Dynamics . . . . .	14
2.2.1	Finite Element Methods . . . . .	14
2.2.2	COMSOL Multiphysics . . . . .	14
2.2.3	Turbulence models . . . . .	14
2.2.4	Discretization . . . . .	15
2.2.5	Mesh theory . . . . .	15
2.2.6	Solvers . . . . .	17
<b>3</b>	<b>Computational Fluid Dynamics setup</b>	<b>18</b>
3.1	Closed incubator . . . . .	18
3.1.1	Geometry of the model . . . . .	18
3.1.2	Material properties of the model . . . . .	20
3.1.3	Physics of the model . . . . .	21
3.1.4	Model discretion and mesh . . . . .	23
3.1.5	Modelling scenarios . . . . .	25
3.1.6	Solution procedure . . . . .	26
3.2	Opened incubator . . . . .	26
3.2.1	Geometry of the model . . . . .	26
3.2.2	Material properties of the model . . . . .	27
3.2.3	Physics of the model . . . . .	27
3.2.4	Model discretization and mesh . . . . .	28
3.2.5	Solution procedure . . . . .	29

<b>4</b>	<b>Experimental setup incubator measurements</b>	<b>30</b>
4.1	Environment . . . . .	30
4.1.1	Neonatal Intensive Care Unit . . . . .	30
4.1.2	Climate Chamber . . . . .	30
4.2	Incubators . . . . .	31
4.2.1	Dräger Caleo™ . . . . .	31
4.2.2	GE Giraffe Carestation . . . . .	33
4.3	Measurement procedure . . . . .	34
4.3.1	Measurement procedure Dräger Caleo™ . . . . .	34
4.3.2	Measurement procedure GE Giraffe Carestation . . . . .	35
4.4	Locations and specifications of measurement equipment . . . . .	36
4.4.1	Specifications of measurement equipment . . . . .	36
4.4.2	Location of measurement equipment . . . . .	36
<b>5</b>	<b>Results and discussion CFD simulations</b>	<b>38</b>
5.1	Closed incubator . . . . .	38
5.1.1	Scenario 1: Incubator setpoint 33°C - 45% RH . . . . .	41
5.1.2	Scenario 2: Incubator setpoint 36°C - 70% RH . . . . .	45
5.1.3	Scenario 3: Climate recovery of the incubator . . . . .	46
5.2	Opened incubator . . . . .	47
5.3	Discussion CFD results . . . . .	48
<b>6</b>	<b>Results and discussion incubator measurements</b>	<b>49</b>
6.1	Results Dräger Caleo™ measurements . . . . .	49
6.1.1	Variation in incubator settings . . . . .	49
6.1.2	Variation in climate chamber settings . . . . .	52
6.1.3	Comparison simulation and measurements . . . . .	53
6.2	Results GE Giraffe Carestation measurements . . . . .	54
6.3	Comparison GE Giraffe Carestation and Dräger Caleo™ . . . . .	58
6.3.1	Incubator setpoint 38°C - 99% RH . . . . .	58
6.3.2	Incubator setpoint 34°C - 50% RH . . . . .	59
6.4	Discussion measurement results . . . . .	60
<b>7</b>	<b>Clinical Relevance and the effect on the neonate</b>	<b>61</b>
7.1	Closed incubator - simulations . . . . .	61
7.2	Opened incubator - measurements . . . . .	64
7.2.1	General guideline NICU personnel . . . . .	64
7.2.2	Typical incubator opening scenarios: the effect on the neonate's body temperature, a guideline for NICU personnel . . . . .	65
7.3	Discussion clinical relevance . . . . .	67
<b>8</b>	<b>Conclusion and recommendations</b>	<b>68</b>
<b>9</b>	<b>Bibliography</b>	<b>69</b>
<b>A</b>	<b>Calculating relative humidity from concentration and visa versa</b>	<b>73</b>
<b>B</b>	<b>Detailed product specifications of measurement equipment</b>	<b>74</b>
<b>C</b>	<b>Detailed description of measurement locations</b>	<b>80</b>
<b>D</b>	<b>Mesh refinement analysis</b>	<b>81</b>



<b>E</b>	<b>Simulation graphs</b>	<b>83</b>
E.1	Scenario 1: Incubator setpoint 33°C-45% RH . . . . .	83
E.2	Scenario 2: Incubator setpoint 36°C-70% RH . . . . .	84
<b>F</b>	<b>All measurement results Dräger Caleo™</b>	<b>86</b>
F.1	Climate chamber setpoint: 25°C-45% RH . . . . .	86
F.1.1	Air temperature and relative humidity . . . . .	86
F.1.2	Surface temperature . . . . .	88
F.2	Incubator setpoint: 36°C-70% RH . . . . .	90
F.2.1	Air temperature and relative humidity . . . . .	90
F.2.2	Surface temperature . . . . .	91
<b>G</b>	<b>All measurement results GE Giraffe Carestation</b>	<b>92</b>
G.1	Air temperature and relative humidity . . . . .	92
G.2	Surface temperature . . . . .	99
<b>H</b>	<b>Comparison Dräger Caleo™ and GE Giraffe Carestation</b>	<b>106</b>
<b>I</b>	<b>Typical incubator opening scenarios: the effect on the neonate’s body temperature, a guideline for NICU personnel</b>	<b>109</b>

# Chapter 1

## Introduction

### 1.1 Preterm birth and maintaining body temperature

According to the WHO (World Health Organization) [1], every year, an estimated 15 million babies are born preterm. That is more than 10 % of all babies born. Almost a million children worldwide die each year due to complications of preterm birth. Many children that survive suffer from lifetime disabilities. Premature birth rates differ between regions in the world. The Netherlands has a preterm birth rate prevalence of 8.0 % in 2010 [2]. Preterm birth is defined as babies born before 37 weeks after gestation. These are further categorized into:

- Extremely preterm (<28 weeks)
- Very preterm (28 to 32 weeks)
- Moderate to late preterm (32 to 37 weeks)

Preterm births generally correspond to a low birth weight. Low birth weight infants are those born weighing less than 2500 g. In more detail they are categorized as follows:

- Extremely Low Birth Weight, <1000 g
- Very Low Birth Weight, <1500 g
- Low Birth Weight, <2500 g

Low birth weight infants suffer from many disabilities. One of their biggest problems is maintaining their core body temperature [3].

The World Health Organization recommends that an infant's body temperature is kept between 36.5 °C and 37.5 °C [4]. The WHO categorizes cold stress into:

- Potential Cold Stress (36.0°C-36.5°C): Cause for concern.
- Moderate hypothermia (32°C-36.0°C): Dangerous, requires immediate warming of the infant.
- Severe hypothermia (<32°C): Outlook grave, skilled care is urgently needed.

When adults experience a low body temperature, the body responds by means of peripheral vascular constriction, inhibition of sweating, voluntary muscle movements, involuntary muscle movements (shivering) and nonshivering thermogenesis [5]. On the other hand, when adults experience a high body temperature, they can increase the evaporative heat loss by sweating.

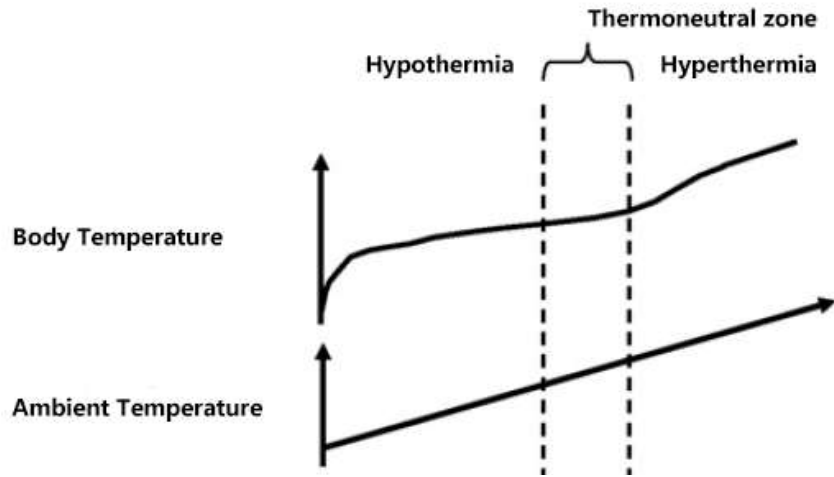


**Figure 1.1** – A preterm infant has a reduced capability to maintain their core body temperature. Their body temperature strongly depends on the ambient temperature. Consequently, their thermoneutral zone is very small. Adapted from [3].

That is the reason why adults are able to maintain their core body temperature in a wide range of ambient temperatures. Therefore the adult's thermoneutral zone is large. Preterm infants lack many of these responses or they have a diminished effect [6]. That is the reason why preterm infants' body temperatures vary strongly with changing ambient temperature. Consequently, the preterm infant's thermoneutral zone is very small. Figure 1.1 illustrates the preterm infant's thermoneutral zone.

In 1957 it was already shown that cold stress in neonates is related to a higher mortality rate [7][8]. Therefore, preventing cold stress in neonates is vital. However, Laptook's large study in 2007 showed that cold stress in neonates is more common than generally thought. He showed that 46.6% of the infants had a lower body temperature than 36.0 °C upon admission of the NICU (Neonatal Intensive Care Unit) [9].

To aid the preterm infants in maintaining their core body temperature, they are often taken care of in neonatal incubators.

## 1.2 Neonatal incubators and nursing procedures

Neonatal incubators are closed environments in which the air temperature and humidity are controlled. The purpose of an incubator is to maintain thermal stability in the preterm infant. A photograph of a neonatal incubator is shown in Figure 1.2.

Even inside an incubator, several studies show that air temperature fluctuations of 2 °C can induce thermal stress in premature infants [10][11][12]. This shows the importance of maintaining a stable climate in incubators. Occasionally a neonatal incubator needs to be opened for nursing procedures. The procedures vary from feeding and changing diapers to radiologic screening. While an incubator is opened it is in direct contact with the air of the environment. In other words, air from the ambient room will mix with the air inside the incubator. Therefore it is recommended to maintain an ambient room temperature between 22 and 26 °C with a relative humidity of at least 50% [13].

Deguines et al (2013) measured the changes in air temperature, body temperature and relative humidity during various nursing procedures, in 31 preterm neonates under 32 weeks of

gestation. The study showed an abdominal body temperature drop of up to  $1.08^{\circ}\text{C/h}$  during nursing procedures. Such changes can induce major disorders of neonatal autonomic function [14]. The results from Deguines' study are presented in Figure 1.3. The climate inside the incubator is essential to control the infant's body temperature. Therefore, it is of importance to gain more insight in the temperature and relative humidity distribution inside the incubator.



**Figure 1.2** – Photograph of the GE Giraffe Carestation neonatal incubator.

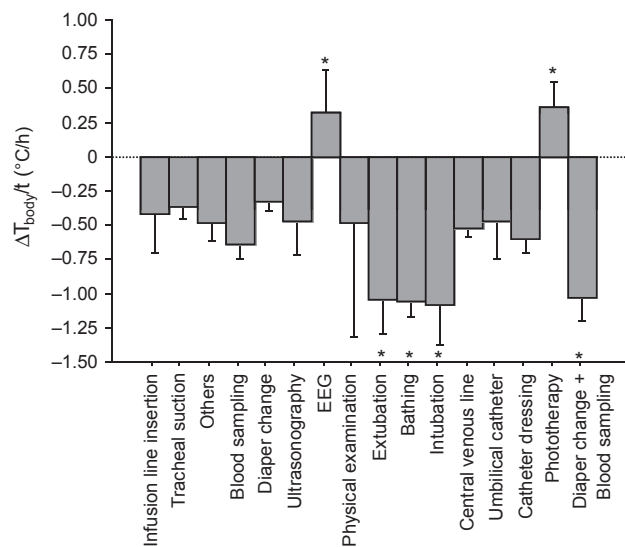


**Figure 1.3** – Impact of nursing procedures on the body temperature of the preterm infant. The temperature drop in case of intubation is  $1.08^{\circ}\text{C/h}$ , which can cause major disorders of neonatal autonomic function. Adapted from [14].

### 1.3 Computational Fluid Dynamics in incubators

Computational Fluid Dynamics (CFD) is a widely used simulation technique to model complex flows. It developed over the last decades, mostly due to rapid increase in computation power of computers. CFD simulations can be very useful in many situations, because they provide clear insight in the physics of the problem. On top of that, they allow for easy parametric

testing to find the optimal configuration. Finally, CFD is usually a lot more cost-efficient than experiments or making proto-types.

Previous studies have already successfully used CFD techniques to describe thermal interaction between the human body and its environment [15][16][17]. These studies were all carried out with respect to adults, whose physical shape and thermophysiological properties differ from neonates. Ginalski et al successfully modelled an incubator by Dräger (Caleo) [45]. Their findings for the air flow and heat losses are in good agreement with previous research [19]. However, Ginalski et al did not model the opening of the incubator. In addition, Ginalski et al did not model the air humidity, which is also presumed to be an important factor for thermal stability of the neonate, based on our own NICU (Neonatal Intensive Care Unit) experiences. The next section explains what is meant by our own NICU experiences.

## 1.4 Maxima Medisch Centrum Veldhoven

This research is executed by the Maxima Medisch Centrum Veldhoven, The Netherlands, in collaboration with the Eindhoven University of Technology. The Maxima Medisch Centrum provided the research with relevant clinical information, as well as an incubator to perform measurements on. Therefore, if a reference 'our' is used, it is referred to as the Maxima Medisch Centrum.

## 1.5 Goal of this research

The goal of this research is to determine the influence of opening an incubator on the temperature and relative humidity inside the incubator. From this temperature and relative humidity, the heat loss and corresponding change in body temperature of the infant can be calculated. Using this knowledge, strategies for reducing thermal losses can be further developed. It can provide insight in the thermal state of the infant and predict whether the infant is at risk for hypo- or hyperthermia. On top of that, it might give insight on how to set up the climate settings of the incubator.

The research consists of two parts:

- Develop a Computational Fluid Dynamics model to compute climate effects due to incubator opening. Climate effects involve temperature and relative humidity. CFD can predict the outcome in advance or recommend the climate configuration of an incubator. It provides accurate information of the thermal state of the neonate.
- Perform climate measurements on incubators to validate the CFD model. The measurements involve opening of the incubator and serve as a verification of the outcomes of the CFD model.

## 1.6 Structure of this thesis

In this thesis, each chapter starts with a brief overview of the information provided in the chapter. Furthermore, the chapters are structured as follows: chapter 2 provides the relevant theory for this research. Chapter 3 describes the setup of the computational fluid dynamics model. Chapter 4 explains the experimental setup involving the incubator measurements. The results for the CFD simulations and the incubator measurements are treated in chapter 5 and 6, respectively. The clinical relevance and the effect on the neonate's body temperature is explained in chapter 7. Finally, the conclusion and future recommendations can be found in chapter 8.

# Chapter 2

## Theory

In this chapter the relevant theory is explained. The first section, 2.1, describes heat transfer in neonates. The second section, 2.2, addresses the theory of computational fluid dynamics.

### 2.1 Heat transfer in neonates

Heat transfer in neonates occurs due to several fundamental physical processes. This section addresses all processes. The processes are visualized in Figure 2.1.

Thermal stability is achieved when the metabolic heat production of the infant equals the heat transfer with the environment. Heat transfer is generally described by the sum of conduction, convection, radiation, evaporation and respiratory transfers [21]. This is expressed by the following equation:

$$M + R + C + K + E + C_{\text{resp}} + E_{\text{resp}} = S, \quad (2.1)$$

where  $M$  is the metabolic heat production,  $R$  is the radiative heat transfer,  $C$  is the convective heat transfer,  $K$  is the conductive heat transfer,  $E$  is the evaporative heat transfer,  $C_{\text{resp}}$  the convective heat transfer through respiratory exchanges,  $E_{\text{resp}}$  the evaporative heat transfer through respiratory exchanges and  $S$  the total heat gain or heat loss. The infant reaches thermal stability when  $S = 0$ .

A more detailed description of the different components of heat transfer is given in the following subsections. Each section will briefly describe the heat transfer mechanism and the impact on the infant. A parametric calculation of typical values of the different components of heat transfer is given in section 2.1.7. In this section, the significance of each heat transfer mechanism on the neonate will be determined. The impact of heat transfer on the neonate's body temperature will be explained in section 2.1.8. Finally, the impact of climate changes on the neonate is treated in section 2.1.9. In all sections, it is assumed that the neonate is naked. Clothing will reduce heat transfer but is not taken into account.

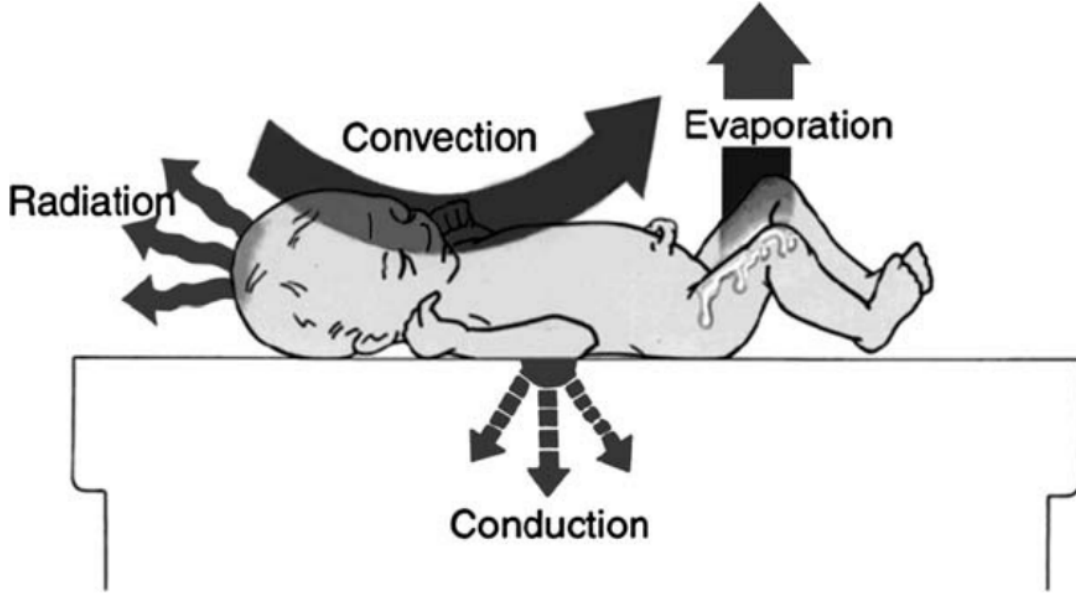


**Figure 2.1** – The physics of heat transfer. Heat transfer occurs through convection, conduction, radiation and evaporation. Adapted from [20].

### 2.1.1 Conduction

The physical mechanism of conduction occurs due to atomic and molecular interactions. It causes a net energy transfer due to random molecular motion. The particles with higher temperature possess higher energy and will transfer energy when colliding with other, colder particles. Therefore, heat transfer takes place in the direction of decreasing temperature.

The rate of heat transferred by conduction is described by Fourier’s law. It is given by

$$Q_{cond} = -k\nabla T, \quad (2.2)$$

where  $Q_{cond}$  is the total heat transferred per unit of time ( $\text{W}/\text{m}^2$ ),  $k$  is the thermal conductivity which is material dependent ( $\text{W}/(\text{m}\cdot\text{K})$ ),  $\nabla$  is the three-dimensional gradient operator ( $1/\text{m}$ ) and  $T(x,y,z)$  is the scalar temperature field ( $\text{K}$ ).

Note that the thermal conductivity,  $k$ , is material, pressure and temperature dependent. In this research however, the thermal conductivity is considered to be dependent of the material only. This is due to the fact that temperature variations are small ( $\pm 2\text{-}3\text{ }^\circ\text{C}$ ) and therefore temperature dependence can be neglected. Figure 2.2 presents the thermal conductivity as function of temperature for different materials. Since thermal conductivity is much less dependent on pressure than on temperature [22], its pressure dependence is neglected as well.

In case of a neonate in an incubator, it is in direct contact with a mattress and air. Heat transfer due to the infant being in contact with the mattress is low, because the mattress is usually prewarmed and the temperature of the mattress is (nearly) equal to the temperature of the neonate’s skin. Conductive heat transfer due to the contact with air is also low, because air has a low thermal conductivity ( $k_{air} \approx 0.02\text{ W}/(\text{m}\cdot\text{K})$ ).

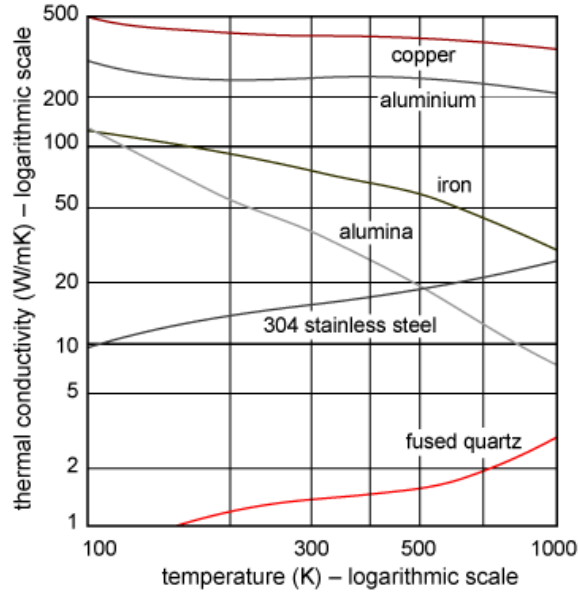


**Figure 2.2** – Thermal conductivity of different materials as a function of temperature. Adapted from [23].

### 2.1.2 Convection

Convective heat transfer occurs when a fluid flows over a surface and there is a temperature difference between the fluid and the surface. Convective heat transfer is widely used in cooling applications (i.e. the cooling of electronic components in a computer).

Convective heat transfer depends on the details of the flow field. Therefore it is important to consider how the flow is generated. In forced convection the fluid motion is caused by an external force such as a fan or a pump. Free convection is caused by body forces of the fluid itself. This is induced by density gradients which are in itself caused by temperature gradients. Flows involving both forced and free convection are termed combined- or mixed convective flows [24].

The rate of convective heat transfer is given by [24]

$$Q_{conv} = h(T_s - T_f), \quad (2.3)$$

where  $Q_{conv}$  is the heat transfer rate ( $\text{W}/\text{m}^2$ ),  $h$  is the heat transfer coefficient ( $\text{W}/(\text{m}^2 \cdot \text{K})$ ),  $T_s$  is the temperature of the surface and  $T_f$  is the temperature of the fluid flowing over the surface.

The convective heat transfer coefficient  $h$  is a difficult parameter to determine. It depends on the flow situation. Variables such as the fluid involved, velocity of the fluid, viscosity of the fluid and shape of the surface alter the value of  $h$  [24]. A list of typical heat transfer coefficients in several scenarios is presented in Table 2.1.

In case of the neonate in an incubator, convection has a considerable impact on the heat transfer of the neonate, because the heat transfer coefficient is  $\sim 250$  times bigger than the thermal conductivity of air ( $h = 5.4 \pm 0.3 \text{ W}/(\text{m}^2 \cdot \text{K})$  [25]).



**Table 2.1** – Typical values for mean heat transfer coefficients. Data provided by [24].

Flow situation and fluid	Mean heat transfer coefficient $h$ (W/(m <sup>2</sup> ·K))
Forced convection in air	10-200
Forced convection in water	40-10,000
Forced convection in liquid metals	10,000-100,000
Free convection in air	3-20
Free convection in water	20-200

### 2.1.3 Radiation

Radiation is the transmission of electromagnetic waves from surfaces. The total power emitted from a surface,  $P_{rad}$  (W/m<sup>2</sup>), is given by [26]

$$P_{rad} = \epsilon\sigma T^4, \quad (2.4)$$

where  $\epsilon$  is the emissivity of the material,  $\sigma$  ( $5.675 \cdot 10^{-8}$  W/m<sup>2</sup>K<sup>4</sup>) the Stefan-Boltzmann constant and  $T$  the temperature in Kelvin.  $\epsilon$  is defined as the power emitted by a nonblack body divided by the power emitted by a black body. In equation form [26],

$$\epsilon = \frac{P_{rad,e}}{P_{rad,b}}, \quad (2.5)$$

where  $P_{rad,e}$  is the power emitted by a nonblack body and  $P_{rad,b}$  is the energy emitted by a black body. The emissivity is material dependent and depends on the opaqueness of the material, but also depends on more variables such as the wavelength, surface temperature and direction of emitted radiation [27].

In case of a neonate, the radiative heat transfer between two surfaces,  $Q_{rad}$  (W/m<sup>2</sup>), is given by [26]

$$Q_{rad} = A_f \epsilon_s \epsilon_r \sigma (T_s^4 - T_r^4), \quad (2.6)$$

where  $A_f$  is the fraction of the infant's body surface area available for radiative heat transfer,  $\epsilon_s$  and  $\epsilon_r$  are the emissivities of the skin and radiant surface respectively and  $T_s$  and  $T_r$  are the mean skin and mean radiant temperature of the surroundings, respectively.

Equation 2.6 can be rewritten to a simpler linear form in case of a neonate in an incubator, because  $(T_s - T_r) \ll T_s$  and the range of the skin temperature is small. Equation 2.6 becomes [25]:

$$Q_{rad} \simeq h_r (T_s - T_r). \quad (2.7)$$

In equation 2.7, the radiant heat transfer coefficient,  $h_r$  (W m<sup>-2</sup> K<sup>-1</sup>), is given by

$$h_r = 4A_f \epsilon_r \epsilon_s \sigma T_s^3 \quad (2.8)$$

In case of a neonate nursed inside an incubator, the neonate will transfer radiative heat with the (inner) walls of the incubator. According to [28], this effect is non-neglectable and should be taken into account.

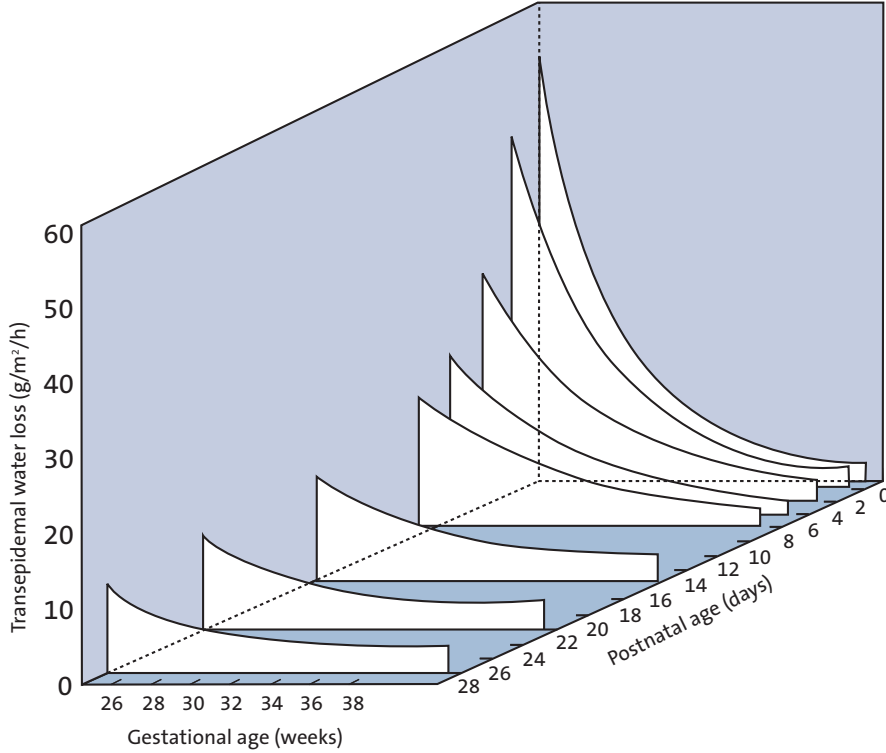


**Figure 2.3** – Transepidermal water loss as a function of postnatal and gestational age. The ambient relative humidity was set to 50%. Transepidermal water loss directly influences the evaporative heat loss. Adapted from [35].

#### 2.1.4 Evaporation

Evaporation is the vaporization of a liquid to a gas. Vaporization requires energy. In case of a neonate, the energy is extracted from the skin and therefore the body suffers from evaporative heat exchange, which is always a loss.

Hammarlund was the first to quantify evaporative heat loss in premature infants. Hammarlund’s study showed that evaporative heat loss has a significant impact on the body temperature of the neonate [28]. Especially during the first hours after birth, evaporative heat loss has a significant impact on the total heat loss of the infant. This is due to the fact that the infant is covered with amniotic fluid. This evaporative heat loss remains high until the infant is dried. Therefore, a couple of studies suggest using a plastic (polythene) wrap immediately after or before drying, to reduce convective and evaporative heat losses [29][30][31]. Evaporative heat loss decreases gradually during the first hours of life [32].

Hammarlund’s study also showed a relatively high evaporative heat loss at low gestational age and low postnatal age. This is due to the high transepidermal water loss (TEWL) [33]. Transepidermal water loss is defined as the measurement of the quantity of water that passes from inside a body through the epidermal layer to the surrounding atmosphere via diffusion and evaporation processes [34]. Figure 2.3 shows the relationship between age (both postnatal and gestational) and the transepidermal water loss of an infant. The relationship is experimentally derived [35].

The TEWL retrieved from Figure 2.3 is from now on denoted as  $TEWL_{50}$ , because it was derived at a relative humidity (RH) of 50 %. The correction for RH is given by [36][37]

$$TEWL = \frac{(100 - RH)}{50} \cdot TEWL_{50}. \quad (2.9)$$

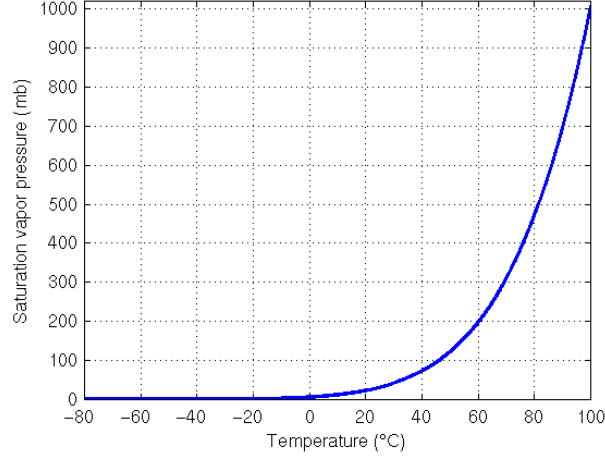


**Figure 2.4** – Temperature dependence of the saturation water vapor pressure. Source: University of Washington

According to Hammarlund, the evaporative heat loss is given by [32]

$$Q_{evap} = k_1 \cdot TEWL \cdot [3.6 \cdot 10^3]^{-1}, \quad (2.10)$$

where  $Q_{evap}$  is the evaporative heat loss ( $\text{W}/\text{m}^2$ ),  $k_1$  is the latent heat of evaporation of water ( $2.4 \cdot 10^6 \text{ J}/\text{kg}$  [32]), TEWL is the Transepidermal water loss ( $\text{g}/\text{m}^2/\text{h}$ ) and  $3.6 \cdot 10^3$  is a correction factor.

The relative humidity, RH, is defined as the ratio of actual water vapor pressure to the saturation water vapor pressure [38][39]:

$$\text{RH} = \frac{p_{H_2O}}{p_{H_2O}^*}. \quad (2.11)$$

The saturation water vapor pressure depends both on the air temperature and pressure. The pressure dependence is negligible compared to the temperature dependence [38][39]. The temperature dependence is illustrated in Figure 2.4. The saturation pressure is strongly dependent on temperature, which implies that relative humidity also strongly depends on temperature.

### 2.1.5 Heat transfer through respiration

Heat transfer through respiration has a convective and an evaporative component. The convective heat transfer depends on the difference in temperature between inspired and expired air and the ventilation rate. Evaporative heat loss depends on the humidity difference between inspired and expired air, as well as the ventilation rate. Convective heat transfer by respiration is given by [21]

$$Q_{conv,resp} = V_E C_p (T_E - T_I). \quad (2.12)$$

In equation 2.12,  $Q_{conv,resp}$  is the heat exchange (W),  $V_E$  is the pulmonary ventilation rate ( $\text{kg}/\text{s}$ ) [40],  $C_p$  is the heat capacity of air ( $1044 \text{ J}/\text{kg}/\text{K}$ ),  $T_E$  (K) is the temperature of the expired air and  $T_I$  (K) is the temperature of the inspired air.

The evaporative heat transfer by respiration is as follows [21]:

$$Q_{evap,resp} = V_E k_1 (M_E - M_I), \quad (2.13)$$

where  $Q_{evap,resp}$  is the heat transfer (W),  $k_1$  is the latent heat of water vaporization ( $2.4 \cdot 10^6$  J/kg [32]),  $M_E$  is the water content (kg water/kg dry air) of expired air and  $M_I$  the water content (kg water/kg dry air) of inspired air.

### 2.1.6 Metabolic heat production of the infant

The metabolic heat production has been determined experimentally in 1961 by Brück and depends on the weight ( $m$ , in kg) and the postnatal age ( $p$ , in days) of the infant. The metabolic heat production  $Q_{meta}$  (W) is given by [41]

$$Q_{meta} = 0.0522 \cdot m \cdot p + 1.64. \quad (2.14)$$

### 2.1.7 Significance of heat transfer mechanisms on the neonate

To determine the importance of each mechanism of heat transfer, this section will calculate typical values for the mechanisms described in previous sections. The respiratory losses through convection and evaporation are not calculated but extracted from Agourram [21].

The physical parameter values, as well as the parameters for the physical shape of the neonate and the neonate's thermophysiological properties used for the calculations are presented in Table 2.2.

The results are shown in Table 2.3. Conduction and respiratory losses are of least significance on the total heat transfer of the baby. Therefore, these are from now on neglected. The total heat loss is 3.69 W, which means the neonate is not thermally stable and will lose heat. The air temperature and relative humidity inside the incubator have to be increased to stabilize the neonate. In conclusion, setting up the incubator's climate is of vital importance in keeping the neonate stable.

Hammarlund et al did measurements on neonates determining the evaporative, radiative and convective heat transfer. The results are shown in Figure 2.5. The results of the typical values calculated in Table 2.2 are also visualized and highlighted with red dots. Figure 2.5 shows some interesting results. First of all, evaporative heat transfer decreases with increasing gestational age. This is due to the fact that the transepidermal water loss decreases when the gestational age increases, see Figure 2.2. Secondly, radiative heat transfer increases with increasing gestational age. This is caused by a lower incubator temperature setpoint. Due to this, the temperature difference between the neonate's skin and the incubator's inner walls increases, causing a higher radiative heat transfer. Additionally, convective heat transfer increases due to the same principle as radiative heat transfer. Finally, the typical values calculated in this section are in good agreement with Hammarlund's study.

**Table 2.2** – Parameter values used to calculate typical values for the mechanisms of heat transfer.

Parameter	Value
Surface area infant	0.10 m <sup>2</sup> [42]
Surface area fraction for radiation $A_f$	0.76 [25]
Weight infant	1 kg
Thermal conductivity mattress $k$	0.04 W/(m·K) [43]
Temperature infant's skin	36 °C [44]
Temperature mattress	35.8 °C
Temperature incubator air	34 °C [45]
Temperature incubator walls	33 °C
Relative humidity incubator	50 %
Gestational age infant	28 weeks
Postnatal age infant	1 day
Convective heat transfer coefficient $h$	5.4 W/(m <sup>2</sup> ·K) [25]
Emissivity of the skin	0.95 [45]
Emissivity of incubator walls	0.9 [45]

**Table 2.3** – Typical values of heat transfer assuming the parameter values in Table 2.2. The metabolic heat production, convection, radiation and evaporation have the largest influence on the total heat transfer.

Heat transfer mechanism	Value, loss (W)	Source
Conduction	0.004	Equation 2.2
Convection	1.08	Equation 2.3
Radiation	1.31	Equation 2.7
Evaporation	2.86	Equation 2.10
Convection respiratory	0.01	Agourram [21]
Evaporation respiratory	0.02	Agourram [21]
Metabolic heat production	-1.69	Equation 2.14
Total heat loss	3.69	

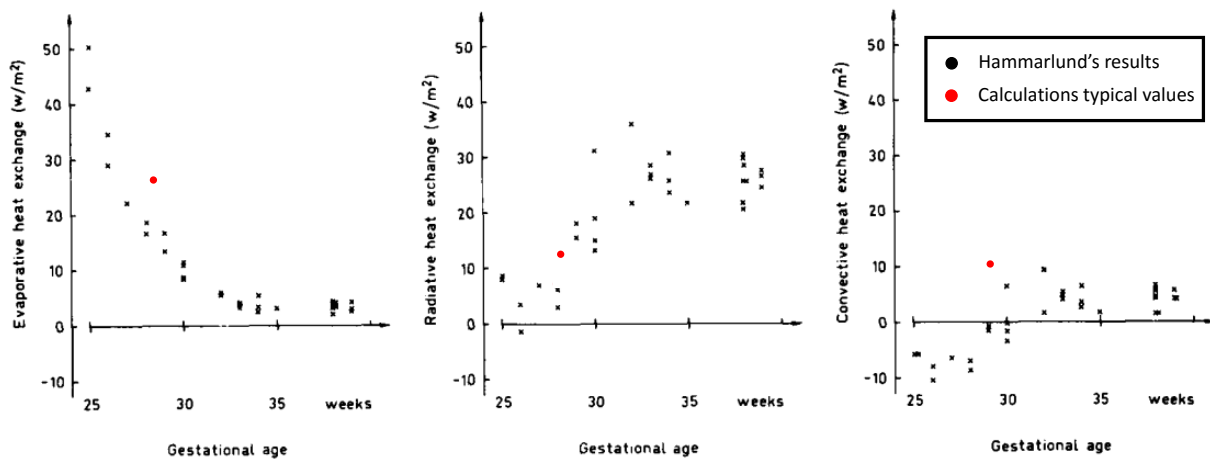


**Figure 2.5** – Evaporative heat transfer, radiative heat transfer and convective heat transfer in neonates related to gestational age. The relative humidity was set to 50% and the ambient air temperature was controlled to maintain the infant's body temperature between 36.0-37.0 °C. Adapted from [28]. The results of the typical values in Table 2.2 are highlighted by the red dots.

### 2.1.8 Impact heat transfer on neonate's body temperature

The effect of heat transfer on the temperature can be calculated using

$$\frac{\Delta T}{\Delta t} = \frac{Q}{cm}, \quad (2.15)$$

where in  $\Delta T/\Delta t$  is the induced temperature difference per time ( $\Delta^\circ\text{C}/\text{s}$ ),  $Q$  is the added/extracted heat per second (W),  $c$  (J/kg·K) is the specific heat of the material and  $m$  is the total mass (kg). For a typical neonate weighing 1 kg and with a specific heat of  $c = 3391$  J/kg·K [46], this means the neonate loses  $0.017$   $^\circ\text{C}/\text{min}$  per Watt heat loss. For the typical values calculated in Table 2.2 this implies the neonate loses  $0.065$   $^\circ\text{C}/\text{min}$ .

### 2.1.9 Changes in climate and the effect on the neonate

This section describes the effect of varying climate on the neonate, assuming the neonate is thermally stable. A change in the incubator's inner wall surface temperature, air temperature and/or relative humidity will induce a disbalance in the neonate's heat balance equation. An air temperature decrease will (linearly) increase the convective heat loss, a relative humidity drop will give rise (linearly) to an increased evaporative heat loss and a drop in the surface temperature of the incubator will (linearly) increase radiative heat loss.

#### Convective heat losses

The convective heat transfer coefficient,  $h$ , is  $5.4$  W/(m<sup>2</sup>·K) [25]. Equation 2.3 is used to calculate the increase in convective heat loss. Every  $^\circ\text{C}$  the air temperature drops, the neonate will lose  $5.4$  W/m<sup>2</sup> heat.

#### Evaporative heat losses

The TEWL<sub>50</sub> can be retrieved from Figure 2.3. The increased evaporative heat loss per drop in relative humidity of 1%,  $\Delta Q_{evap}^*$  (W/m<sup>2</sup>), can be derived from equation 2.10 and is given by:

$$\Delta Q_{evap}^* = 0.0133 \cdot \text{TEWL}_{50} + 0.001. \quad (2.16)$$

#### Radiative heat losses

The increase in radiative heat loss is calculated by using equation 2.7. Every  $^\circ\text{C}$  decrease of the incubator's inner wall temperature leads to an increase in radiative heat loss of  $4.36$  W/m<sup>2</sup>.

#### Total heat loss and effect on the temperature

The total heat loss is given by addition of convective, evaporative and radiative heat loss. Combined with the area of the infant, specific heat (3391 J/kg·K [46]) of the infant and the mass of the infant, the resulting body temperature change can be calculated using equation 2.15.

## 2.2 Computational Fluid Dynamics

This section gives an overview of Computational Fluid Dynamics (CFD). CFD generally makes use of Finite Element Methods (FEMs) to solve the problem. This section elaborates on FEMs and different turbulence models. Finally, the section ends with information about mesh theory and solvers.

### 2.2.1 Finite Element Methods

Physics problems, which are space- and time-dependent, are generally described by Partial Differential Equations (PDEs). Due to complex geometries and mixed PDEs, these problems can usually not be solved using analytical methods. These often complex functions can be solved by discretization methods. By using well-chosen discretization methods, these PDEs can often be approximated fairly well.

Finite Element Methods (FEMs) make use of these discretization methods to solve PDEs. The usefulness of FEM techniques was first recognized by Richard Courant in 1940 [47]. Nowadays it is a worldwide used approach to solve complex physical problems.

### 2.2.2 COMSOL Multiphysics

This subsection addresses COMSOL Multiphysics, which is a FEM computer program able to solve CFD problems. This section is part of the theory because the turbulence models and solvers, which are described further in this chapter are related to COMSOL. There are several computer programs able to solve CFD problems by making use of Finite Element Methods. In this research, COMSOL Multiphysics is chosen because the Eindhoven University of Technology offered a license. Furthermore, COMSOL provided a separate license for this research which allowed making use of their support center.

### 2.2.3 Turbulence models

In fluid dynamics (which includes gases and liquids), as the Reynolds number increases, the flow regime can switch from laminar to turbulent flow. The Reynolds number ( $Re$ ) depends on the characteristic velocity  $v$  (m/s), characteristic length scale  $L$  (m) and the kinematic viscosity  $\nu$  ( $m^2/s$ ) and is defined as

$$Re = \frac{v \cdot L}{\nu}. \quad (2.17)$$

In pipe flows the flow regime switches from laminar to turbulent at a Reynolds number of  $\approx 10^4$ . As the Reynolds number increases even more, the flow field exhibits small eddies and the timescales of the oscillations become so short that it is computationally unfeasible to solve the Navier-Stokes equations [48]. In case of an incubator,  $v \approx 0.41$  m/s [45],  $L = \approx 1$  m and  $\nu \approx 1.6 \cdot 10^{-5}$   $m^2/s$ . Using these values, the Reynolds number can be calculated and is given by  $\approx 2.5 \cdot 10^4$ . Therefore it is assumed that the flow regime is governed by turbulent flow. In this regime the RANS (Reynolds Averaged Navier Stokes) formulation is commonly used to average these oscillations. This will add additional unknowns to the problem [48]. There are several formulated RANS turbulence models which all compute the extra unknown equations differently. In this research, the  $k - \epsilon$  model is used which is described in the following paragraph. It is beyond the scope of this research to determine the influence of the multiple turbulence models on the solution of the model. Therefore, other turbulence models are treated only briefly after the  $k - \epsilon$  model is described.

### 2.2.3.1 $k$ - $\epsilon$ model

The  $k$ - $\epsilon$  model solves for two variables:  $k$ , which is the turbulent kinetic energy, and  $\epsilon$ , which is the rate of dissipation of turbulent kinetic energy.  $k$  determines the energy of the turbulence, while  $\epsilon$  is the variable that determines the scale of turbulence.

It is the most commonly used and validated turbulence model due to its relatively good convergence and relatively low memory requirements [48]. The "standard"  $k - \epsilon$  model was developed by Launder and Spalding [49]. The model generally was not used when there were wall effects present. However, nowadays it can be applied to models where wall effects are present due to the implementation of wall functions. Wall functions are used to connect the free stream and the near-wall flow [49]. The model may perform poorly in a variety of cases such as unconfined flows, curved boundary layers and rotating flows [50].

### 2.2.3.2 Other turbulence models

Apart from the  $k - \epsilon$  model, there are several other models available to compute turbulence. The L-VEL and yPlus models compute the turbulent viscosity, based only on the local fluid velocity and distance to the closest wall [48]. These models generally have a good convergence and are least computationally intensive of all the models described in this section, but are also least accurate.

The  $k$ - $\omega$  model is similar to the  $k$ - $\epsilon$  model, but instead of  $\epsilon$  it solves for  $\omega$ , which is the specific rate of dissipation of kinetic energy [48]. It has worse convergence than the  $k$ - $\epsilon$  model but is useful in many cases where the  $k$ - $\epsilon$  model is not accurate.

The SST (Menter's Shear Stress Transport) model combines the free stream of the  $k$ - $\epsilon$  model and the  $k$ - $\omega$  model near walls. It tends to be most accurate when solving flows near walls but does not always converge to the solution quickly [48].

## 2.2.4 Discretization

COMSOL allows several approaches to discretize physical quantities. They can be discretized by so-called element orders. Element orders can be either linearly, quadratically, cubically, quartically or quintically. Once the solution is computed, COMSOL constructs the solution field by interpolating the solution vector [51]. Single-physics finite element problems will converge towards the same answer, regardless of the element order. Increasing the element order will increase the computation time. COMSOL will choose a default element order by the type of differential equations. I.e. Poisson-type partial differential equations are second-order partial differential equations, so second-order (quadratic) elements are COMSOL's default choice [51].

It is beyond the scope of this research to determine what element order is most appropriate for each physical quantity. Therefore, COMSOL's default choice is used in the simulations.

## 2.2.5 Mesh theory

The meshing of the geometry significantly influences the accuracy of the solution. Meshing is dividing your geometry into subdomains to represent the geometry in a discretized manner [52]. It partitions the geometry into elements over which the governing physics equations can be approximated. The mesh quality is of great importance when solving FEM simulations, because it has influence on several factors, such as the rate of convergence, the solution accuracy and the computation time required. Especially when considering fluid flow, the mesh quality should not be inferior. An inferior mesh quality can leave out important physical phenomena such as boundary layers in fluid flows. This might cause delays in convergence, or even become a model



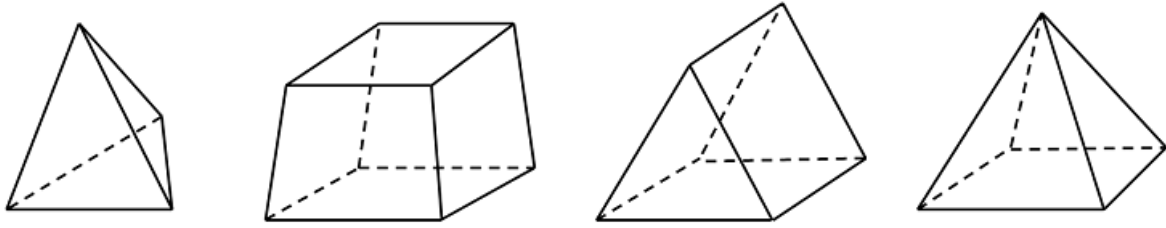


**Figure 2.6** – Four basic meshing elements used for meshing a 3D geometry. From left to right: tetrahedral, brick, prism and pyramid. Adapted from [52].

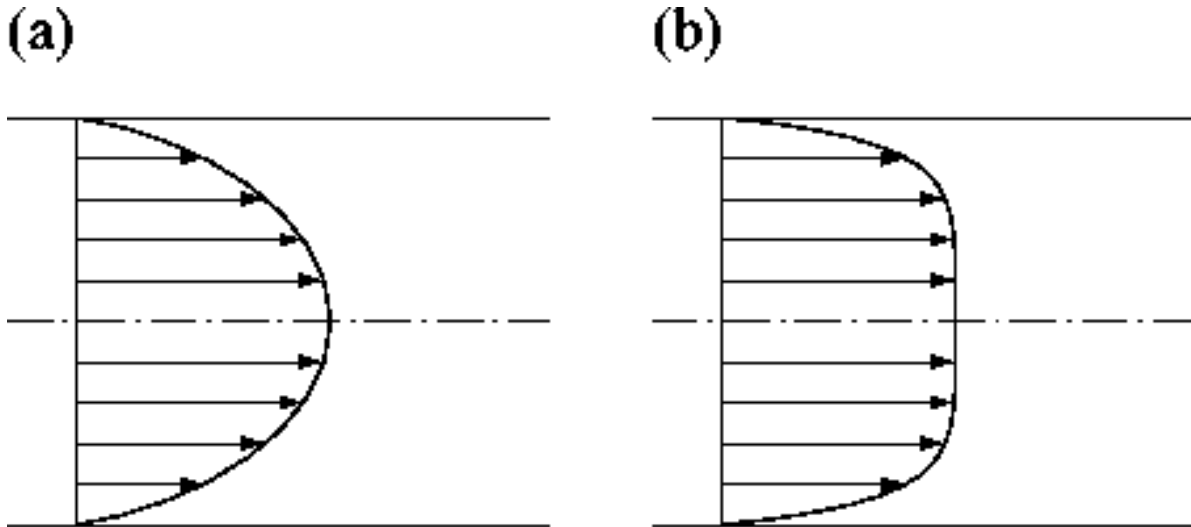


**Figure 2.7** – (a) Laminar fully developed channel flow. It is characterized by a parabolic profile. (b) Turbulent fully developed channel flow. It is characterized by a flat mean velocity profile caused by turbulent mixing in the centre and high gradients near the walls.

that does not converge at all.

Several element types can be used to build the mesh. In 2D this includes triangles and quadrilaterals. In 3D the element types are given by tetrahedra, bricks, prisms and pyramids. Figure 2.6 shows the four basic element types used for meshing in 3D. Tetrahedra are the default element type for most physics within COMSOL Multiphysics. The main reason is because tetrahedra are known as being simplex, which means that any 3D volume can be meshed with tetrahedra [52].

When modelling flow, one should be aware when meshing in- and outlets. Turbulent flow through in- and outlets generally behaves as a flattened out velocity profile [53]. In- and outlets behave as a short channel. Therefore, gradients are high near the walls in case the flow is turbulent. This requires fine meshing of the in- and outlets. A velocity profile of a laminar and turbulent fully developed channel flow is shown in Figure 2.7.

In COMSOL Multiphysics, two variables are automatically computed that allow verification of the mesh quality. These are given by the wall lift-off,  $\delta_w$  (m), and the wall-lift off in viscous units,  $\delta_w^+$ . The wall-lift off is defined as the distance between the (solid) wall and the region where the computational domain starts. Between the wall and the computational domain, that is in the region of the wall lift-off, wall functions are used. Wall functions are used to connect the flow at a solid wall, where a no-slip condition applies, and the free stream flow. The wall lift-off is represented in Figure 2.8. The wall lift-off,  $\delta_w$ , is automatically computed so that

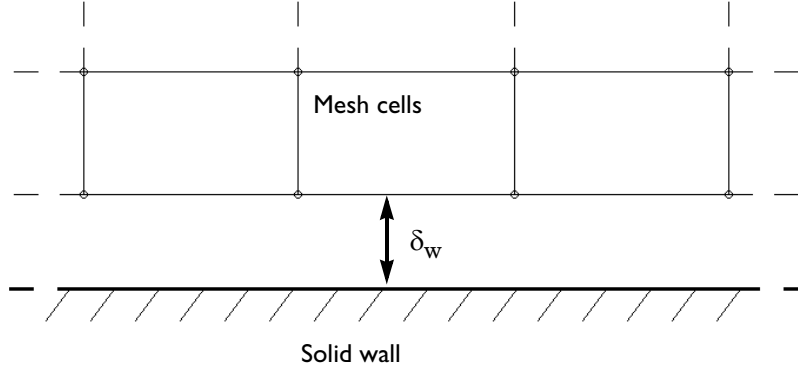


**Figure 2.8** – The wall-lift off,  $\delta_w$  (m), is defined as the distance between the (solid) wall and where the mesh cells (computational domain) start. Wall functions are used in this regime. Adapted from [54].

the wall lift-off in viscous units,  $\delta_w^+$ , becomes 11.06. Therefore, the optimal value for  $\delta_w^+$  is 11.06.  $\delta_w$  is limited from below so that it never becomes smaller than half of the height of the boundary mesh element. Because  $\delta_w^+$  is a linear function of  $\delta_w$ , this implies that, if the mesh is too coarse,  $\delta_w^+$  can become higher than 11.06.  $\delta_w^+$  should be 11.06 on most of the walls. If  $\delta_w^+$  is much higher ( $>100$ ) over a significant part of the walls, the accuracy might be compromised [54]. Subsequently, to verify the quality of the mesh, both wall lift-off and wall lift-off in viscous units should be plotted after running a simulation. The value of wall lift-off should be small compared to the dimensions of the geometry, while the wall lift-off in viscous units should be 11.06 on most of the walls.

Finally, the mesh should be refined until the solution does not change. This is called the mesh refinement technique and will give further insight in the quality of the mesh. Once the solution does not further change, your mesh is sufficient [53].

## 2.2.6 Solvers

COMSOL Multiphysics uses two kinds of solvers, namely direct and iterative. Based on the amount of mesh elements and the degrees of freedom, COMSOL automatically determines the best solver for the model. Therefore, in this research, solvers are not treated in detail. Several examples of solvers COMSOL applies are given below.

The direct solvers are MUMPS, PARDISO and SPOOLES. It is irrelevant which one is chosen since they will all converge to the same solution. They differ primarily in relative speed. All direct solvers occupy a lot of memory [55].

The second type of solvers are iterative solvers. The big advantage of iterative solvers is their memory usage, which is significantly less for the same problem compared to a direct solver. The biggest issue considering iterative solvers is the convergence.

Different physics require different solver settings, depending on the governing equations being solved [55].

## Chapter 3

# Computational Fluid Dynamics setup

This chapter describes the setup of the CFD simulations done in COMSOL Multiphysics. The first part describes the setup for the closed incubator while the second part describes the setup for the opened incubator. Two incubators, the GE Giraffe Carestation and the Dräger Caleo<sup>TM</sup>, are used for the experiments (see chapter 4). Because there is no specified outlet in the GE Giraffe Carestation (see section 4.2.2), simulating this incubator becomes practically impossible. This is due to the fact that the exact number, locations and size of the outlets is unknown. The Dräger Caleo<sup>TM</sup> has specific outlets. Therefore, the Dräger Caleo<sup>TM</sup> is used in all simulations.

### 3.1 Closed incubator

This section describes the setup and settings of the closed incubator model. First, the geometry of the model will be explained. Secondly, the material properties of the air, incubator and neonate are given. Thirdly, the different physics modules of the model, including the boundary conditions, are described. Finally, the model discretization, mesh, modelling scenarios and solution procedure will be treated.

#### 3.1.1 Geometry of the model

The geometry of the closed incubator is shown in Figure 3.1. The inlets, outlets and neonate are highlighted by arrows. The incubator has eight inlets, four on each side, and six outlets, three on each side. Since the incubator is symmetric, only half of the geometry is used to compute the solution. This will reduce the computation time. The halved geometry is shown in Figure 3.2. The symmetry plane is highlighted in blue. A more detailed overview of the geometrical data of the incubator is given in Table 3.1. The data is provided by Dräger [56].

The neonate is modelled by using a sphere mimicking the head, a block mimicking the body and four cylinders mimicking the arms and legs. The surface areas, dimensions and skull circumference are all based on measurements done by our own NICU department on neonates weighing 1 kg. Neonates weighing 1 kg are common within the NICU. A table of the physical and thermophysiological properties of the modelled neonate is given in Table 3.2.

**Table 3.1** – Geometrical data of the incubator. Data provided by Dräger [56].

Parameter	Value
Length Incubator	73 cm
Width Incubator	50 cm
Height Incubator	40 cm
Thickness Incubator Walls	0.9 cm
Length Inlet	12.1 cm
Width Inlet	2.3 cm
Length outlet	8.7 cm
Width outlet	0.8 cm

**Table 3.2** – Geometrical and physiological data of the neonate. Based on measurements performed by our own NICU department.

Parameter	Value
Total length	37 cm
Skull circumference	25 cm
Back length	20 cm
Arm length	14 cm
Leg length	16 cm
Skin area	0.105 m <sup>2</sup>
Weight	1 kg
Postnatal age	1 day
Gestational age	28 weeks

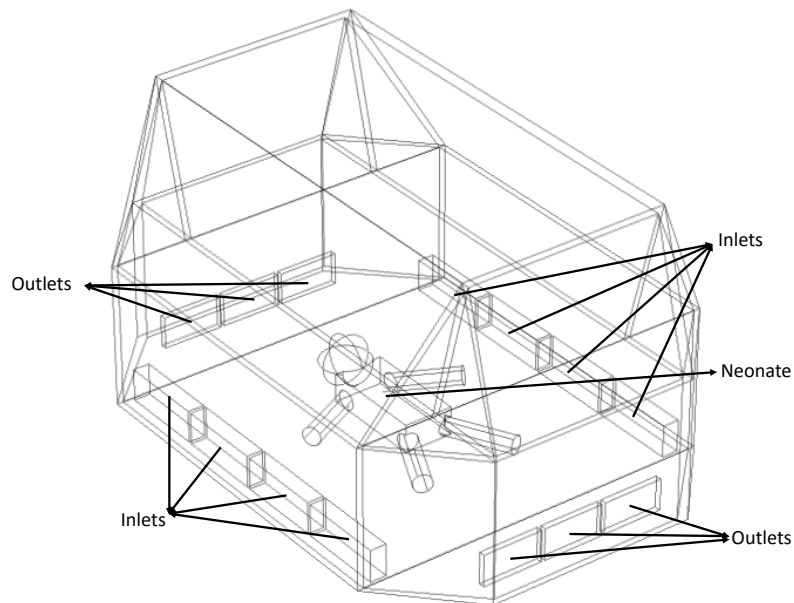


**Figure 3.1** – Geometry of the Dräger Caleo<sup>TM</sup>. This geometry represents the closed incubator. The inlets, outlets and neonate are highlighted by the arrows.

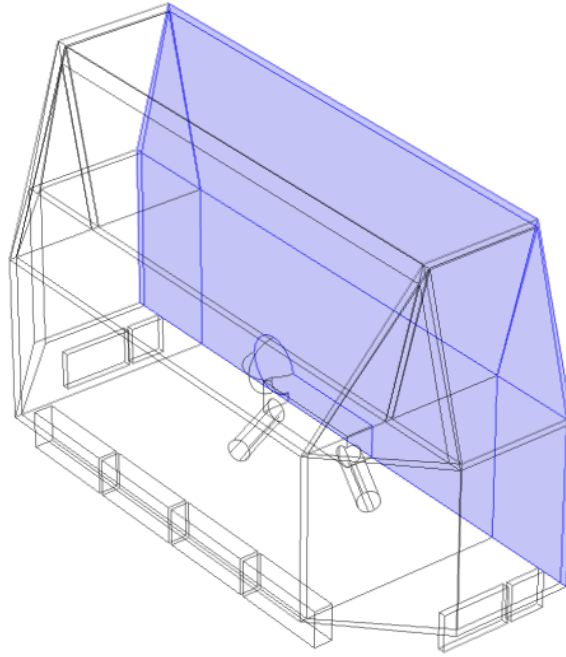


**Figure 3.2** – Geometry of the Dräger Caleo™ which is used for the CFD simulations. It is similar to the geometry in Figure 3.1 except that this geometry is cut in half due to symmetry. This will reduce the computation time. The symmetry plane is highlighted in blue.

### 3.1.2 Material properties of the model

The model consists out of three materials, namely the neonate, air and plexi glass (incubator walls). For air, COMSOL Multiphysics has inbuilt material properties. They are dependent on variables such as temperature and pressure. The neonate’s body as well as the plexi glass’ material properties are user defined. They are shown in Table 3.3.

**Table 3.3** – Material properties of the neonate and the plexiglass. Data provided by Ginalski et al [45] and Cengel [57].

<i>Neonate</i>		
<b>Property</b>	<b>Physical quantity</b>	<b>Value</b>
Heat capacity at constant pressure	$C_p$	3391 J/(kg·K)
Density	$\rho$	1109 kg/m <sup>3</sup>
Thermal conductivity	$k$	0.37 W/(m·K)
Surface emissivity	$\epsilon$	0.95
<i>Plexi glass</i>		
<b>Property</b>	<b>Physical quantity</b>	<b>Value</b>
Heat capacity at constant pressure	$C_p$	1000 J/(kg·K)
Density	$\rho$	1700 kg/m <sup>3</sup>
Thermal conductivity	$k$	0.14 W/(m·K)
Surface emissivity	$\epsilon$	0.9 <sup>1</sup>

<sup>1</sup>Emissivity is strongly dependent on wavelength. The emissivity of 0.9 corresponds to a wavelength of  $\lambda = 2 - 5.6 \mu\text{m}$  [58].

### 3.1.3 Physics of the model

Three different physics modules are used in the model. A flow module is used to compute the velocity profile of the air, a heat transfer module is used to calculate the temperature distribution and a transport of diluted species module is used to compute the relative humidity distribution.

The flow is assumed to be stationary. This is an adequate assumption because in all simulations the temperature differences within the incubator are small ( $\approx 0.1-1$  °C). Therefore, density effects are small and are neglected. On top of that, assuming the flow is stationary also reduces the complexity of the model and the computation time.

#### 3.1.3.1 Flow module

COMSOL Multiphysics offers several flow modules. In section 2.2.3 it is calculated that the Reynolds number for an incubator is given by  $Re \approx 2.5 \cdot 10^4$ . Therefore, a turbulence model has to be used to compute the fluid flow.

The turbulence model chosen for the simulations is the  $k - \epsilon$  model. First of all because it is the most commonly used turbulence model worldwide, because of its relatively good convergence and relatively low memory requirements. Secondly, because Ginalski et al [45] used the  $k - \epsilon$  model for their simulations. It is beyond the scope of this research to determine which turbulence model suits best for this specific model.

There are several boundary conditions within the flow module. First of all, all initial values are set to 0. This means the initial velocity field is given by  $\mathbf{v} = (v_x, v_y, v_z) = (0, 0, 0)$  m/s and the initial pressure is set to  $p = 0$  Pa.

The first boundary condition is defined as inlet at every inlet of the incubator. The velocity at the inlet is given by  $\mathbf{v} = (0, 0, 0.41)$  m/s [45], which is perpendicular to the inlet's surface, pointing upwards.

The second boundary condition involves adding the outlet boundary condition at every outlet of the incubator. A generic used approach to do this is by setting a pressure boundary condition of  $p = 0$  Pa [45].

The final boundary condition is the symmetry constraint. It is assigned to the whole symmetry plane.

The boundaries not used for any user-applied boundary conditions are automatically set to walls. This implies that COMSOL uses in-built wall functions to calculate the velocity profile near these walls.

#### 3.1.3.2 Heat transfer module

The heat transfer module consists out of two parts. Heat transfer in solids is applied to the plexi glass and the neonate while heat transfer in fluids is applied to the air domain.

Heat transfer in solids is governed by two heat transfer mechanisms. First of all, COMSOL calculates heat transfer through conduction. It is known from section 2.1.7 that the conductive heat transfer between the infant in contact with the air and the mattress is small. However, there is conduction within the neonate and plexi glass. The second heat transfer mechanism which is involved in heat transfer in solids is radiation. The boundary conditions concerning radiation are given by diffuse surface and diffuse mirror boundary conditions. Diffuse surface boundary are COMSOL's default boundary condition for radiation if  $\epsilon \neq 0$  [59]. Diffuse mirror boundary conditions are used if the boundary does not participate in the radiative heat transfer. It provides the model with information with which boundaries should be included when

computing radiation. The first diffuse surface boundary condition is applied to the inner walls of the incubator while the second diffuse surface boundary condition is applied to the neonate’s skin. A diffuse mirror boundary condition is assigned to the bottom surface of the incubator, because it does not participate in the radiative heat transfer.

Heat transfer in fluids is governed by convection. The output of the flow field which is computed by the flow module is applied as input for the heat transfer module.

The initial temperature values depend on the simulation scenario. The neonate’s initial temperature is given by  $T_{0,baby}$ . The initial temperature of the air and plexi glass is set to  $T_{0,incubator}$ .

Other boundary conditions include a heat flux, a heat source, a temperature constraint and a symmetry boundary condition. The heat flux is applied to the external boundaries of the incubator and computes the convective heat transfer between the incubator and the (NICU) environment. The external temperature is set to  $T_{NICU} = 25^{\circ}\text{C}$  and the convective heat transfer coefficient is given by  $h_{ext} = 0.19 \text{ W}/(\text{m}^2\cdot\text{K})$  [45]. It is assumed the external NICU temperature is constant. A heat source,  $Q_{baby}$  (W), is added to the domain of the baby to mimic the metabolic heat production. Equation 2.14 is used to determine the value of  $Q_{baby}$ . The temperature boundary condition is applied to the inlets to give the air at the inlets the desired temperature. The temperature is set to  $T_{air}$ . Finally, the same symmetry constraint is used as in the previous section. The remaining boundaries not used for user-applied boundary conditions are automatically set to thermally insulated. This implies that no heat is allowed to pass through these boundaries.

### 3.1.3.3 Transport of diluted species module

The final physics module is transport of diluted species, which is only implemented in the air domain. It is used to calculate the humidity of the air. The velocity field from the flow module is used as input for the transport of diluted species module to compute the humidity.

The concentration of water vapour  $c$  ( $\text{mol}/\text{m}^3$ ) is computed by the transport of diluted species module. The module does not compute the relative humidity, but it is more convenient to use relative humidity as in- and output of the model. Therefore, several equations are used to calculate the concentration from the relative humidity, and visa versa. For an overview of how these calculations are done, see Appendix A.

There are multiple boundary conditions applied to the model. The initial value for the concentration is set to  $c_0$  ( $\text{mol}/\text{m}^3$ ). An inflow boundary condition is applied to the air inlets. The inflow’s value is  $c_{in}$  ( $\text{mol}/\text{m}^3$ ). The outlets’ boundary condition is an outflow, which implies that concentration is allowed to pass through these boundaries. Similar to the previous two physics modules, a symmetry boundary condition is applied to the symmetry plane. Finally, all boundaries not used for user-applied boundary condition are automatically constrained with a no flux boundary condition. This implies that no concentration is allowed to pass through these walls.

### 3.1.4 Model discretion and mesh

This section describes the model discretization and meshing of the model.

COMSOL's blog [51] warns users for using conjugate heat transfer with fluid flow. Conjugate heat transfer is an interface that is composed of two physics interfaces: heat transfer in solids and heat transfer in fluids. COMSOL's default choice for solving fluid velocity and pressure fields within the flow module is by using linear elements. COMSOL's default choice for solving the temperature distribution is by making use of linear elements as well. However, if heat transfer in solids is selected as the heat transfer interface and the heat transfer in fluids interface is manually added, COMSOL will automatically use quadratic elements for the temperature field in the fluid domain. This is not advised by COMSOL [51], so the element order in the fluid domain was manually set to linear. In total this means every physics module is solved using linear elements.

The mesh of the model is user-defined. COMSOL has an in-built option to build a physics controlled mesh. However, as explained in section 2.2.5, using in- and outlets combined with turbulent flow requires careful meshing.

The meshing of the in - and outlets is done as follows: First of all, the boundaries of the in- and outlets are meshed with a triangular mesh. It is recommended to have at least 10 cells across the in- and outlets [53]. Therefore, the element size is customized in such a way that the number of elements across the in- and outlets is 11, which meets the requirement of at least 10. The in- and outlet's boundaries are then swept across the domain of the in- and outlets. Next, boundary layers are added because of the strong gradients near the walls. Finally, all boundary elements are converted by inserting a diagonal edge to connect the 2D triangular mesh to the 3D tetrahedral mesh.

The mesh of the neonate's skin is important because the heat transfer which place on these boundaries can be used to calculate the neonate's body temperature. The neonate's boundaries are meshed with a triangular mesh. The size is not custom defined, but set to 'extremely fine', calibrated for general physics, which is a drop down menu in COMSOL. A screenshot of the drop down menu is given in Figure 3.3. Other options in the drop down menu are fluid dynamics, plasma and semiconductor. Because heat transfer is the only physics of importance on the neonate's body surface, it is calibrated for general physics. The remaining geometry is meshed with tetrahedra. The size is set to normal, calibrated for fluid dynamics.

An overview of all mesh steps and their accounting number of elements is given in Table 3.4. The corresponding Figures are shown in Figures 3.4 and 3.5. The Figures showing mesh step 2 and 3 have been left out because they are indistinguishable from Figure 3.4b.

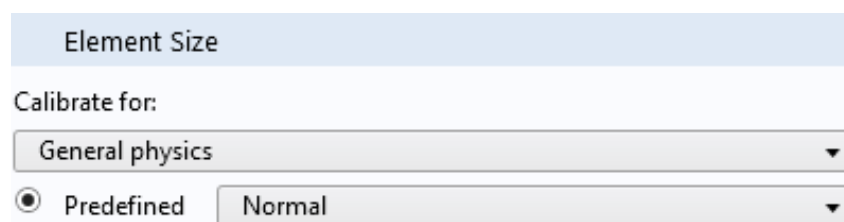
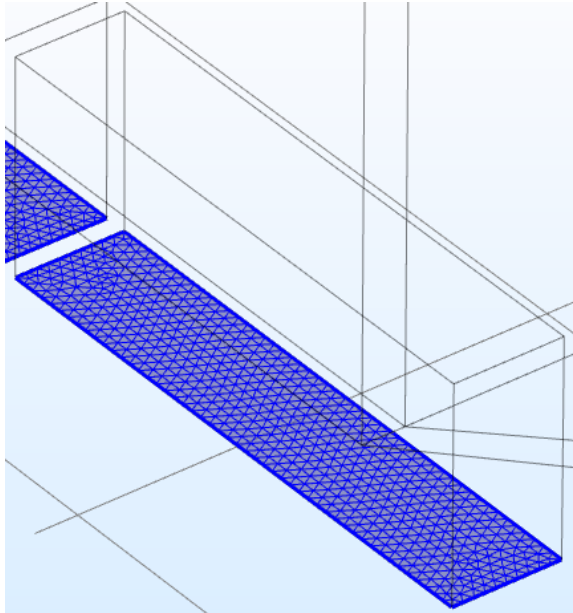


**Figure 3.3** – Screenshot of COMSOL's drop down menu to set the element size. The predefined size, as well as the calibration for the type of physics, can be chosen.

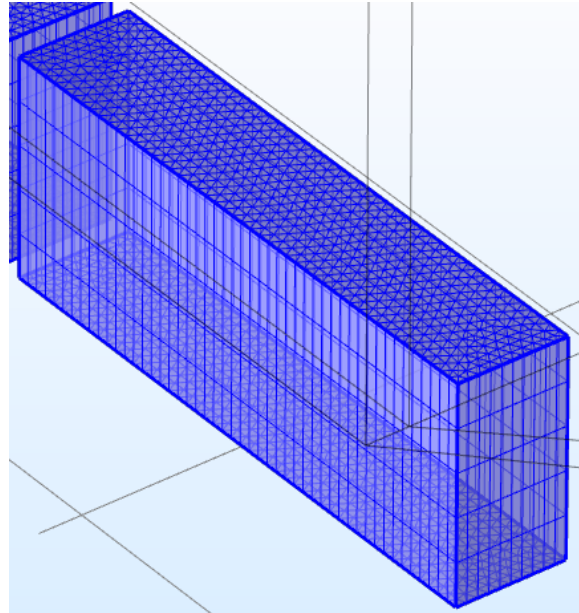


**Table 3.4** – Meshing steps for the incubator. Figures of the meshing steps are shown in Figures 3.4 and 3.5.

Mesh step	Cumulative Total Domain elements	Cumulative Total Boundary elements	Cumulative Total Edge elements
1: Triangular in/outlets	0	5322	716
2: Swept across domain in/outlets	26610	14224	1592
3: Adding boundary layers in/outlets	70998	14390	1592
4: Converting boundaries in/outlets	90241	17804	1592
5: Triangular on boundaries neonate	90241	26794	2465
6: Tetrahedral remaining geometry	298265	50300	3864



(a) Mesh step 1



(b) Mesh step 4

**Figure 3.4** – Mesh steps 1 and 4. Mesh step 1 involves meshing the boundaries of the in- and outlets with a triangular mesh. Mesh step 4 involves converting the boundaries of the in-and outlets with a diagonal edge so they are connected with the tetrahedral mesh. The Figures showing mesh step 2 and 3 have been left out because the Figures are indistinguishable from Figure 3.4b.

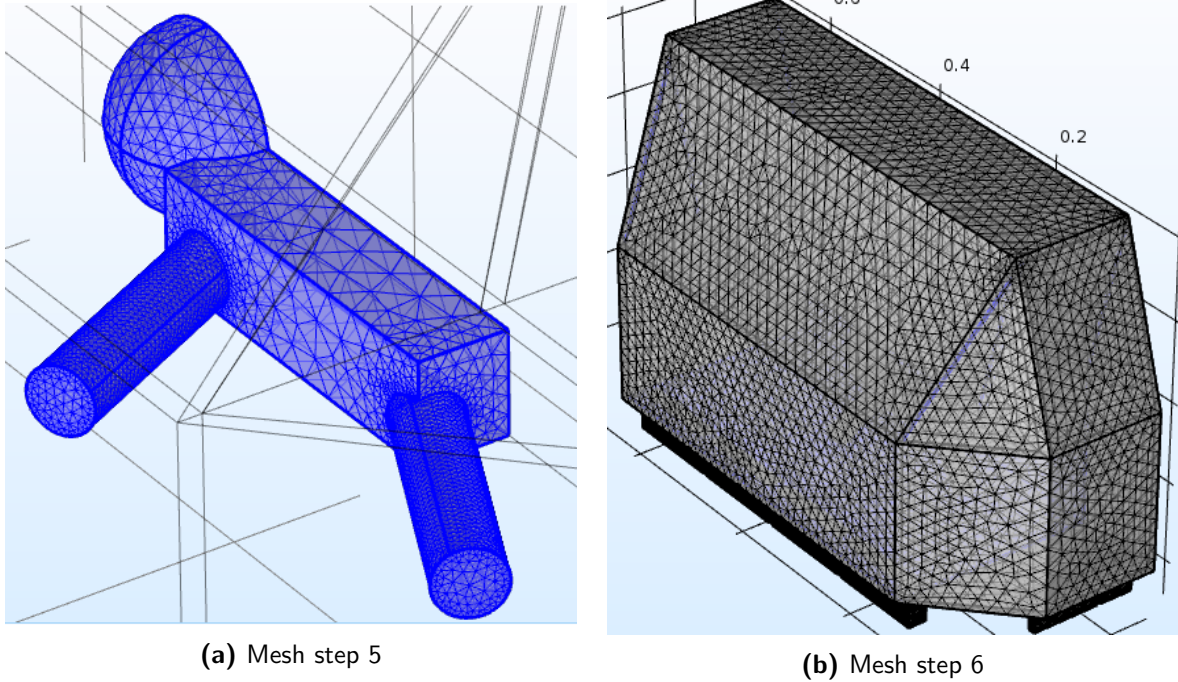


**Figure 3.5** – Mesh steps 5 and 6. Mesh step 5 is meshing the neonate’s skin with a triangular mesh. Mesh step 6 involves filling the remaining geometry with a tetrahedral mesh.

### 3.1.5 Modelling scenarios

Three different scenarios are modelled in case of the closed incubator.

Scenario 1 involves a constant incubator climate, which is set to 33°C-45%RH. It mimics a common incubator setting.

Scenario 2 mimics warming up of the neonate. The incubator is set to 36°C-70%RH and the neonate’s initial body temperature is set to 35 °C. The incubator’s climate is held constant.

Scenario 3 models the recovery of the climate after closing the incubator. Its initial values are set to 35°C-50%RH while the inlet air temperature and RH are given by 38°C-85%RH.

An overview of the different scenarios, including their model parameters and initial values, is represented in Table 3.5.

**Table 3.5** – Three different scenarios are simulated. Scenario 1 and 2 involve a constant climate, where as scenario 3 models the recovery of the climate after the incubator has been opened.

Scenario	$T_{0,baby}$	$T_{0,incubator}$	RH <sub>0</sub>	$T_{air}$	RH <sub>air</sub>
1	37 °C	33 °C	45%	33 °C	45%
2	35 °C	36 °C	70%	36 °C	70%
3	37 °C	35 °C	50%	38 °C	85%

### 3.1.6 Solution procedure

The solution procedure consists of two steps. The first step involves a stationary study and the second step a time-dependent study.

The stationary study only solves for the flow interface. It computes the velocity and pressure profile. COMSOL automatically selected the direct solver PARDISO for this study.

The time-dependent study only solves for the heat transfer and transport of diluted species. The velocity and pressure profile from the stationary study are used as input for the time-dependent study. The total time-scale of the simulations is five minutes. The time step increments are given by 5 seconds. This implies that the solution is computed every five seconds, until five minutes total is reached. The heat transfer interface is solved using the direct PARDISO solver, while the transport of diluted species interface is solved using the iterative GMRES (Generalized Minimal Residual Method) solver. These solvers are automatically selected by COMSOL.

## 3.2 Opened incubator

This section describes the settings and setup for the opened incubator model.

### 3.2.1 Geometry of the model

The geometry of the model is mostly similar to the closed incubator, except for the portholes and symmetry. Portholes are lids that can be opened for nursing procedures or parental care. A porthole has a length of 19.1 cm and a height of 12 cm. The thickness is equal to the incubator's thickness and is equal to 0.9 cm. The other difference is the symmetry plane. Due to the addition of the portholes, the symmetry plane has disappeared. The geometry of the opened incubator is shown in Figure 3.6. The portholes are highlighted in blue.

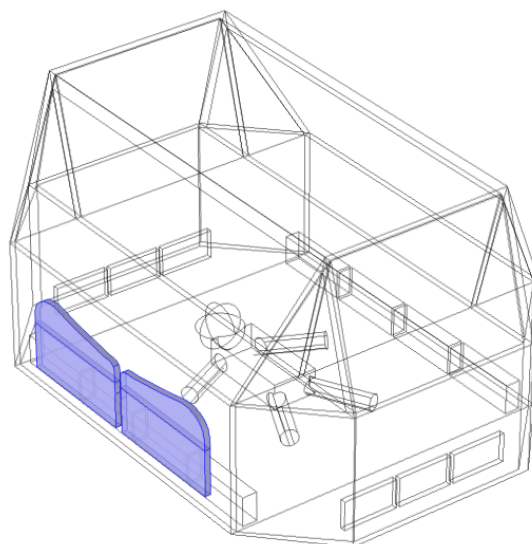


**Figure 3.6** – Geometry of the opened incubator. It is equal to the geometry of the closed incubator except that two portholes are added. The portholes' domains are highlighted in blue. The material properties of the portholes are set to air.

### 3.2.2 Material properties of the model

The material properties of the opened incubator are nearly identical to the closed incubator, see section 3.1. The only difference is the assignment of the materials to the domains. The material air is now also assigned to the domain of the portholes because in case of an opened incubator this space is filled with air.

### 3.2.3 Physics of the model

In case of the opened incubator, an exterior boundary condition for the temperature and water vapor concentration has to be applied. Our NICU department did measurements on relative humidity in one of their NICU rooms from 9 to 16 May 2014. The results are visualized in Figure 3.7. As can be seen, fluctuations of several percent are observed in the relative humidity within seven days. No measurements of the temperature are available, but it is plausible that the temperature also does not remain completely constant over several days, but will vary around 25 °C, to which the temperature is regulated. Since the variations are quite small, the ambient temperature and relative humidity are assumed to be constant.

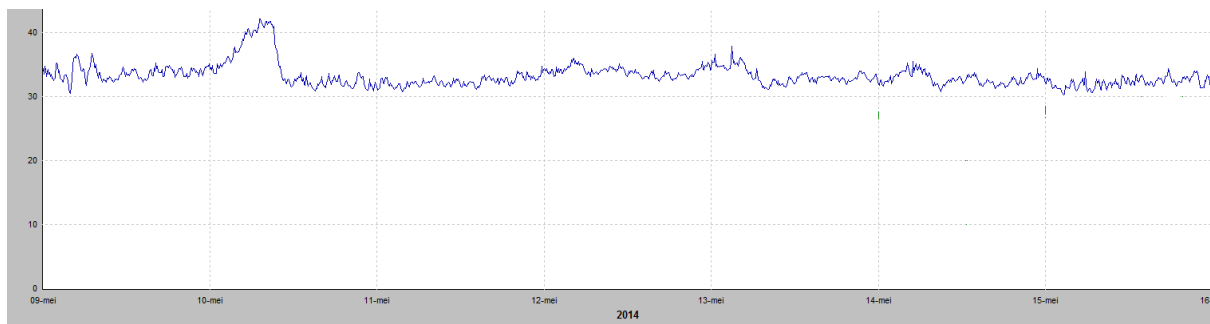


**Figure 3.7** – Relative humidity measured in one of our NICU rooms. Data was acquired from 9 to 16 May 2014. The relative humidity setpoint was 40%. Fluctuations of the relative humidity can be observed.

#### 3.2.3.1 Flow module

Two boundary conditions are added compared to the flow module of the closed incubator. The first boundary condition includes gravity. The mixing of outside air with the air inside the incubator will induce temperature differences. Temperature differences will result in density differences. Therefore, COMSOL’s inbuilt option ‘gravity’ is switched on.

Secondly, an ‘open boundary’ boundary condition is applied to the outer boundaries of the porthole domains. Air is allowed to flow in or out through the open boundary. COMSOL automatically calculates whether air will flow through and in which direction, based on the pressure distribution.

The initial values of the velocity profile are set equal to the result of the velocity profile calculated for the closed incubator.

#### 3.2.3.2 Heat transfer module

The only difference with the heat transfer module for the closed incubator is that an extra boundary condition is added. The boundary condition ‘open boundary’ has been assigned to the outer boundaries of the portholes, with a temperature given by  $T_{NICU}$ , which is the temperature of the environment.

The initial values for the temperature field are set equal to the result of the temperature field calculated for the closed incubator.

### 3.2.3.3 Transport of diluted species module

An extra 'open boundary' boundary condition has been added to the outer boundary of the portholes. The open boundary's concentration is given by  $c = c_{NICU}$ .

The initial concentration distribution is set equal to the result of the concentration distribution of the closed incubator.

### 3.2.4 Model discretization and mesh

The model discretization is equal to the model discretization in case of the closed incubator (see section 3.1.4). This means all physics modules are solved using linear elements.

Compared to section 3.1.4, only the portholes are meshed differently. A triangular mesh is applied to the outer boundaries of the portholes. The element size is set to extremely fine, calibrated for fluid dynamics. The triangular mesh on the boundary is then swept across the domain of the portholes. The distribution of the swept meshing step is automatically chosen by COMSOL. Finally, all boundaries are converted with inserted diagonal edges to connect the mesh to the tetrahedral mesh in the rest of the geometry. The meshing steps for the portholes are schematically shown in Table 3.6. A Figure of the mesh of a porthole is shown in Figure 3.8.

**Table 3.6** – Meshing procedure for the portholes

Mesh step	Cumulative Total Domain elements	Cumulative Total Boundary elements	Cumulative Total Edge elements
1: Triangular outer boundaries portholes	0	4812	358
2: Swept across domain portholes	4812	9982	728
3: Converting boundaries portholes with diagonal edges	6172	10254	728

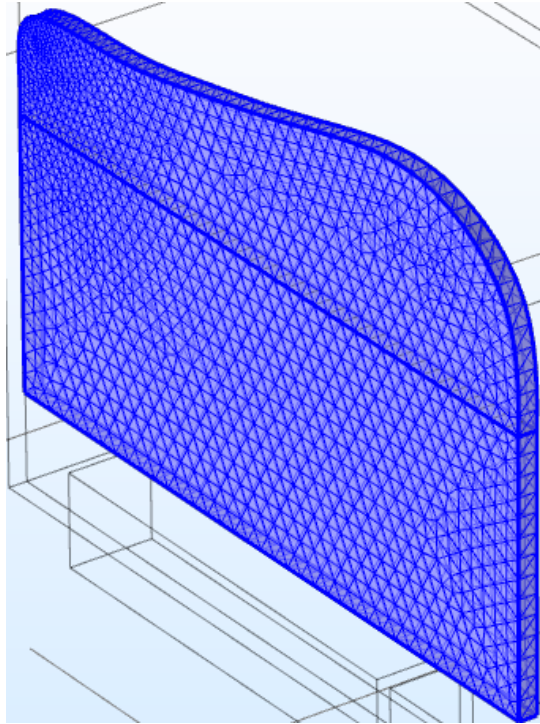


**Figure 3.8** – Mesh of a porthole. A triangular mesh on the outer boundary is swept across the domain of the porthole. The triangular mesh is then converted with inserted diagonal edges to connect the mesh to the remaining geometry's mesh.

### 3.2.5 Solution procedure

The solution procedure for solving the opened incubator includes one study step. The results of the temperature, concentration and velocity field from the closed incubator simulations are set as initial values for the opened incubator. The study step solves all three physics modules time-dependently. The same time-scale and time increments are used as for the closed incubator. The direct solver PARDISO is automatically selected by COMSOL.

## Chapter 4

# Experimental setup incubator measurements

This chapter describes the experiments done on the incubators. Two incubators are used for the experiments. The first incubator is the Dräger Caleo<sup>TM</sup>. It is chosen because Dräger was willing to provide this research with an incubator for scientific purposes. The second incubator is the GE Giraffe Carestation. This incubator is provided by our own NICU department. Both incubators are well-known and often used within neonatology.

The climate, which includes air temperature, relative humidity and surface temperature, was measured accurately at different locations inside the incubators. The first section describes the environment of the measurements. The second section addresses the incubators used for the measurements. Next, the third section provides information on the measurement procedure. The chapter ends with sections about the locations of the measurement equipment and the specifications of the measurement equipment.

### 4.1 Environment

#### 4.1.1 Neonatal Intensive Care Unit

The Neonatal Intensive Care Unit (NICU) is a controlled environment in which air temperature and humidity are set to and maintained on a certain set point. The World Health Organization recommends NICU room temperatures of at least 25 °C [4]. Currently there is no standard of care for the set point of the relative humidity (RH) in the NICU [60], however most NICU's relative humidities are between 40 and 50 %.

#### 4.1.2 Climate Chamber

The NICU ward is not a viable location to measure because most of the time the chambers are occupied. Therefore, to perform the measurements, the NICU environment was mimicked by a climate chamber. It is located at the buildings physics laboratory at the Eindhoven University of Technology. The chamber's dimensions are 5.4 m x 3.6 m x 2.7 m and air temperature ( $\pm 0.2$  °C) and relative humidity ( $\pm 3\%$ ) can be controlled.

## 4.2 Incubators

### 4.2.1 Dräger Caleo™

One of the two incubators used for the measurements is the Caleo™, which is manufactured by the German company Dräger. A photograph of the incubator is shown in Figure 4.1.

The incubator injects warmed and moisturised air into the incubator. The humidity of the air is increased by adding steam. The air is warmed by a heating element. A sensor inside the incubator measures the air temperature and humidity. The incubator controls the climate by reading out the sensor values. If the values measured by the inbuilt sensor differ from the incubator settings, the incubator responds by heating/cooling down the inlet air temperature and/or decreasing/increasing the amount of moist injected. Because the incubator uses ambient air as inlet air, the inlet's air temperature can be lowered by switching off or decreasing the power of the heating element. The relative humidity can be lowered by decreasing the amount of moist added. The air supply, or air inlet, is located at the long side of the incubator. The air exhaust, or air outlet, is located at the short side of the incubator. Part of the air escapes through narrow ventholes, which are located at all bottom corners of the incubator. The in- and outlets, as well as the location of the incubator's air temperature and relative humidity sensor, are schematically shown in Figure 4.2.

To access the neonate for nursing interventions or parental care, the Caleo™ can be opened in two ways. For smaller nursing procedures or parental care, the portholes can be used to access the neonate. For bigger interventions, such as intubation or radiologic examination, the neonate can be accessed through the accessdoor. Figure 4.3 illustrates the geometry and location of the portholes and access doors.



**Figure 4.1** – Photograph of the Caleo™ incubator manufactured by Dräger. Source: Mediproma



### Air temperature and relative humidity sensor

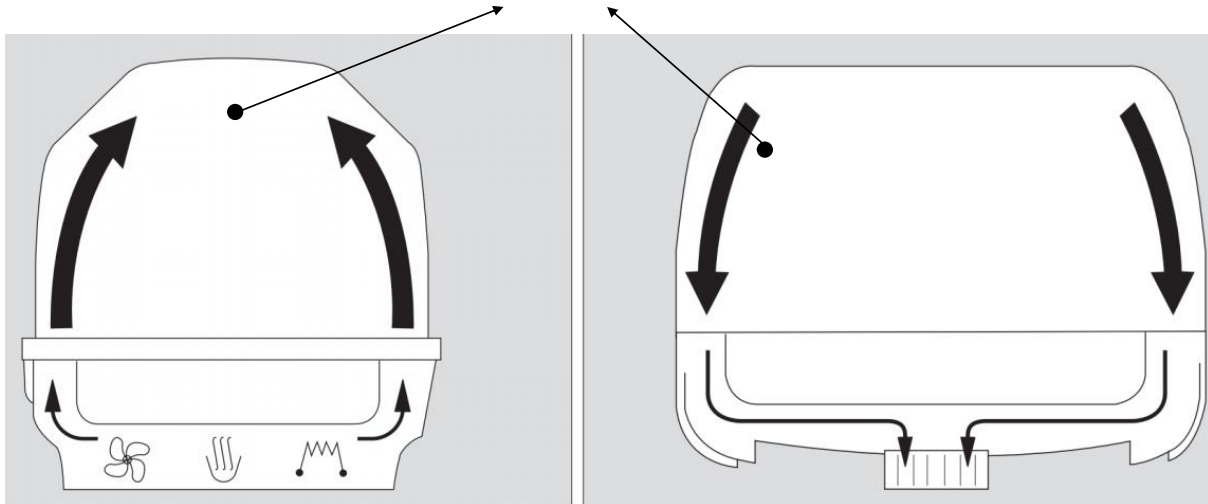


**Figure 4.2** – In- and outlets of the Caleo™ incubator. Air supply occurs at the long side, air exhaust at the short side. The in- and outlets are visualized by the black arrows. The incubator's air temperature and relative humidity sensor is highlighted by the black dots. They highlight the same sensor. Source: Dräger [56]

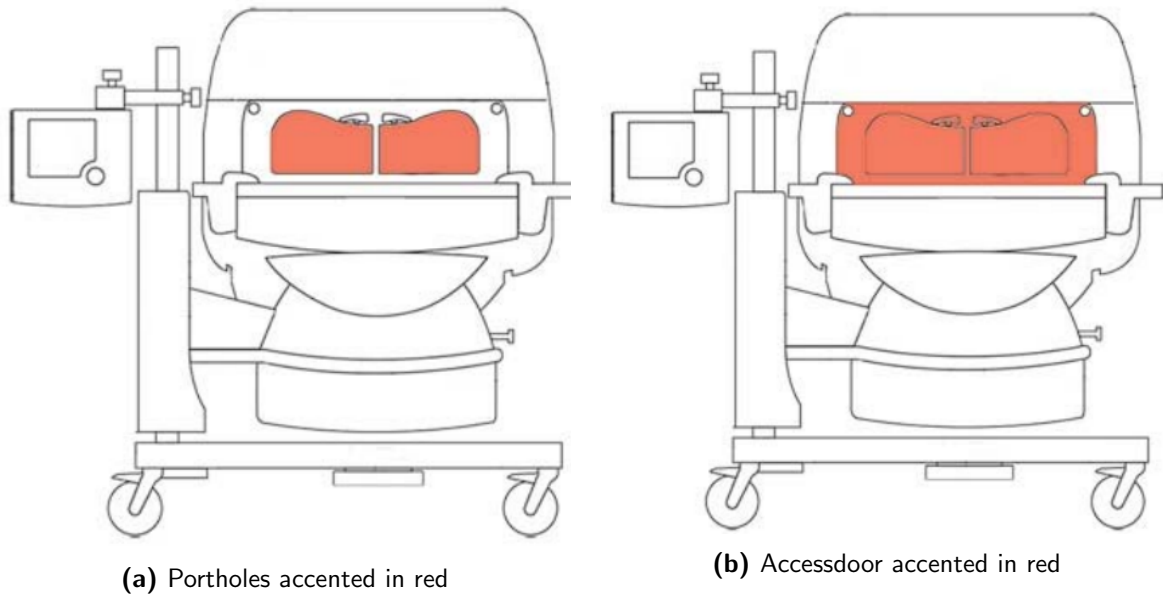


**Figure 4.3** – The neonate can be accessed through two ways. (a) Portholes, used for smaller nursing procedures. (b) Accessdoor, used for bigger interventions. The incubator which is illustrated is the Caleo™.

#### 4.2.2 GE Giraffe Carestation

The GE Giraffe Carestation incubator is the second incubator used for the measurements in the climate chamber. A photograph of the GE Giraffe Carestation is shown in Figure 4.4. The Giraffe generally acts similar to the Caleo™. The locations of the portholes and access door are equal to the Caleo™, although the portholes vary in shape. For more insight in the shape of the portholes, see Figure 4.4.

The Giraffe has two differences in lay-out and settings compared to the Caleo™. The air inlet is located at the short side of the incubator. There is no specific air outlet. There are a lot of small gaps and narrow ventholes which serve as outlet, but the exact locations are unknown. The location of the incubator's air temperature and humidity sensor is equal to the Caleo™. Figure 4.5 schematically shows the air inlets, as well as the incubator's air temperature and relative humidity sensor.

In the Giraffe, there is an extra option to activate an air curtain. The air curtain prevents environmental air from entering the incubator when the incubator is opened. During air curtain mode the inlet air speed increases by 30-35 %. All data is provided by GE.



**Figure 4.4** – Photograph of the GE Giraffe Carestation Incubator.

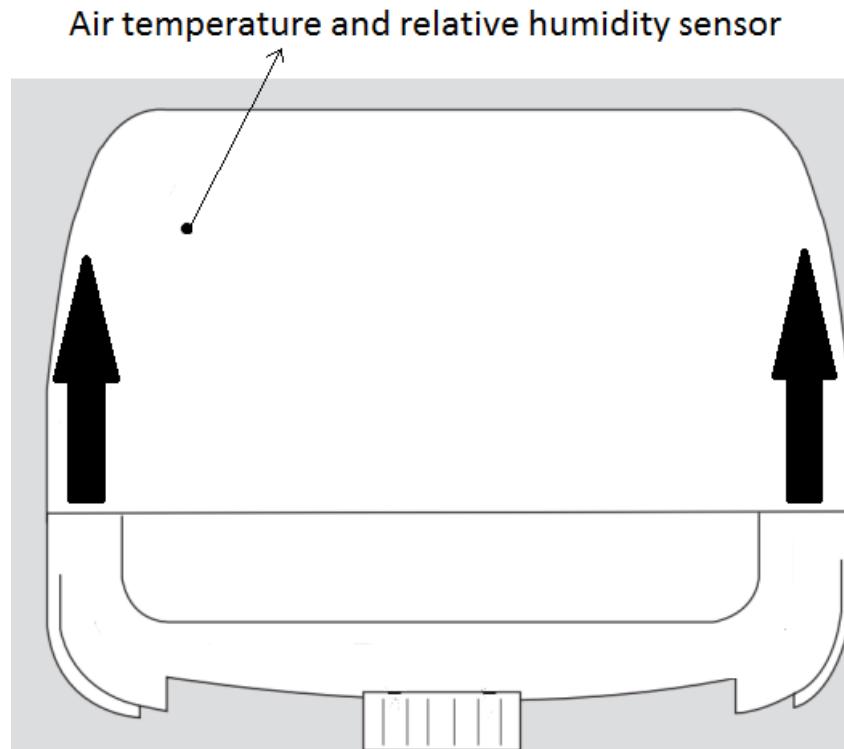


**Figure 4.5** – Inlets of the GE Giraffe Carestation incubator. The incubator’s air temperature and relative humidity sensor is highlighted by the black arrow.

### 4.3 Measurement procedure

The influence of opening the incubator on the climate inside the incubator was measured in different scenarios. In all measurements, the height of the incubators was set to 1m, measured from the mattress to the floor. This is the optimal configuration for nurses with a length of 1.70m.

The measurement schemes differ between the two incubators. This is due to the fact that the results of the performed measurements on the Caleo™ gave insight for new interesting climate scenario measurements. These new insightful measurements were performed with the Giraffe. On top of that, the measurements performed on the Caleo™ were done in collaboration with other research. This other research focuses on the climate in the NICU [61]. Therefore, several measurements involved varying the climate chamber’s climate.

#### 4.3.1 Measurement procedure Dräger Caleo™

The measurements involving the Caleo™ include two different scenarios.

In the first scenario, the climate chamber’s air temperature and relative humidity are fixed and set to 25°C-45%RH. The air temperature and relative humidity settings for the incubator are varied. The incubator is opened for five minutes, where after it is closed.

In the second scenario, the incubator’s climate is fixed and set to 36°C-70%RH. The air temperature and relative humidity’s setpoints for the climate chamber are varied. The incubator was not closed in the second scenario.

In both scenarios, all measurements are performed twice. The first measurement involves opening the portholes while the second measurement involves opening the access door.

The measurement scheme for the Caleo™ is presented in Table 4.1.

**Table 4.1** – Measurement scheme for the Caleo™. In the first three measurements the climate chamber settings are fixed and the incubator climate is varied. In the last two measurements, the incubator settings are fixed and the climate chamber settings are varied. In all five measurements the opening of the portholes and the opening of the accessdoor were measured separately.

Climate Chamber		Incubator	
Temperature	Relative Humidity	Temperature	Relative Humidity
25 °C	45%	34 °C	70%
25 °C	45%	36 °C	70%
25 °C	45%	38 °C	99%
21 °C	45%	36 °C	70%
21 °C	60%	36 °C	70%

### 4.3.2 Measurement procedure GE Giraffe Carestation

The climate chamber’s settings are fixed and set to 25°C-45%RH for all measurements performed on the Giraffe. The incubator’s temperature and relative humidity’s setpoint are varied.

All measurement are performed by opening the incubator for 15 minutes. Four different opening scenarios are measured at every setpoint. These four different opening scenarios are as follows:

- 1: Opening the portholes, air curtain switched off
- 2: Opening the portholes, air curtain switched on
- 3: Opening the access door, air curtain switched off
- 4: Opening the access door, air curtain switched on

**Table 4.2** – Measurement scheme for the GE Giraffe Carestation. The climate chamber settings are fixed in all measurements. All measurements are repeated four times, namely opening the accessdoor/portholes and switching on/off the air curtain. In all measurements, the incubator was opened for 15 minutes.

Climate Chamber		Incubator	
Temperature	Relative Humidity	Temperature	Relative Humidity
25 °C	45%	28 °C	70%
25 °C	45%	34 °C	50%
25 °C	45%	34 °C	70%
25 °C	45%	34 °C	99%
25 °C	45%	36 °C	70%
25 °C	45%	38 °C	50%
25 °C	45%	38 °C	99%

## 4.4 Locations and specifications of measurement equipment

### 4.4.1 Specifications of measurement equipment

To measure the climate inside the incubators, several types of equipment are used. Air temperature, relative humidity and surface temperature is measured at different locations inside the incubators. These are all simultaneously logged on a logger. The measurement locations are further specified in section 4.4.2.

An overview of the measurement equipment is given in Table 4.3. A more detailed description is given in Appendix B.

**Table 4.3** – Equipment used to for the incubator measurements.

Parameter	Type	Range	Accuracy
Air temperature	Pt 1000 IEC 751 Class B	-55°C - 80°C	0.05 °C
Relative humidity	INTERCAP Humidity sensor, part no. 15778	0-100% RH	3-5% RH (depending on the measured value)
Surface temperature	Grant NTC thermistor	-50°C - 150°C	0.2 °C
Data logging	Grant Squirrelview 2040	0-10 V	0.1%

### 4.4.2 Location of measurement equipment

This section describes the location of the measurement equipment. For a more detailed description, see Appendix C. The measurement locations concerning the Caleo™ and the Giraffe are identical.

In total, there are four measurement locations. Every measurement site logs different physical values. The locations and the physical values measured at that location are given by:

- 1. Location of neonate: air temperature and relative humidity
- 2. Next to incubator sensor: air temperature and relative humidity
- 3. Outside and inside of incubator hood: surface temperature
- 4. Inside porthole: surface temperature

These four positions are illustrated by photographs, presented in Figure 4.6 and Figure 4.7.

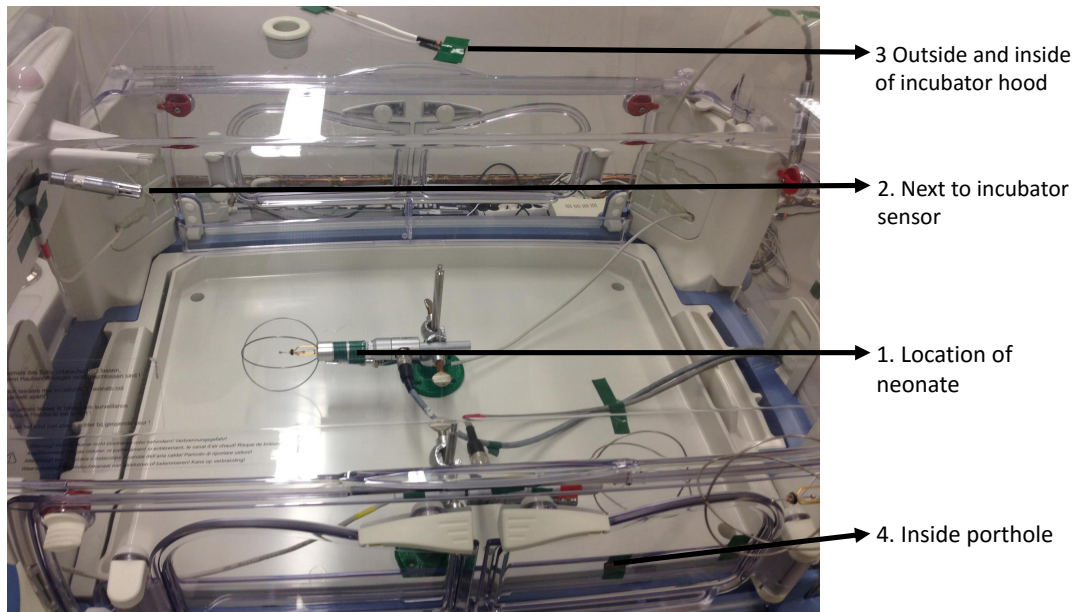


**Figure 4.6** – Photograph of the experimental setup with the Caleo™. Measurement positions on the in- and outside of the incubator hood, next to the incubator sensor, location of the neonate and on the inside of a porthole are shown.

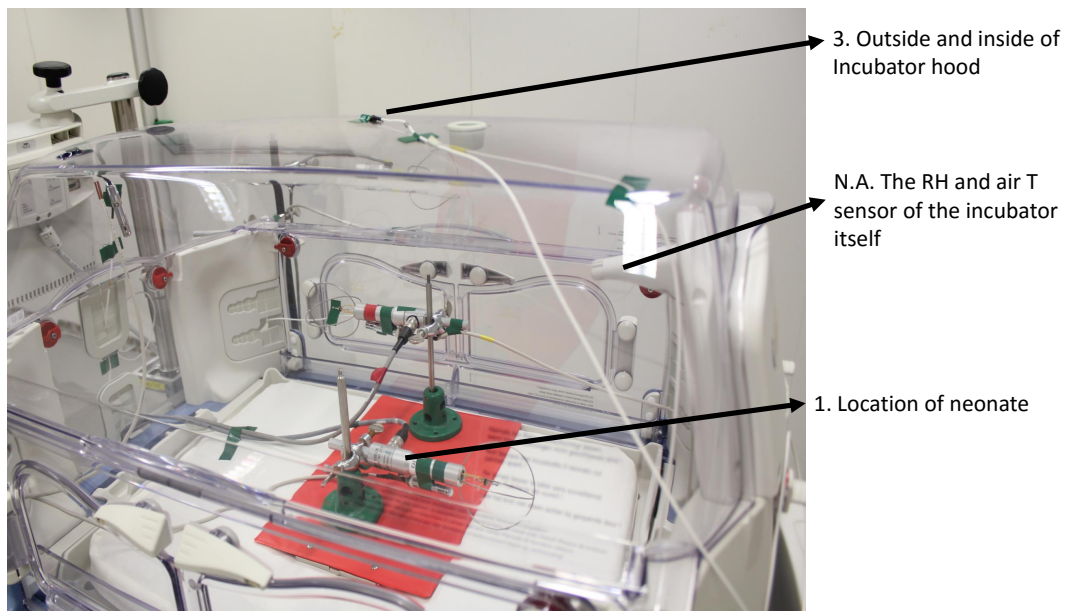


**Figure 4.7** – Photograph of the experimental setup with the Caleo™. Measurement positions on the in- and outside of the incubator hood and at the location of the neonate are shown. The inbuilt incubator sensor is pointed out as well.

## Chapter 5

# Results and discussion CFD simulations

This chapter addresses the results of the CFD simulations. The first part describes the results of the simulations of the closed incubator. The second section treats the results of the simulations of the opened incubator.

### 5.1 Closed incubator

#### Mesh Analysis

To test the model on the adequacy of the mesh, the wall lift-off in viscous units has been plotted for two different mesh types. The result is represented in Figure 5.1. Figure 5.1a shows the plot for the normal-sized mesh described in section 3.1.4, while Figure 5.1b shows the plot for a fine-sized mesh. The fine-sized mesh is equal to the normal-sized mesh, except that the remaining geometry, meshed with tetrahedra, is set to the predefined size 'fine' instead of 'normal'. The fine-sized mesh has 373930 total domain elements, 62769 total boundary elements and 4292 total edge elements where as the normal-sized mesh has 298265 total domain elements, 50300 total boundary elements and 3864 total edge elements.

Figure 5.1 illustrates that the surface plot of the wall lift-off in viscous units,  $\delta_w^+$ , is equal to 11.06 on most walls, as it should be (see section 2.2.5). In both meshes, this is the case. At the bottom of the incubator there are two relatively small regions where the values differ from 11.06. In case of the normal mesh this value goes up to 17.5 while in case of the fine mesh this value goes up to 14. Although these values are higher than 11.06, they are significantly lower than 100. Therefore, both these plots confirm an adequate mesh quality.

The second plot that tests mesh quality is a surface plot of the wall lift-off (m). It should be smaller than the typical dimension of the geometry. It is plotted for the normal-sized mesh and presented in Figure 5.2. All values are smaller than  $2 \cdot 10^{-2}$  m, which is small compared to the typical length scale. Therefore, the mesh satisfies this condition.

The final step in analysing the mesh is the mesh refinement technique. The results from the normal-sized mesh and fine-sized mesh can be compared. If no difference in results is observed, the normal-sized mesh is sufficient. The results have been compared and small differences ( $\Delta T = 0.004^\circ\text{C}$  and  $\Delta\text{RH}=0.2\%$  after five minutes) in the results were observed. Due to the computation time of the normal-sized mesh being shorter than the fine-sized mesh ( $\pm 8$  hours vs  $\pm 24$  hours), the normal-sized mesh is chosen for the remaining simulations. For a more detailed overview on the mesh refinement analysis, see Appendix D.

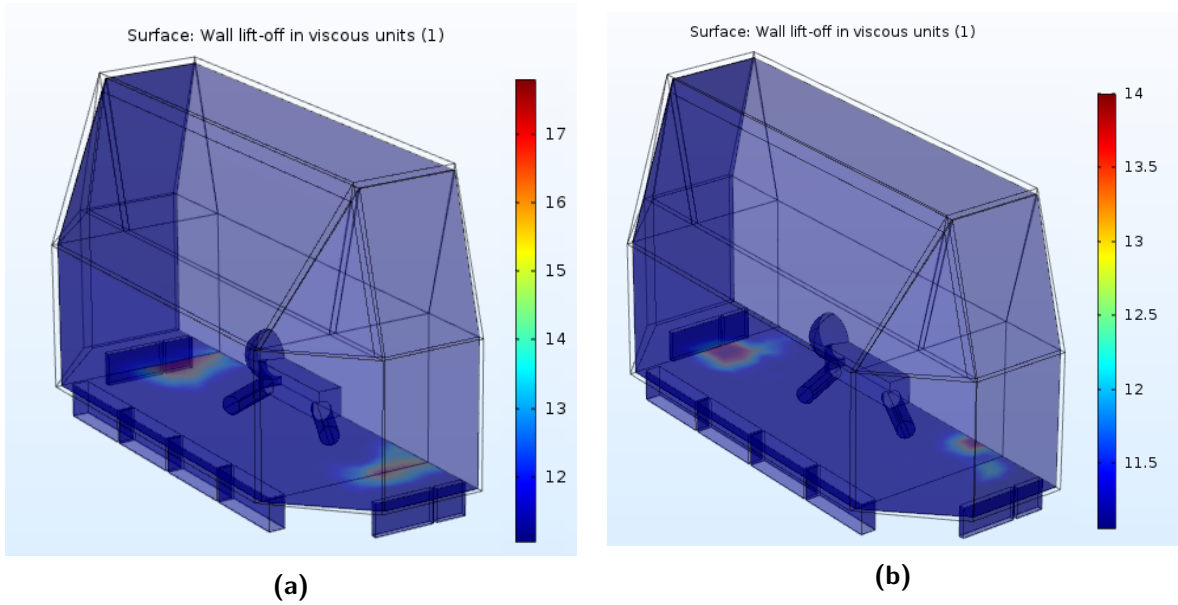


**Figure 5.1** – Wall lift-off in viscous units ( $\delta_w^+$ ) surface plot. Figure 5.1a shows the results for the normal-sized mesh. Figure 5.1b represents the results for the fine-sized mesh.

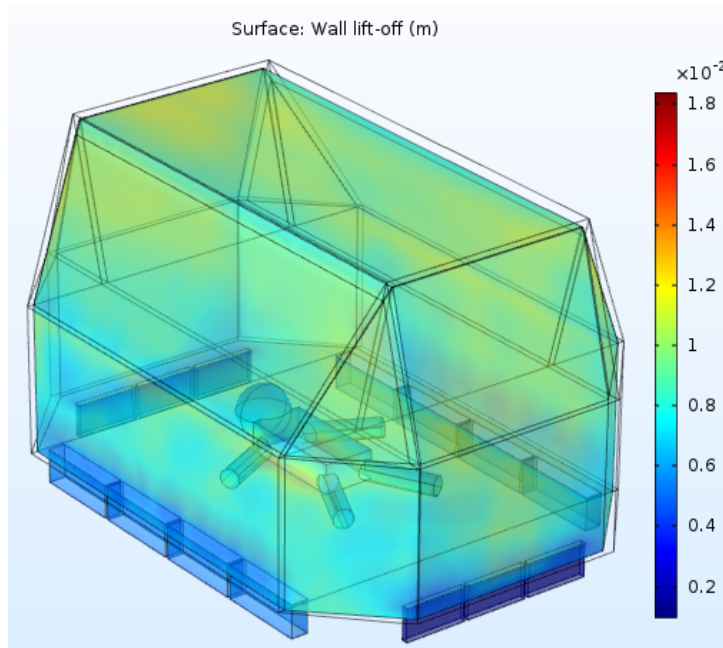


**Figure 5.2** – Surface plot of the wall lift-off ( $\delta_w$ ) for the normal-sized mesh.



## Velocity profile

The velocity profile is similar in all simulations, because it is modelled stationary. Therefore, the results obtained by one simulation apply to all simulations. The results for the velocity profile are shown in Figure 5.3.

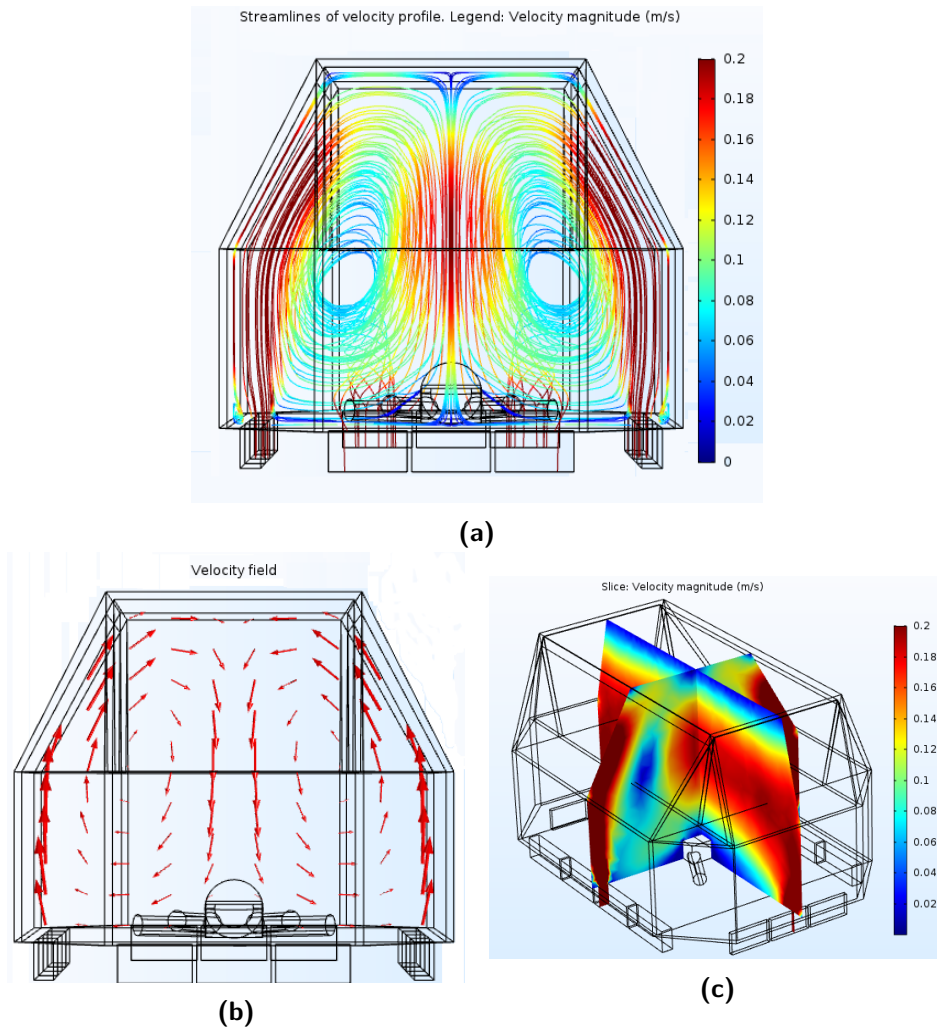


**Figure 5.3** – Results of the flow simulations. Figure (a) represents the streamlines and the corresponding velocity magnitude (m/s). Figure (b) shows the directional velocity field in an arrow plot. The length of the arrows directly relate to the velocity magnitude. Figure (c) shows two slice plots with the velocity magnitude (m/s). Note: While the inlet air speed is given by 0.41 m/s, the color map for the velocity magnitude is maximized to 0.2 m/s. This is done to better visualize the difference in velocity magnitudes.

All plots are symmetric. This is expected due to the symmetry boundary condition.

The plots show high velocities at the locations of the in/outlets as well as low ( $\pm 0.09$  m/s) velocity magnitudes near the neonate. The profile is in good agreement with Ginalski's simulated velocity profile [45].

### 5.1.1 Scenario 1: Incubator setpoint 33°C - 45% RH

#### Temperature and relative humidity distribution

The temperature distribution is not simulated stationary and thus depends on time. In case of the closed incubator, temperature variations are small because there is no interaction with the air from the environment. Therefore, the distribution of temperature occurs due to the environment cooling the outside wall of the incubator, the neonate and the incubator transferring radiative heat, the metabolic heat production of the neonate and the convective heat transfer between the neonate and the air. The incubator's initial value is set to  $T_0 = 33^\circ\text{C}$  and the air inlet is set to  $T_{air} = 33^\circ\text{C}$ . The neonate's initial temperature is set to  $T_{0,baby}=37^\circ\text{C}$  and its weight is 1 kg. A representation of the temperature distribution as function of time is shown in Figure 5.4.

The color map legend has a minimum of  $32.8^\circ\text{C}$  and a maximum of  $33.2^\circ\text{C}$ , which is a small range. The reason for this is because variations in temperature are small. Due to the color map legend's range being small, it seems as if the air temperature next to the neonate is equal to the neonate's temperature in Figure 5.4b to 5.4b. This is not the case. The air temperature next to the neonate is given by  $\approx 33.2^\circ\text{C}$  while the neonate's temperature is  $\approx 37^\circ\text{C}$ .

As time progresses, the wall temperature remains constant. Apparently the radiative heat transfer between the baby and the walls is in balance with the convective heat transfer between the walls and the environmental air. A small increase in air temperature of  $\approx 0.1^\circ\text{C}$  is observed, which is caused by the convective heat transfer between the neonate's skin and the air.

The relative humidity is time dependent as well. Similar to the temperature distribution, relative humidity also has a small range of variation, due to the air not being in contact with environmental air. The time-dependent relative humidity distribution is presented in Figure 5.5.

A small decrease of  $\approx 1\%$  RH can be observed after 1.5 minute. The RH remains constant in the remaining 3.5 minutes. The decrease is caused by the high outflow of water vapor concentration at the outlets. The RH at the outlets is given by  $\approx 47\%$ .

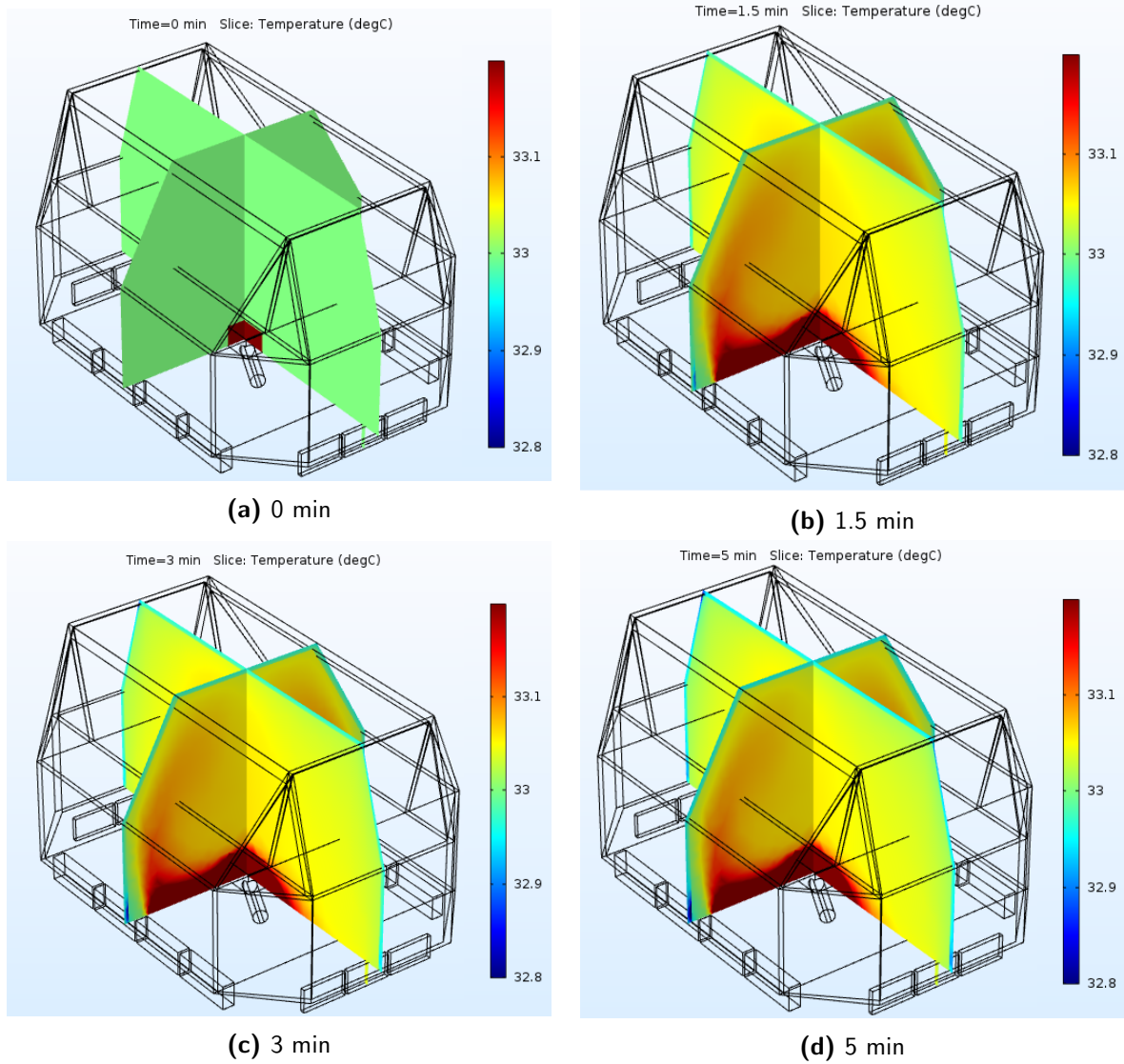
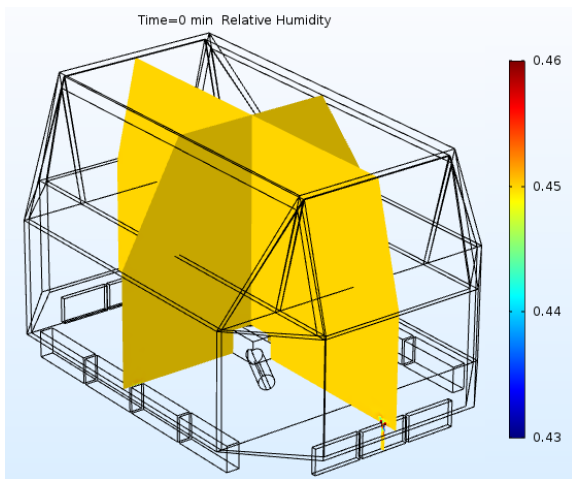
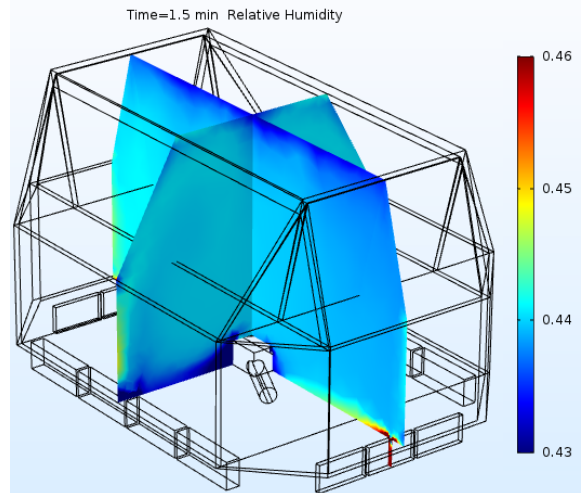


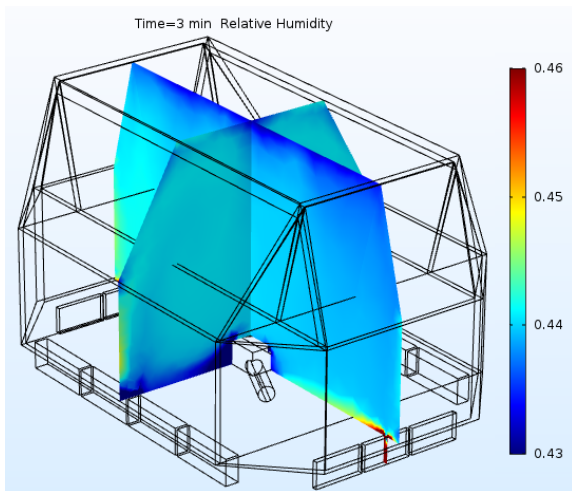
**Figure 5.4** – Slices of the temperature distribution ( $^{\circ}\text{C}$ ) as function of time for the incubator setpoint  $33^{\circ}\text{C}$ -45%RH. Figure (a) shows the distribution at  $t=0$  min, Figure (b) at  $t=1.5$  min, Figure (c) at  $t=3$  min and Figure (d) at  $t=5$  min.



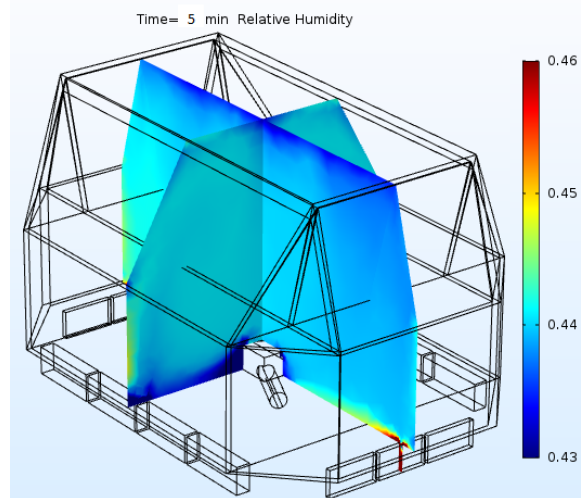
(a) 0 min



(b) 1.5 min



(c) 3 min



(d) 5 min

**Figure 5.5** – Slices of the relative humidity distribution as function of time for the incubator setpoint 33°C-45%RH. Figure (a) shows the distribution at t=0 min, Figure (b) at t=1.5 min, Figure (c) at t=3 min and Figure (d) at t=5 min.

## Convective, radiative and evaporative heat flux

COMSOL is able to calculate the convective and radiative heat flux after computing the model. Unfortunately, COMSOL is not able to directly calculate the evaporative heat loss from the RH. Therefore, evaporative heat loss has to be calculated manually using equation 2.10. Because the temperature and relative humidity remain nearly constant ( $\pm 0.1^\circ\text{C}$  and  $\pm 1\%$  RH) throughout the time-dependent simulation, it is redundant to show time-dependent plots of the convective and radiative heat flux. Therefore, the average over time is plotted. The result is shown in Figure 5.6.

The convective heat transfer plot shows cooling only. Some spots on the neonate's body surface suffer from higher cooling. The plot shows a significant amount of local peaks and dips. This is caused by the relatively high differences in air velocity in the air surrounding the neonate.

The radiative heat transfer shows much less local peaks and dips. This is due to the fact that radiative heat transfer is not related to air velocity, but depends on the incubator inner wall's temperature distribution. Since the inner wall's temperature distribution is nearly constant, the surface plot is very smooth.

It is interesting to compute the average convective heat flux and average radiative heat flux across the surface of the infant, separately. The convective and radiative heat flux can also be calculated manually by using equations 2.3 and 2.7. To calculate the heat fluxes manually, the average air temperature around the neonate, the average inner incubator wall temperature and the average skin temperature have to be known. These are extracted from the model results. The average air temperature around the neonate, computed by the model, is given by  $33.1^\circ\text{C}$ , the average incubator (inner) wall temperature is given by  $33.0^\circ\text{C}$  and the average skin temperature is given by  $36.0^\circ\text{C}$ .

The average convective heat transfer, calculated by the model, is equal to  $-24\text{ W/m}^2$  and the convective heat transfer calculated manually is equal to  $-15.7\text{ W/m}^2$ . The difference might be caused by a mismatch in the convective heat transfer coefficient used for the calculations and the convective heat transfer coefficient used by COMSOL. Unfortunately, the heat transfer coefficient COMSOL uses is not visible. Therefore, further research on the correct heat transfer coefficient is required.

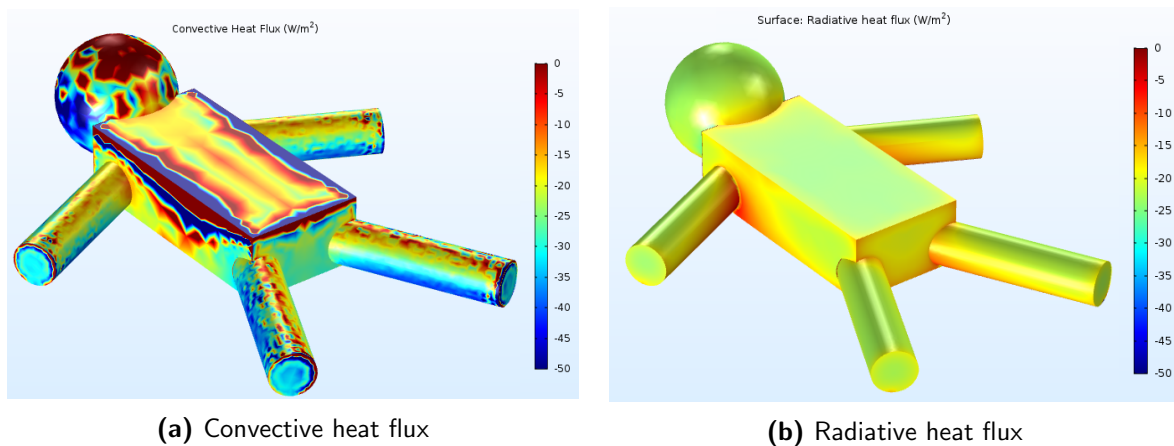


**Figure 5.6** – Time-averaged convective (a) and radiative (b) heat flux surface plots for scenario 1: incubator setpoint  $33^\circ\text{C}$  - 45% RH.

The average radiative heat flux, calculated by the model,  $-13.5 \text{ W/m}^2$ . The radiative heat flux, calculated manually, is  $-13.2 \text{ W/m}^2$ . These results are in good agreement.

The average RH around the neonate computed by the model is 44%. Because the evaporative heat loss strongly depends on the TEWL, which in turn strongly depends on gestational and postnatal age, the impact of the relative humidity on the infant depends on the infant. The evaporative heat loss can be calculated using equation 2.10.

### 5.1.2 Scenario 2: Incubator setpoint $36^\circ\text{C}$ - 70% RH

The second scenario that is simulated involves warming up the neonate. Assume a cooled down neonate who's body temperature initially is given by  $35^\circ\text{C}$ . The incubator is set  $36^\circ\text{C}$ -70% RH. The temperature and relative humidity distributions are similar to Figure 5.4 and 5.5 and thus not insightful enough to display here. Therefore, they are represented in Appendix E.

#### Convective, radiative and evaporative heat flux

The (time-averaged) convective and radiative heat transfer plots are represented in Figure 5.7.

The resulting Figures are similar to Figure 5.4 and 5.5, except that the color map legends are different. Therefore, it is insightful to calculate the average convective heat transfer and radiative heat transfer across the neonate's surface. Similar to scenario 1, they are calculated by COMSOL, and manually by using equation 2.3 and 2.7. To calculate the convective and radiative heat transfer manually, several physical values are extracted from the model. The average air temperature around the neonate is given by  $35.9^\circ\text{C}$ , the average (inner) wall surface temperature by  $35.9^\circ\text{C}$  and the average skin temperature by  $35.6^\circ\text{C}$ .

The average convective heat transfer across the infant's body surface, calculated by COMSOL, is given by  $+3.4 \text{ W/m}^2$ . Manual calculations compute the average convective heat transfer as  $+1.6 \text{ W/m}^2$ . Similar to the previous section (5.1.1), this mismatch might be caused by a difference in the convective heat transfer coefficients between the calculations done by COMSOL and the manual calculations.

The average radiative heat transfer should be positive, due to the incubator walls having a higher temperature than the neonate's skin. Manually calculating the average radiative heat transfer gives  $+1.3 \text{ W/m}^2$ . It is relatively small because the difference between the neonate's

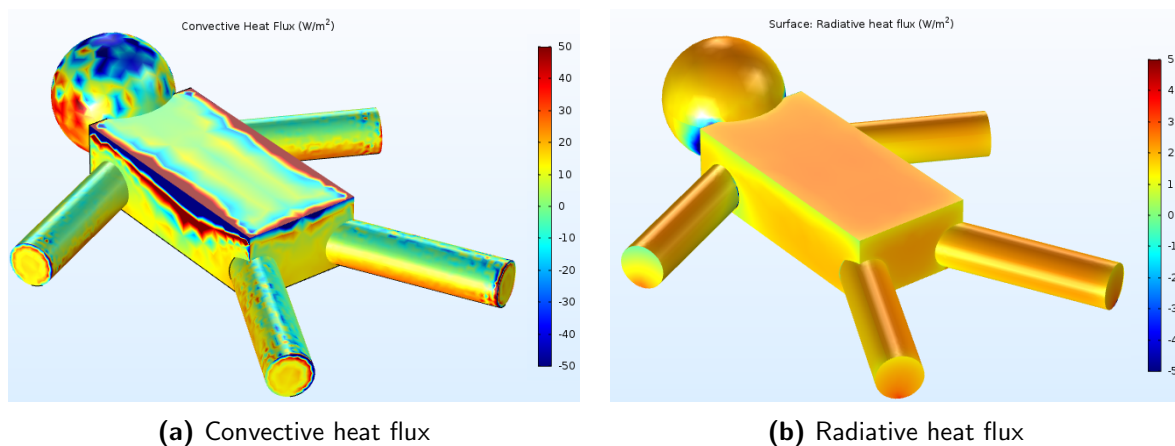


**Figure 5.7** – Time-averaged convective (a) and radiative (b) heat flux surface plots for scenario 2: incubator setpoint  $36^\circ\text{C}$  - 70% RH. Note the color map's ranges are different.

skin temperature and the inner wall temperature is small. COMSOL computes the average radiative heat flux as  $+0.7 \text{ W/m}^2$ . These results are in good agreement.

The average RH around the neonate computed by the model is 69%. Because the evaporative heat loss strongly depends on the TEWL, which in turn strongly depends on gestational and postnatal age, the impact of the relative humidity on the infant depends on the infant. The evaporative heat loss can be calculated using to equation 2.10.

### 5.1.3 Scenario 3: Climate recovery of the incubator

The closed incubator model can be used determine the rate of recovery from a drop in temperature and relative humidity. On top of that, it can be used to compare the simulations with the measurements. For this scenario, the incubator's initial values are set to  $35.5^\circ\text{C}$ - $50\%$ RH. The inlet's air parameters are set to  $38^\circ\text{C}$ - $85\%$ RH. These settings are chosen because it mimics a measurement described in section 6.1. The air temperature and relative humidity at the same location as the measurement location (at the location of the neonate) are computed as a function of time.

The result for air temperature and relative humidity is presented in Figure 5.8.

The air temperature recovers in  $\approx 0.5 \text{ min}$ . The incubator is unable to reach  $38^\circ\text{C}$  when the air inlet's temperature is set to  $38^\circ\text{C}$ . With respect to the relative humidity, the incubator restores its original value after  $\approx 0.5 \text{ min}$  as well. The overall comparison is analysed after presenting the measurement results, in section 6.1.3.

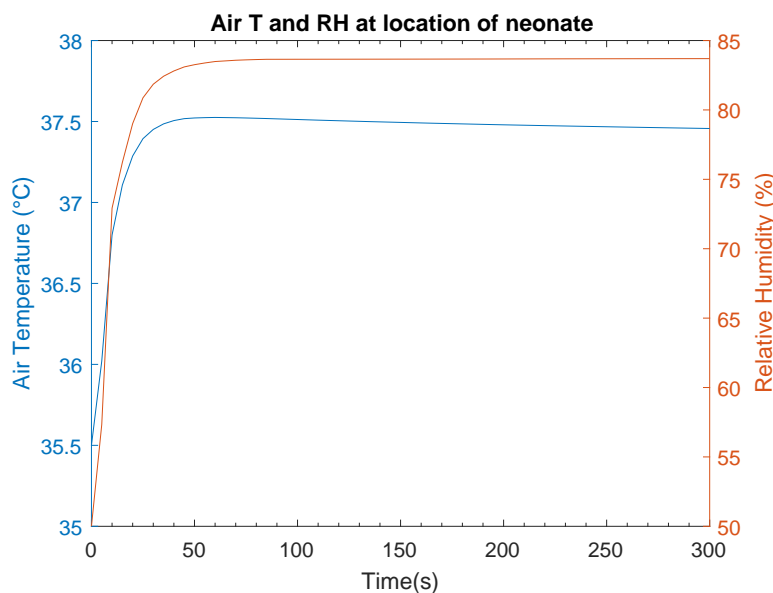


**Figure 5.8** – Simulated air temperature and relative humidity at the location of the neonate in case of scenario 3.

## 5.2 Opened incubator

Unfortunately, the simulations involving the opened incubator did not converge before the end of the project. A typical convergence plot and a picture of a typical convergence error are presented in Figure 5.9.

The convergence plot in Figure 5.9a shows a decreasing graph of the reciprocal of step size versus the time step. In case of the closed incubator, the solver typically reached convergence when the reciprocal of step size was  $\sim 10^{-2}$ . However, the solver for the opened incubator never reached this value and always encountered an error. Figure 5.9b represents the error corresponding to Figure 5.9a's convergence plot.

Several actions to solve these problems have been undertaken. All without success. First of all, several different direct and iterative solvers in COMSOL have been tested (MUMPS, PARDISO, SPOLES and GMRES).

As explained in section 2.2.5, an inferior mesh quality may lead to convergence problems. Therefore, as second option, the mesh was refined multiple times.

Next, the relative tolerance in the solution in COMSOL is defaultly set to 0.001. It was manually changed to 0.01, unfortunately without success.

Finally, COMSOL offered guidance in the setup of the simulations. They could not help within time to provide an answer for this model. Therefore, the further implementation for an opened incubator will be future work.

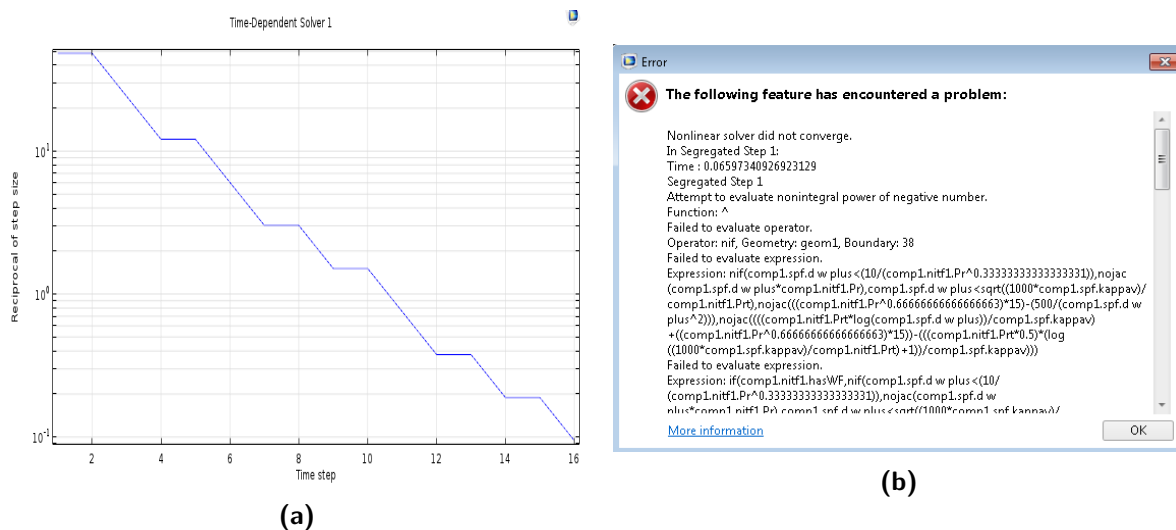


**Figure 5.9** – A typical convergence plot (a) and a picture of a typical convergence error (b) for the opened incubator simulations.



### 5.3 Discussion CFD results

In this section several remarks on the simulations are discussed.

First of all, as explained in the theory section, the  $k - \epsilon$  turbulence model might not be accurate in case of unconfined flows. In case the opened incubator is simulated, the flow is unconfined because it is able to flow through the open boundary. Perhaps this is the cause why the opened incubator model did not converge. A suggestion for future research would be to apply a different turbulence model in case an opened incubator is simulated.

The second remark relates to the convective heat transfer coefficient. A reason why the computed and calculated convective heat transfer mismatch might be caused by different heat transfer coefficients  $h$ . Therefore, future research could further examine the correct value of  $h$ .

Third, in scenario 3, the incubator's climate is recovering. It involves both warming up the air temperature, as well as increasing the relative humidity. As explained in this chapter, all simulations are simulated with a stationary flow. However, due to temperature differences of  $\approx 4.5$  °C, density effects will become more important and influence the flow profile. On top of that, the differences in water vapor concentration will also influence the density distribution. Therefore, the flow should have been modelled time-dependent and the density effects due to temperature and humidity differences should have been taken into account.

Finally, the geometry of the neonate used for the simulations is simplified compared to reality. Computer Aided Design (CAD) programs allow a more accurate representation of the geometry compared to geometry packages included in CFD software. Combining CAD software with CFD packages will increase the accuracy of the results.

## Chapter 6

# Results and discussion incubator measurements

This chapter presents the results of the incubator measurements and provides a discussion on the results. The first section addresses the measurements performed on the Dräger Caleo<sup>TM</sup>, while the second section addresses the GE Giraffe Carestation. The third section compares the performance of both incubators.

In several cases, the measured relative humidity at the location of the incubator's sensor is different from the relative humidity shown on the display of the incubator. The explanation for this is that humidity can be difficult to measure accurately. The sensor used in these experiments (see Appendix B) has an accuracy of several percent, depending on the measured RH. It is plausible to assume that the incubator sensor has an accuracy of several percent as well. Therefore, user-measured RH at the location of the incubator sensor and the RH displayed by the incubator might mismatch by  $\approx 5\%$ . The measured RH by the incubator is not taken into account in the measurements.

### 6.1 Results Dräger Caleo<sup>TM</sup> measurements

The section is structured as follows: the results of a typical measurement are presented in graphs. From these graphs, several values such as the air temperature drop, the relative humidity drop and the typical time scale of the drops can be determined. The results of the other measurement scenarios are only presented in these values. For an overview of all measurement result graphs, see Appendix F.

The first section addresses the measurements where the climate chamber settings are constant and set to 25°C-45%RH. In this setup, the incubator's climate is varied. The second section addresses the measurements where the incubator's climate is kept constant and the climate chamber's settings are varied.

#### 6.1.1 Variation in incubator settings

The measurement results for air temperature and relative humidity, in case the incubator is set to 38°C-99%, are visualized in Figure 6.1. The measurement results for the surface temperature are presented in Figure 6.2. The dashed vertical lines indicate the time at which the incubator was closed again. The initial value of the relative humidity is set to 99%, while the incubator is not able to achieve a relative humidity higher than 85%. In case of the air temperature and relative humidity plots, the measurement location at the neonate is most important, because these values can directly be translated into convective and evaporative heat transfer. Therefore,

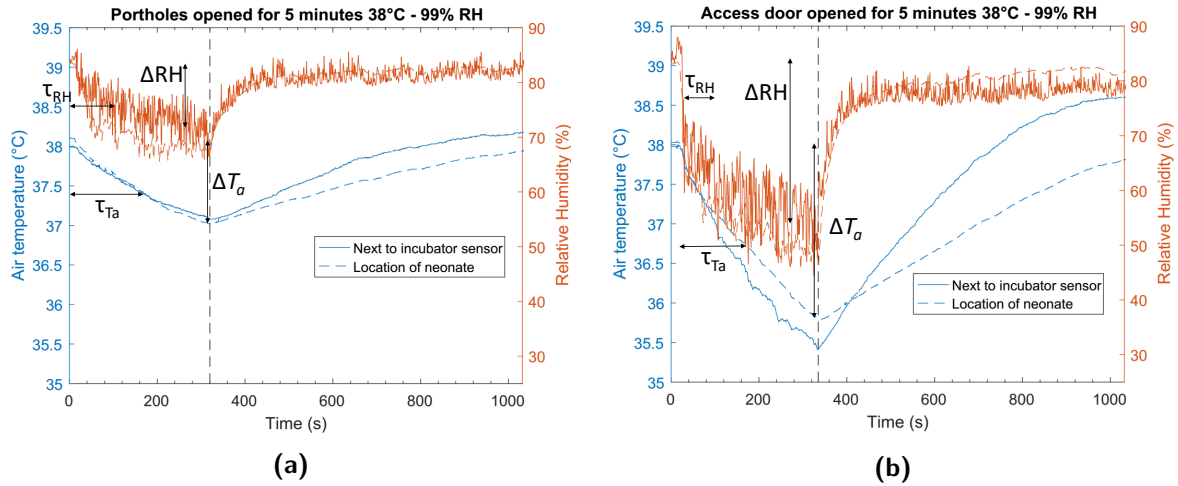


**Figure 6.1** – Results for opening the portholes (a) and access door (b) for 5 minutes on the air temperature and relative humidity. The incubator (Caleo<sup>TM</sup>) was set to 38°C-99%. The drop in relative humidity ( $\Delta RH$ ) and air temperature ( $\Delta T_a$ ) at the location of the neonate are visualized. Their corresponding time constants are denoted by  $\tau$ .

at the location of the neonate, the drop in air temperature and relative humidity after opening are denoted by  $\Delta T_a$  (°C) and  $\Delta RH$  (%), respectively. With respect to the surface temperature plots, the measurement location on the inside of the incubator hood is most important, because it can directly be translated into radiative heat transfer. The surface temperature drop on the inside of the incubator hood is given by  $\Delta T_s$  (°C). The time constants,  $\tau$  (s), are a measure for how rapidly the value drops. The shorter the time constant, the faster the value drops.  $\tau$  is defined as the time in which the value drops 63 % of its total drop.

These typical values can be obtained for all measurement scenarios. The corresponding graphs are presented in Appendix F. The results of the typical values for all measurements are presented in Table 6.1.

Several observations can be done. Firstly, increasing the incubator's climate settings has more influence on the air temperature, surface temperature and relative humidity drop.

Secondly, opening the access door has more impact on the air temperature, surface temperature and relative humidity drop compared to opening the portholes.

Thirdly, the relative humidity drops' time constants are much lower than the air temperature drops' time constants. This implies that the relative humidity decays much faster.

Furthermore, it is interesting to observe that the relative humidity drop in scenario 2 is higher compared to scenario 3, while the initial relative humidity is lower. On top of that, the relative humidity's time constant is  $\approx 3$  times higher in scenario 3 compared to scenario 2. This is caused by the incubator not being able to reach 99% RH. Therefore, the incubator runs at maximum capacity to raise the RH. If the incubator is opened, the incubator will still run at maximum capacity, better preserving the humidity.

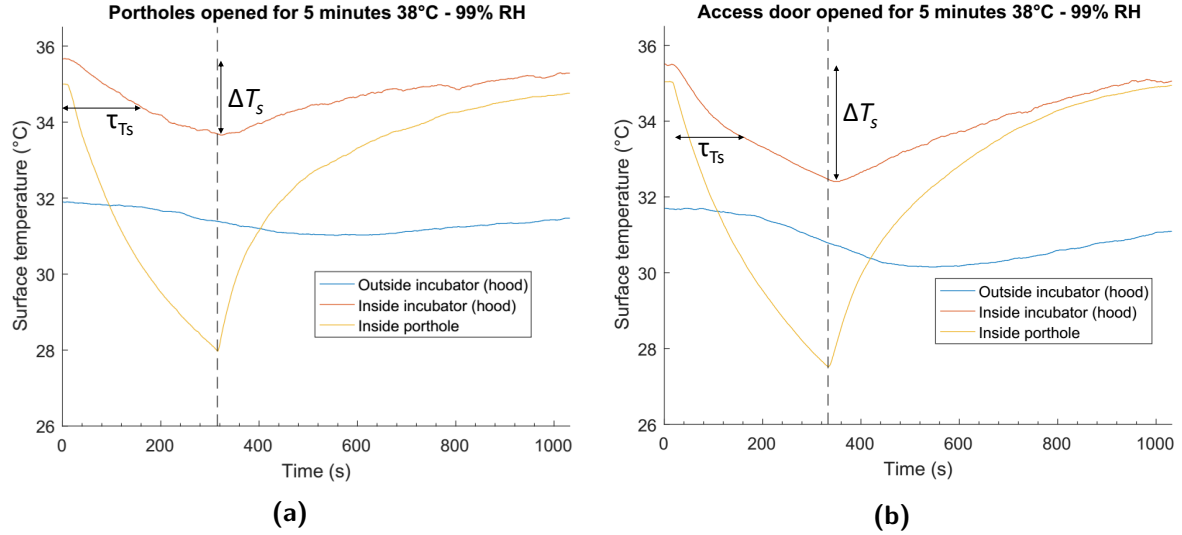


**Figure 6.2** – Results for opening the portholes (a) and access door (b) for 5 minutes on the surface temperature. The incubator (Caleo<sup>TM</sup>) was set to 38°C-99%. The drop in surface temperature ( $\Delta T_s$ ) on the inside of the incubator hood is visualized. Its corresponding time constant is denoted by  $\tau$ .

**Table 6.1** – The air temperature drop ( $\Delta T_a$ ), relative humidity drop ( $\Delta RH$ ) and surface temperature drop ( $\Delta T_s$ ) for the Caleo<sup>TM</sup> in case the incubator's settings are varied. Their time constants are denoted by  $\tau$ .

<b>1: Incubator 34°C-50%</b>	$\Delta T_a$ (°C)	$\tau_{T_a}$ (s)	$\Delta RH$ (%)	$\tau_{RH}$ (s)	$\Delta T_s$ (°C)	$\tau_{T_s}$ (s)
Opening portholes	0.3	170	8	30	0.2	180
Opening access door	0.8	150	14	13	0.5	120
<b>2: Incubator 36°C-70%</b>	$\Delta T_a$ (°C)	$\tau_{T_a}$ (s)	$\Delta RH$ (%)	$\tau_{RH}$ (s)	$\Delta T_s$ (°C)	$\tau_{T_s}$ (s)
Opening portholes	0.5	140	19	30	0.4	150
Opening access door	1.2	150	34	30	0.8	101
<b>3: Incubator 38°C-99%</b>	$\Delta T_a$ (°C)	$\tau_{T_a}$ (s)	$\Delta RH$ (%)	$\tau_{RH}$ (s)	$\Delta T_s$ (°C)	$\tau_{T_s}$ (s)
Opening portholes	1.1	160	13	97	2.2	160
Opening access door	2.2	170	29	74	3.1	350

### 6.1.2 Variation in climate chamber settings

The second set of measurements is performed on a constant incubator environment. The incubator is set to 36°C-70% RH. The climate chamber's settings are varied. All measurements were performed without closing the incubator. The same physical values as in previous section are extracted from the data. For the corresponding graphs, see Appendix F. The results are presented in Table 6.2.

Interesting observations can be done. First of all, the only difference between scenario 1 and 2 is a difference in the chamber's RH. The temperatures are set equal, although a higher drop in air and surface temperature is observed in scenario 1. Apparently, increasing the ambient relative humidity has a positive effect on the humidity drop, as well as the temperature drop.

Secondly, because the time constants are much lower, the rate of drop in RH is higher than in the air and surface temperature. This is similar to the measurement results in the previous section.

**Table 6.2** – The air temperature drop ( $\Delta T_a$ ), relative humidity drop ( $\Delta RH$ ) and surface temperature drop ( $\Delta T_s$ ) for the Caleo<sup>TM</sup> in case climate chamber's settings are varied. Their time constants are denoted by  $\tau$ .

<b>1: Chamber 21°C-45%</b>	$\Delta T_a$ (°C)	$\tau_{T_a}$ (s)	$\Delta RH$ (%)	$\tau_{RH}$ (s)	$\Delta T_s$ (°C)	$\tau_{T_s}$ (s)
Opening portholes	0.6	160	19	30	1.1	160
Opening access door	1.8	150	33	30	2.1	160
<b>2: Chamber 21°C-60%</b>	$\Delta T_a$ (°C)	$\tau_{T_a}$ (s)	$\Delta RH$ (%)	$\tau_{RH}$ (s)	$\Delta T_s$ (°C)	$\tau_{T_s}$ (s)
Opening portholes	0.5	170	16	30	0.7	170
Opening access door	1.5	140	27	30	2.0	140
<b>3: Chamber 25°C-45%</b>	$\Delta T_a$ (°C)	$\tau_{T_a}$ (s)	$\Delta RH$ (%)	$\tau_{RH}$ (s)	$\Delta T_s$ (°C)	$\tau_{T_s}$ (s)
Opening portholes	0.5	140	19	30	0.4	150
Opening access door	1.2	145	34	30	0.8	100

### 6.1.3 Comparison simulation and measurements

Unfortunately, as explained in section 5.2, the simulations involving the opened incubator did not converge. Therefore, only the recovery of the climate after the incubator is reclosed can be compared. In Figure 6.1b, the incubator recovers starting at an initial value of  $\approx 35.5^{\circ}\text{C}$ -50%RH. The incubator's setpoint is  $38^{\circ}\text{C}$ -99%RH. Because in practice the incubator is unable to reach 99% RH, the setpoint for the RH is set to 85% in the simulations (see section 5.1.3). The results at the measurement location of the neonate, and the simulation results, can be plotted in one graph. This is done in Figure 6.3.

The graph with respect to the air temperature does not agree between the simulation and measurement. This is most probably caused by an error in the simulation settings. The flow in all simulations is assumed to be stationary, which is a reasonable assumption in case the incubator's initial temperature and setpoint are equal. In case the incubator is warmed up, temperature differences will increase significantly and this leads to (higher) density differences. These density effects will influence the flow profile. Therefore, these simulations should have been run with a time-dependent flow. Unfortunately, this has not been taken into account, as explained in the discussion of chapter 5.

The graph with respect to the relative humidity shows more agreement between the measurement and simulation compared to the temperature graph. However, similar to the temperature, differences in relative humidity will lead to density differences. In case the incubator's initial RH is equal to the setpoint, this effect is small. If the RH changes significantly during the simulations, the density differences will influence the flow profile. Therefore, the flow should have been computed time-dependently.

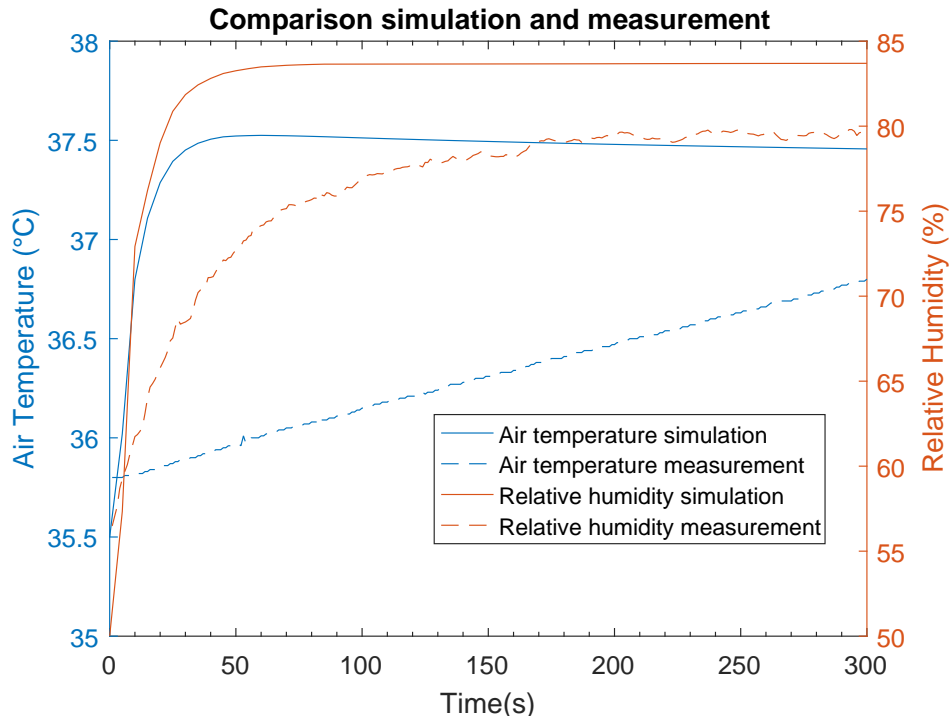


**Figure 6.3** – Recovery of the air temperature and relative humidity from initial value  $35.5^{\circ}\text{C}$ -50%RH to  $38^{\circ}\text{C}$ -85%RH. The results have been shown for both the simulation and the measurement.

## 6.2 Results GE Giraffe Carestation measurements

The section is structured similar as the previous section: the results of a typical measurement are presented in graphs. From these graphs, several values such as the air temperature and relative humidity drop and their corresponding typical time scales can be determined. The results from the other measurements are only presented in these values. For corresponding graphs of all measurement result graphs, see Appendix G.

As explained in section 4.3, all measurements are done with and without activation of the inbuilt air curtain. All measurements performed on the GE Giraffe carestation are done with climate chamber settings of 25°C-45%RH.

The measurement results for air temperature and relative humidity, in case the incubator is set to 38°C-99% RH, are visualized in Figure 6.4. Results are shown for the four different opening scenarios described in section 4.3.2. The vertical purple dashed line in Figure 6.4b indicates a shut-down of the air curtain by the incubator itself. Similar to previous section, the drop in air temperature and RH at the location of the neonate are denoted by the symbol  $\Delta$ . Their corresponding time constants are shown as well. In Figure 6.4b, the incubator shows a recovery of the air temperature. The absolute value of the recovery is denoted by  $\Delta T_{a,r}$  and the corresponding time constant by  $\tau_{T_{a,r}}$ . Several measurements showed recovery when the air curtain was activated. The climate recovery is treated separately in the next section.

The results for the surface temperature are illustrated in Figure 6.5. The surface temperature drop, on the inside of the incubator hood, is denoted by  $\Delta T_s$ . The recovery of the surface temperature in Figure 6.5a and 6.5b is denoted by  $\Delta T_{s,r}$ . The corresponding time constants are expressed by  $\tau$ .

The results for all measurements on the GE Giraffe Carestation are shown in Table 6.3. The first value denotes the value without activation of the air curtain, while the second value denotes the value with activation of the air curtain. Some values could not be computed due to several reasons. The main reason was a wrong initial value of the air temperature, relative humidity or surface temperature. These are indicated by NA. During several measurements, the incubator was able to recover from a drop during the time the incubator was opened. If this occurred, an asterisk is assigned to the value.

The results in Table 6.3 can be interpreted in two ways: the difference between opening the portholes and access door and the difference between with and without air curtain.

Activation of the air curtain only influences the air and surface temperature drop. It does not influence the decrease in relative humidity. The higher the temperature setting, the more impact the air curtain has on lowering the total temperature drop. On top of that, the rapidness of the temperature decays are lower.

Opening the access door has more impact on the climate compared to opening the portholes. It increases the total drop in air temperature, surface temperature and relative humidity. The impact on the air and surface temperature is higher than on the relative humidity. In most scenarios, the time constants in case of opening the access door are lower compared to when the portholes are opened.

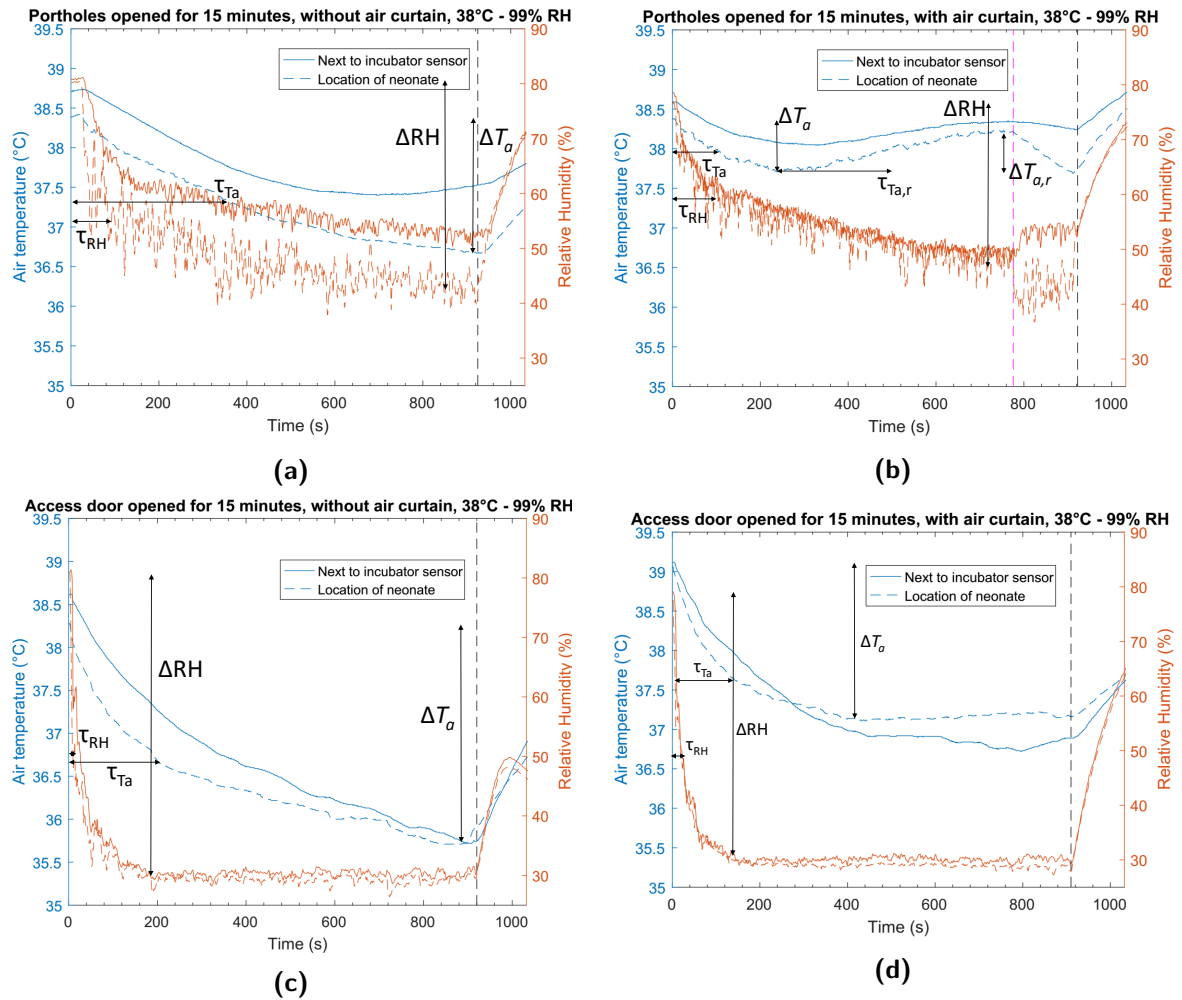
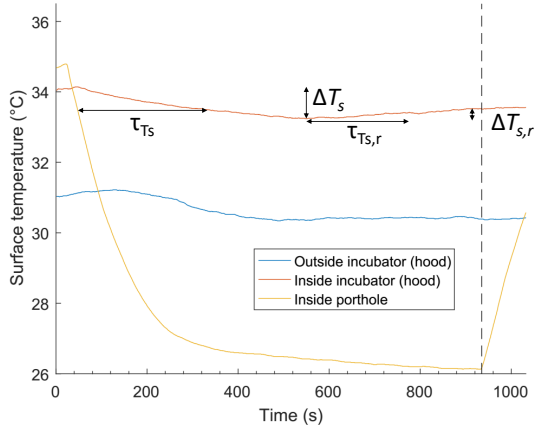


**Figure 6.4** – Results for opening the Giraffe for 15 minutes on the air temperature and relative humidity. The incubator was set to 38°C-99%. The drop in relative humidity ( $\Delta RH$ ) and air temperature ( $\Delta T_a$ ) at the location of the neonate are visualized. Their corresponding time constants are denoted by  $\tau$ .

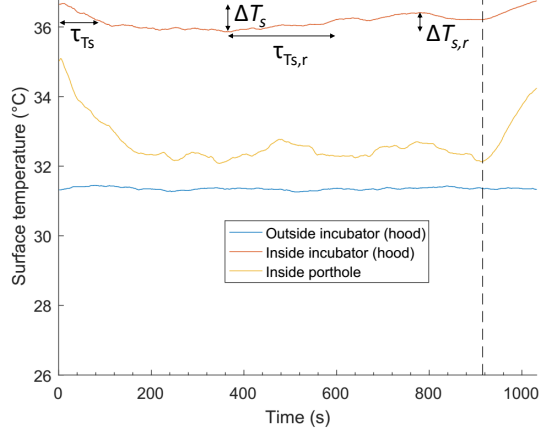


**Portholes opened for 15 minutes, without air curtain, 38°C - 99% RH**



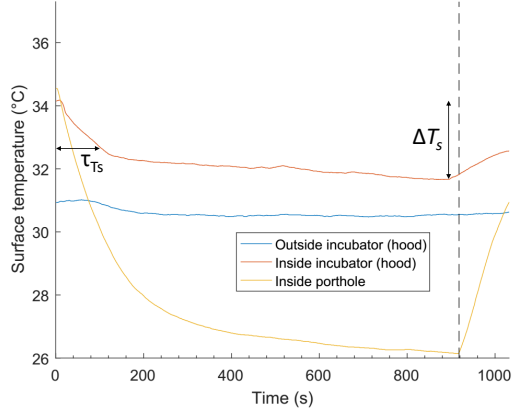
**(a)**

**Portholes opened for 15 minutes, with air curtain, 38°C - 99% RH**



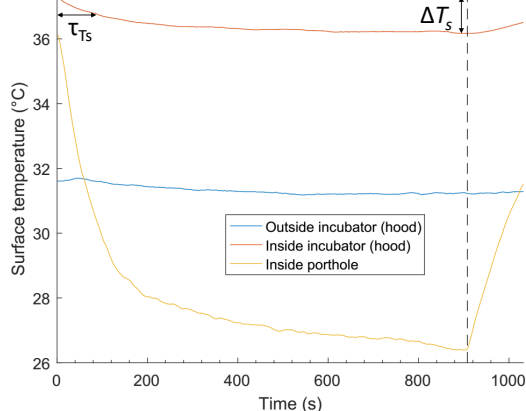
**(b)**

**Access door opened for 15 minutes, without air curtain, 38°C - 99% RH**



**(c)**

**Access door opened for 15 minutes, with air curtain, 38°C - 99% RH**



**(d)**

**Figure 6.5** – Results for opening the Giraffe for 15 minutes on the surface temperature. The incubator was set to 38°C-99%. The drop in surface temperature ( $\Delta T_s$ ) on the inside of the incubator hood is visualized. Its corresponding time constant is denoted by  $\tau$ .

**Table 6.3** – Results of all incubator measurements performed on the GE Giraffe Carestation. In each cell, the first value indicates the value without air curtain while the second value indicates the value with air curtain. Some values were not computable due to errors in initial values. They are indicated by a NA. During several measurements, the incubator was able to recover from a drop during the time the incubator was opened. If this occurred, an asterisk is assigned to the value.

<b>1: Incubator 28°C-70%</b>	$\Delta T_a$ (°C)	$\tau_{T_a}$ (s)	$\Delta RH$ (%)	$\tau_{RH}$ (s)	$\Delta T_s$ (°C)	$\tau_{T_s}$ (s)
Opening portholes	0.0/0.0	0/0	10/11	70/90	0.0/0.0	0/0
Opening access door	0.0/0.0	0/0	16/17	30/30	0.0/0.0	0/0
<b>2: Incubator 34°C-50%</b>	$\Delta T_a$ (°C)	$\tau_{T_a}$ (s)	$\Delta RH$ (%)	$\tau_{RH}$ (s)	$\Delta T_s$ (°C)	$\tau_{T_s}$ (s)
Opening portholes	0.4/0.2	490/680	NA/NA	NA/NA	NA/0.0	NA/0
Opening access door	1.1/0.9*	500/670	13/13	20/20	0.9/0.1*	210/290
<b>3: Incubator 34°C-70%</b>	$\Delta T_a$ (°C)	$\tau_{T_a}$ (s)	$\Delta RH$ (%)	$\tau_{RH}$ (s)	$\Delta T_s$ (°C)	$\tau_{T_s}$ (s)
Opening portholes	0.7/0.3	140/650	24/15	30/20	NA/0.6	NA/460
Opening access door	1.0/0.9*	140/440	29/33	30/30	0.8/0.3	120/610
<b>4: Incubator 34°C-99%</b>	$\Delta T_a$ (°C)	$\tau_{T_a}$ (s)	$\Delta RH$ (%)	$\tau_{RH}$ (s)	$\Delta T_s$ (°C)	$\tau_{T_s}$ (s)
Opening portholes	0.7/1.3	240/310	33/28	60/60	0.6/1.1	110/250
Opening access door	1.9/1.5	180/190	49/49	40/40	2.9/0.9	190/110
<b>5: Incubator 36°C-70%</b>	$\Delta T_a$ (°C)	$\tau_{T_a}$ (s)	$\Delta RH$ (%)	$\tau_{RH}$ (s)	$\Delta T_s$ (°C)	$\tau_{T_s}$ (s)
Opening portholes	1.0/0.5*	180/760	29/17	20/40	0.3/0.5	420/380
Opening access door	1.7/0.3*	220/240	32/39	20/20	1.2/0.1	140/260
<b>6: Incubator 38°C-50%</b>	$\Delta T_a$ (°C)	$\tau_{T_a}$ (s)	$\Delta RH$ (%)	$\tau_{RH}$ (s)	$\Delta T_s$ (°C)	$\tau_{T_s}$ (s)
Opening portholes	1.2/NA	200/NA	10/12	10/30	NA/0.3	NA/280
Opening access door	2.6/2.5	110/390	18/21	20/20	1.0/0.9	110/350
<b>7: Incubator 38°C-99%</b>	$\Delta T_a$ (°C)	$\tau_{T_a}$ (s)	$\Delta RH$ (%)	$\tau_{RH}$ (s)	$\Delta T_s$ (°C)	$\tau_{T_s}$ (s)
Opening portholes	1.7/0.7*	350/510	38/34	30/20	0.8*/0.8*	280/340
Opening access door	2.6/2.0	210/310	55/50	10/30	2.5/1.1	110/140

## Recovery of the incubator on the climate

In some scenarios, the incubator is able to (partly) recover the air or surface temperature during the time the incubator is opened. These scenarios and corresponding values are denoted with an asterisk in Table 6.3. The recovery can be expressed in terms of  $\Delta T_{a,r}$  and  $\Delta T_{s,r}$ . The rate of recovery is expressed by their time constants  $\tau$ . The results are given in Table 6.4. Values that did not show any recovery are denoted by NA.

**Table 6.4** – Results of the recovery values for all scenarios where recovery occurred. Values that did not show any recovery are denoted by NA.

<b>1: Incubator 34°C-50%</b> Opening access door, with air curtain	$\Delta T_{a,r}$ (°C)	$\tau_{T_{a,r}}$ (s)	$\Delta T_{s,r}$ (°C)	$\tau_{T_{s,r}}$ (s)
	0.4	300	0.4	360
<b>2: Incubator 34°C-70%</b> Opening access door, with air curtain	$\Delta T_{a,r}$ (°C)	$\tau_{T_{a,r}}$ (s)	$\Delta T_{s,r}$ (°C)	$\tau_{T_{s,r}}$ (s)
	0.7	230	NA	NA
<b>3: Incubator 36°C-70%</b> Opening portholes, with air curtain	$\Delta T_{a,r}$ (°C)	$\tau_{T_{a,r}}$ (s)	$\Delta T_{s,r}$ (°C)	$\tau_{T_{s,r}}$ (s)
	0.4	220	NA	NA
Opening access door, with air curtain	0.6	460	NA	NA
<b>4: Incubator 38°C-99%</b> Opening portholes, without air curtain	$\Delta T_{a,r}$ (°C)	$\tau_{T_{a,r}}$ (s)	$\Delta T_{s,r}$ (°C)	$\tau_{T_{s,r}}$ (s)
	NA	NA	0.3	210
Opening portholes, with air curtain	0.5	280	0.4	240

## 6.3 Comparison GE Giraffe Carestation and Dräger Caleo™

To fairly compare the two neonatal incubators, they have to be studied in the exact same way. Two opening scenarios apply to both incubators, i.e. the incubator setpoint 38°C-99% RH the incubator setpoint 34°C-50% RH. On top of that, the measurements applying to the Caleo™ involve opening the incubator for five minutes. Therefore, only the first five minutes of opening the Giraffe are taken into account.

The first section addresses the incubator setpoint 38°C-99%RH. The second section shows the results for the incubator setpoint 34°C-50%RH. The results are presented similar to previous sections, i.e. by presenting their typical values in Tables. For more insight in Figures in which the results for the Caleo™ and Giraffe are simultaneously presented in one graph, see Appendix H.

### 6.3.1 Incubator setpoint 38°C - 99% RH

The results for the air temperature, surface temperature and relative humidity drop for both incubators is given in Table 6.5.

With respect to air temperature, the Giraffe without air curtain performs worst in both opening scenarios. On the other hand, if the air curtain is activated, the Giraffe performs best of all three.

**Table 6.5** – Results for the incubator setpoint 38°C-99%RH for both the Caleo™ and the Giraffe. This allows comparison between the incubators.

<b>Opening portholes</b>	$\Delta T_a$ (°C)	$\tau_{T_a}$ (s)	$\Delta RH$ (%)	$\tau_{RH}$ (s)	$\Delta T_s$ (°C)	$\tau_{T_s}$ (s)
Caleo™	1.1	160	13	100	2.0	160
Giraffe without air curtain	1.7	350	38	30	0.8	280
Giraffe with air curtain	0.7	510	34	20	0.8	340
<b>Opening access door</b>	$\Delta T_a$ (°C)	$\tau_{T_a}$ (s)	$\Delta RH$ (%)	$\tau_{RH}$ (s)	$\Delta T_s$ (°C)	$\tau_{T_s}$ (s)
Caleo™	2.2	170	29	70	3.1	150
Giraffe without air curtain	2.6	210	55	10	2.5	110
Giraffe with air curtain	2.0	310	50	30	1.1	140

With respect to the surface temperature, the Giraffe with air curtain shows the least temperature drop in both opening scenarios. This is followed by the Giraffe without air curtain. The Caleo™ performs worst.

The drop in the Giraffe’s relative humidity is nearly equal with and without air curtain. In both opening scenarios, the Caleo™ shows significantly less drop in relative humidity compared to the Giraffe. Therefore, with respect to the relative humidity, the Caleo™ performs best.

### 6.3.2 Incubator setpoint 34°C - 50% RH

The results are presented in Table 6.6.

The drop in relative humidity is equal in case the access door is opened. Unfortunately, due to deviations in the initial values of the relative humidity, the portholes opening scenario can not be analysed.

With respect to air temperature, the Giraffe without air curtain performs worst in both opening scenarios. Depending on whether the access door is opened, or the portholes are opened, the performance differs between the two others. In the scenario where the portholes are opened, the Giraffe with air curtain performs better than the Caleo. If the access door is opened, the Caleo™ performs better.

Concerning the surface temperature, the Giraffe with air curtain shows the least temperature drop. This is followed by the Caleo™. The Giraffe without air curtain performs worst.

**Table 6.6** – Results for the incubator setpoint 34°C-50%RH for both the Caleo™ and the Giraffe. This allows comparison between the incubators.

<b>Opening portholes</b>	$\Delta T_a$ (°C)	$\tau_{T_a}$ (s)	$\Delta RH$ (%)	$\tau_{RH}$ (s)	$\Delta T_s$ (°C)	$\tau_{T_s}$ (s)
Caleo™	0.3	170	8	30	0.2	180
Giraffe without air curtain	0.4	490	NA	NA	NA	NA
Giraffe with air curtain	0.2	680	NA	NA	0.0	0
<b>Opening access door</b>	$\Delta T_a$ (°C)	$\tau_{T_a}$ (s)	$\Delta RH$ (%)	$\tau_{RH}$ (s)	$\Delta T_s$ (°C)	$\tau_{T_s}$ (s)
Caleo™	0.8	160	14	10	0.5	120
Giraffe without air curtain	1.1	90	13	20	0.9	130
Giraffe with air curtain	0.9	130	13	20	0.1	160

## 6.4 Discussion measurement results

There are several points of discussion on the measurements. The first point is the measurement of relative humidity. The sensor used in this research has an accuracy of  $\pm 5\%$ . Therefore, a lot of fluctuations are measured. The consequence of these fluctuations is that the analysis of the results becomes more complex. It is difficult to determine to absolute relative humidity drop and the corresponding time constant. Therefore, it is recommended for future research to use more accurate RH sensors.

Secondly, the inner wall temperature of the incubator was only measured at one location. The measurement locations on the inside of the porthole and the top of the incubator hood had no utility, because they can not be translated into radiative heat transfer. Therefore, to gain more insight in the inner wall temperature distribution, it would have been a more sophisticated choice to measure the inner wall temperature at more locations.

Finally, the incubators were measured with absence of a neonate. On top of this, measurement equipment was placed inside the incubators. This setup is different compared to the setup in a NICU ward. These differences could influence the flow profile of the incubator, with the result that the flow profile in the experiments differ from the flow profile in the NICU. The impact of the presence of the neonate on the flow profile is unknown, but can be investigated in future research.

## Chapter 7

# Clinical Relevance and the effect on the neonate

This chapter addresses the clinical relevance of the results. For that purpose, the impact of the simulation and measurement results on the neonate is determined. The first section treats the effect of the neonate in case the incubator is closed. The results from the simulations are used. The second section presents the effects on the neonate when the incubator is opened. This is done by using the outcomes of the measurements.

### 7.1 Closed incubator - simulations

This section calculates the body temperature as a function of time for a number of different infants placed in the simulated incubators described in chapter 5. Because the metabolic heat production depends on the mass and postnatal age and the evaporative heat loss depends on the gestational and postnatal age, the scenarios are calculated for infants with different gestational and postnatal age.

The procedure for determining the infant's physical parameters and thermophysiological properties is as follows: First, gestational age (GA) and postnatal age (PA) are chosen. From there, the body weight can be looked up using TNO's growth diagrams [62]. Using the body weight, the surface area can be looked up using a table for the body-surface area in infants and children provided by the CCLG - Chemotherapy Standardization Group 2008 [63]. The infant's metabolic heat production can be calculated using equation 2.14. Finally, to determine the transepidermal water loss, Figure 2.3 is used as look up.

The infants' physical parameters and thermophysiological properties used to calculate their body temperature as a function of time are represented in Table 7.2. They are nursed in the simulated incubator, which is the Dräger Caleo™. The average skin temperature, average incubator inner wall temperature, average air temperature around the neonate and the average relative humidity around the neonate are extracted from the simulation results and shown in Table 7.1. Together with the equations for convective, evaporative and radiative heat transfer, as well as the metabolic heat production (see chapter 2), the body temperature as function of time can be calculated. Note that these values are calculated for naked infants. Using clothing and blankets would reduce the heat loss.

The results for the neonates nursed in incubator scenario 1 (33°C-45%RH) and scenario 2 (36°C-70%RH) are shown in Figure 7.1 and 7.2, respectively.

**Table 7.1** – Computed average skin temperature, average air temperature around the neonate, average (inner) wall temperature and average relative humidity for two incubator settings. The values are extracted from the simulation results. They are used to calculate the neonate's body temperature as a function of time.

Incubator settings	$T_{skin}$ (°C)	$T_{air}$ (°C)	$T_{walls}$ (°C)	RH (%)
33°C-45%RH	36.0	33.1	33.0	44
36°C-70%RH	35.6	35.9	35.9	69

**Table 7.2** – Different infants and their physical and thermophysiological properties.

Gestational age (weeks)	Postnatal age (days)	Body Weight (kg)	Surface Area (m <sup>2</sup> )	Metabolic heat production (W)	TEWL (g/m <sup>2</sup> /h)
28	1	1.25	0.11	1.71	43
28	5	1.30	0.12	1.98	30
30	1	1.40	0.12	1.71	30
30	5	1.45	0.13	2.02	25
32	1	1.75	0.14	1.73	23
32	5	1.80	0.15	2.11	21

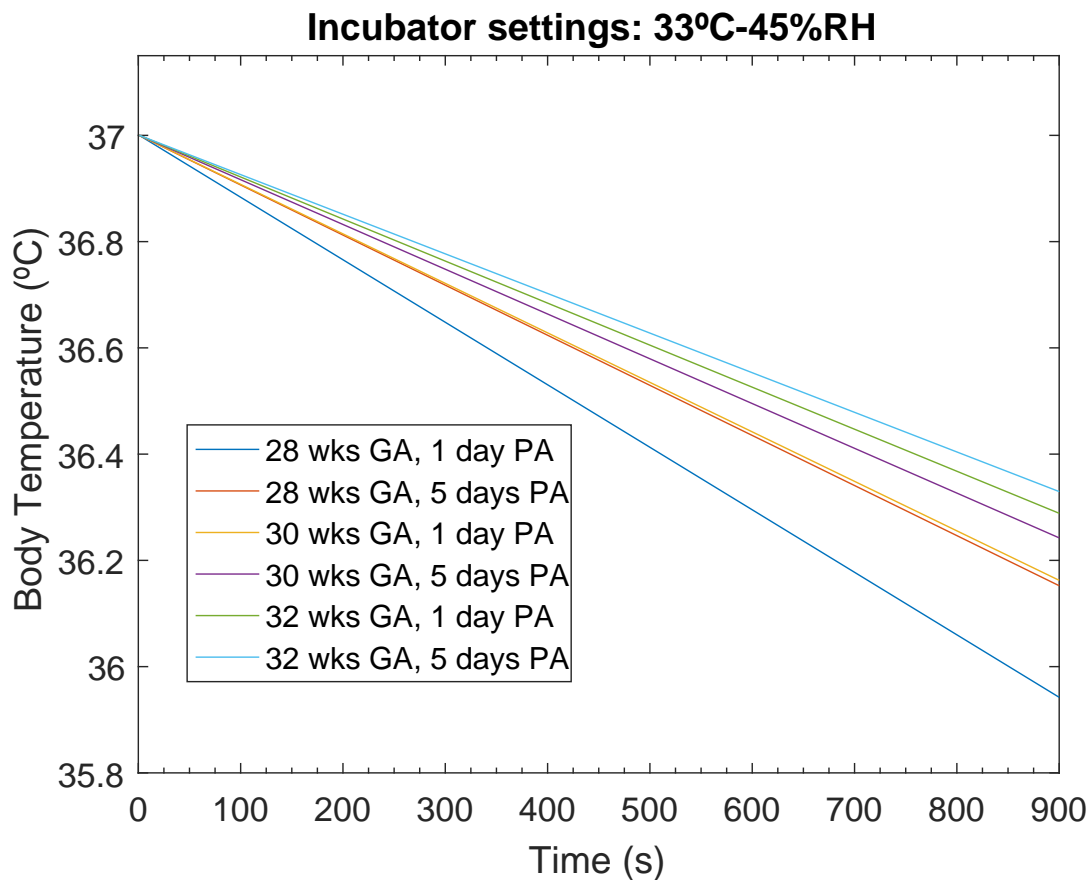


**Figure 7.1** – Body temperature as a function of time for neonates of different gestational age (GA) and postnatal age (PA). The incubator is set to 33°C-45%RH. Not that these values are calculated for naked infants.

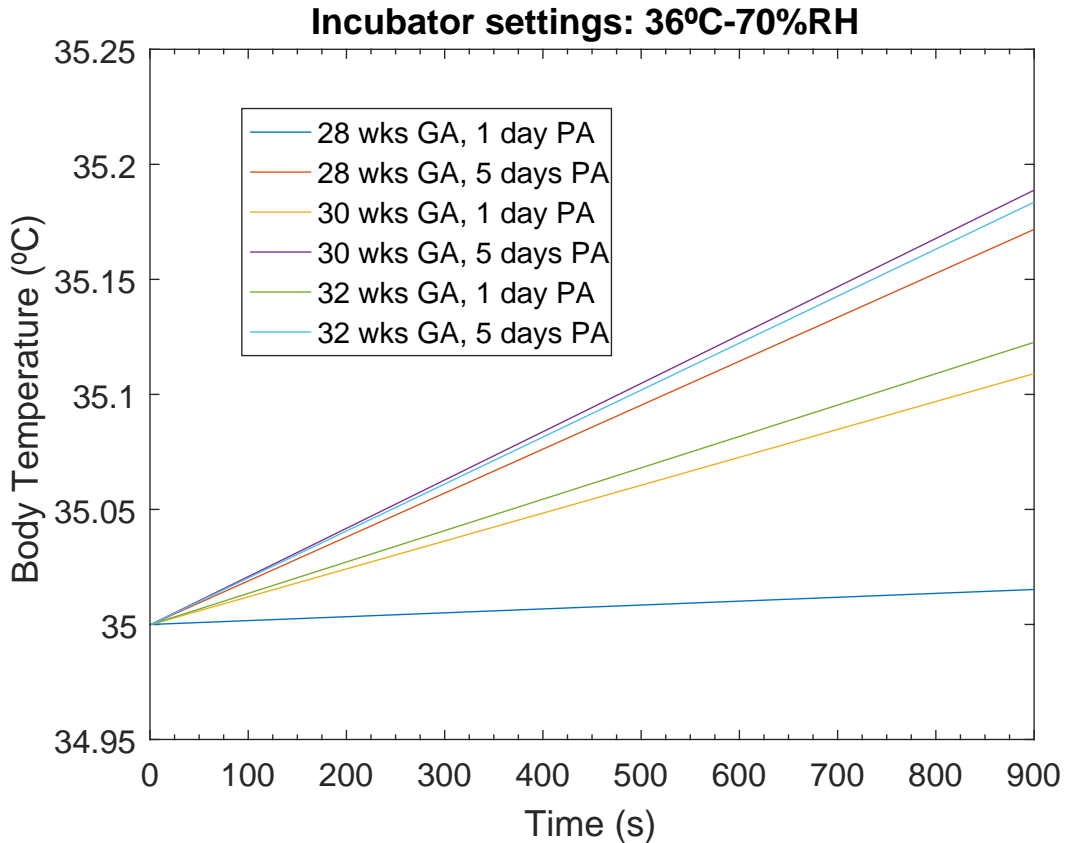


**Figure 7.2** – Body temperature as a function of time for neonates of different gestational age (GA) and postnatal age (PA). The incubator is set to 36°C-70%RH. Not that these values are calculated for naked infants.

In Figure 7.1, it is interesting to observe that all infants cool down in this incubator. The postnatal age has a large impact on the heat balance. I.e. the infant of 28 weeks GA and 5 days PA has a similar body temperature drop compared to infant of 30 weeks GA and 1 day PA. The body temperature drops range from -4.2 °C/h for the youngest infant, to -2.7 °C/h for the oldest infant.

In case of scenario 2 (see Figure 7.2), the neonates' body temperatures start at 35 °C, because this incubator setting mimics warming up the infant. The body temperature increases for every infant. The three infants of 5 days PA show the highest body temperature increase. This is caused by the higher metabolic heat production of the infants compared to the infants of 1 day PA.

On top of that, it is interesting to observe that the infant of 30 weeks GA - 5 days PA has a higher body temperature increase compared to the infant of 32 weeks GA - 5 days PA. The explanation for this is that the infant of 30 weeks GA - 5 days PA has a lower body mass. Therefore, a similar heat gain will lead to a higher increase in body temperature.

The youngest infant of 28 weeks GA - 1 day PA shows a near-constant body temperature. This is due to the transepidermal water loss being high, and the metabolic heat production being relatively low.



## 7.2 Opened incubator - measurements

The first section provides a general guideline for the personnel at the NICU on how to determine the influence of air temperature, RH and/or wall temperature drops on the infant's body temperature. On top of that, a look-up table for several typical infants is presented. The second section provides a table of the infant's body temperature for several common opening scenarios in the NICU. The values to calculate the heat loss when the incubator is opened are extracted from the Giraffe measurement results' section, because the Giraffe is used in our NICU department. Note that all equations used for calculation assume naked infants. With clothes or blankets the effects will be less.

### 7.2.1 General guideline NICU personnel

This guideline might be difficult for people without a physics background. The next section (7.2.2) provides a look-up table for typical opening scenarios at the NICU and the effect on the neonate's body temperature, which might be more insightful.

Step 1: Determine the postnatal (PA, days) and gestational age (GA, weeks) of the infant. From this, the body weight (kg) and body surface area (m<sup>2</sup>) can be looked up [62][63], or measured yourself.

Step 2: Determine the convective, radiative and evaporative heat loss. This is done as follows:

- Convective heat loss: The convective heat loss increases by 5.4 W/m<sup>2</sup> per °C air temperature drop. Determine the air temperature drop in degrees Celsius, and multiply this by 5.4. This gives the total convective heat loss in Watts per square meter.
- Radiative heat loss: The radiative heat loss increases by 4.36 W/m<sup>2</sup> per °C wall temperature drop. Determine the wall temperature drop in degrees Celsius, and multiply this by 4.36. This gives the total radiative heat loss in Watts per square meter.
- Evaporative heat loss: This one is more complicated. First of all, determine the TEWL<sub>50</sub> (g/m<sup>2</sup>/h) from Figure 2.3. The TEWL<sub>50</sub> depends on the GA and PA of the neonate. Next, use the following equation to determine the increase in evaporative heat loss per % RH drop in the relative humidity,  $\Delta Q_{evap}^*$  (W/m<sup>2</sup>):

$$\Delta Q_{evap}^* = 0.0133 \cdot TEWL_{50} + 0.001 \quad (7.1)$$

Multiply the total drop in relative humidity by  $\Delta Q_{evap}^*$ . This gives the total increase in evaporative heat loss in Watts per square meter.

Step 3: Determine the total heat loss. Do this by adding the convective, radiative, and evaporative heat loss calculated in step 2. This total heat loss is in W/m<sup>2</sup>, which means that it needs to be multiplied with the body surface area of the infant. Thus: multiply the answer with the area of the infant. You now have a value for the total heat loss of the infants,  $Q$ , in Watts. You need this value in the following step.

Step 4: Calculate the effect on the neonate's body temperature, per second. The body temperature drop per second,  $\frac{\Delta T}{\Delta t}$  (°C/s), can now be calculated. Use the mass of the infant,  $m$  (kg), and the total heat loss,  $Q$  (W), in the following formula to calculate the neonate's body temperature drop per second:

$$\frac{\Delta T}{\Delta t} = \frac{Q}{3391 \cdot m} \quad (7.2)$$

Step 5: This is the final step. To calculate the total body temperature loss, multiply  $\frac{\Delta T}{\Delta t}$  by the total time, in seconds. I.e. if your incubator is opened for two minutes, multiply  $\frac{\Delta T}{\Delta t}$  by 120.

A look-up table for six typical infants is presented in Table 7.3. The infants and their physical parameters and thermophysiological properties are equal to the infants described in section 7.1. The table calculates the convective heat loss gain per °C air temperature drop, the radiative heat loss gain per °C wall temperature drop and the evaporative heat loss gain per % relative humidity drop. The last column represents the impact on the body temperature of the infant, per Watt heat loss gain. The temperature drops and relative humidity drop can be retrieved from the incubator measurement results. This allows calculation of the body temperature, depending on the infant.

I.e. assume an infant of 30 weeks GA, 1 day PA, nursed inside the Dräger Caleo™ with an incubator setpoint of 34°C-50%RH. A nurse opens the access door for three minutes. The average temperature and relative humidity drops in these three minutes are:  $\Delta T_{air} = 0.3^\circ\text{C}$ ,  $\Delta T_{wall} = 0.2^\circ\text{C}$  and  $\Delta\text{RH}=8\%$ . This induces an increased convective heat loss of 0.2 W, an increased radiative heat loss of 0.1 W and an increased evaporative heat loss of 0.4 W. The total increased heat loss is then given by 0.7 W. Within these three minutes this will induce a decrease of the infant's body temperature of 0.03 °C.

**Table 7.3** – Lookup table for the effect on climate changes inside the incubator on the infant's body temperature. The total heat loss consists out of addition of the convective, radiative and evaporative heat losses.

Age. GA (weeks)- PA (day(s))	$\Delta Q_{conv}$ (W), per °C air temperature drop	$\Delta Q_{rad}$ (W), per °C wall temperature drop	$\Delta Q_{evap}$ (W), per % relative humidity drop	$\Delta T_{body}/\Delta t$ (°C/min), per Watt heat loss gain
28-1	0.59	0.48	0.063	-0.014
28-5	0.65	0.52	0.048	-0.014
30-1	0.65	0.52	0.048	-0.013
30-5	0.70	0.57	0.043	-0.012
32-1	0.76	0.61	0.043	-0.010
32-5	0.81	0.65	0.042	-0.010

### 7.2.2 Typical incubator opening scenarios: the effect on the neonate's body temperature, a guideline for NICU personnel

The results of the incubator measurements on the Giraffe have been used to determine the climate changes when the incubator is opened. The Giraffe is chosen since it is the incubator used within our own NICU department. The results of opening the incubator on the neonates' body temperatures (°C) for typical nursing procedures have been calculated and are presented in Table 7.4. The neonates' physical and thermophysiological properties have been extracted from Table 7.2. The first number represents the body temperature drop (°C) without air curtain while the second number represents the body temperature drop with air curtain. For more information on the body temperature change per minute at typical incubator settings, see the Table in Appendix I.

**Table 7.4** – Body temperature drops ( $^{\circ}\text{C}$ ) due to typical nursing procedures for three different incubator settings and six different infants. The first value indicates the body temperature drop in case the air curtain is switched off, while the second value indicates the body temperature when the air curtain is switched on. The brackets behind the nursing procedures indicate if the access door or portholes is/are opened, and for how long. The total time corresponding to each nursing procedure has been extracted from Deguines et al [14].

Neonate's age (GA (weeks) - PA (days))	28-1	28-5	30-1	30-5	32-1	32-5
<i>Incubator settings: 34° C-50%RH</i>						
Diaper change (portholes, 12 min)	-0.07/-0.05	-0.06/-0.04	-0.06/-0.04	-0.06/-0.04	-0.05/-0.03	-0.05/-0.03
Bathing (portholes, 34 min)	-0.19/-0.14	-0.16/-0.11	-0.16/-0.11	-0.16/-0.10	-0.14/-0.09	-0.14/-0.09
Tracheal suction (portholes, 12 min)	-0.07/-0.05	-0.06/-0.04	-0.06/-0.04	-0.06/-0.04	-0.05/-0.03	-0.05/-0.03
Infusion line insertion (access door, 26 min)	-0.72/-0.52	-0.60/-0.41	-0.61/-0.42	-0.60/-0.40	-0.53/-0.34	-0.53/-0.35
Tracheal intubation (access door, 44 min)	-1.22/-0.88	-1.02/-0.70	-1.03/-0.71	-1.02/-0.68	-0.89/-0.58	-0.89/-0.58
Radiologic screening (access door, 5 min)	-0.14/-0.10	-0.12/-0.08	-0.12/-0.08	-0.12/-0.08	-0.10/-0.07	-0.10/-0.07
<i>Incubator settings: 34° C-70%RH</i>						
Diaper change (portholes, 12 min)	-0.32/-0.24	-0.24/-0.18	-0.24/-0.17	-0.22/-0.17	-0.18/-0.15	-0.18/-0.15
Bathing (portholes, 34 min)	-0.91/-0.67	-0.67/-0.51	-0.68/-0.52	-0.62/-0.49	-0.52/-0.41	-0.51/-0.41
Tracheal suction (portholes, 12 min)	-0.32/-0.24	-0.24/-0.18	-0.24/-0.17	-0.22/-0.17	-0.18/-0.15	-0.18/-0.15
Infusion line insertion (access door, 26 min)	-1.03/-1.01	-0.80/-0.75	-0.81/-0.76	-0.77/-0.71	-0.66/-0.60	-0.65/-0.59
Tracheal intubation (access door, 44 min)	-1.75/-1.72	-1.35/-1.28	-1.37/-1.29	-1.30/-1.20	-1.11/-1.01	-1.10/-1.00
Radiologic screening (access door, 5 min)	-0.20/-0.20	-0.15/-0.15	-0.16/-0.15	-0.15/-0.14	-0.13/-0.12	-0.13/-0.11
<i>Incubator settings: 36° C-70%RH</i>						
Diaper change (portholes, 12 min)	-0.43/-0.26	-0.33/-0.20	-0.33/-0.20	-0.31/-0.19	-0.27/-0.16	-0.26/-0.16
Bathing (portholes, 34 min)	-1.23/-0.74	-0.93/-0.56	-0.94/-0.57	-0.88/-0.54	-0.75/-0.46	-0.74/-0.46
Tracheal suction (portholes, 12 min)	-0.43/-0.26	-0.33/-0.20	-0.33/-0.20	-0.31/-0.19	-0.27/-0.16	-0.26/-0.16
Infusion line insertion (access door, 26 min)	-1.33/-1.00	-1.06/-0.70	-1.08/-0.70	-1.04/-0.63	-0.90/-0.52	-0.90/-0.51
Tracheal intubation (access door, 44 min)	-2.25/-1.69	-1.80/-1.18	-1.82/-1.20	-1.76/-1.07	-1.52/-0.89	-1.53/-0.86
Radiologic screening (access door, 5 min)	-0.26/-0.19	-0.20/-0.13	-0.21/-0.14	-0.20/-0.12	-0.17/-0.10	-0.17/-0.10

### 7.3 Discussion clinical relevance

The calculations provided in this chapter are based on some assumptions. The first and main assumption is that the neonates are naked. In reality neonates wear clothes and/or are covered with blankets. This will reduce heat transfer with the environment. The effect of clothes and blankets has not been analysed in this research, but could be an import factor in the heat transfer of the neonate.

Furthermore, the neonate's skin temperature is assumed to be constant throughout the calculations. This implies that the heat transfer is constant as well. In reality, cooling down of the neonate's skin will reduce convective and radiative heat losses. Therefore, at some point in time, the neonate's body temperature will stabilize. In this research however, these time-dependent heat transfer calculations are not computed. For a more accurate representation of the neonate's body temperature, this effect should be taken into account.

On top of that, the calculations on the neonate's body temperature in case the incubator is opened are based on more assumptions. All physical and thermophysiological properties are extracted from literature. Because these properties are based on average neonates, and some literature is relatively old, specifying these properties by means of measurements on individual neonates will increase the accuracy of the calculations. Additionally, although the infant's thermal control mechanism is poor, it is existing. Because knowledge about the infant's thermal control mechanism is little, it is not taken into account in the calculations.

Moreover, the calculations' input values for the drop in air temperature, surface temperature and relative humidity are extracted from the measurements. These input values will vary when the ambient climate is different, or an other incubator is used.

Additionally, the calculations for the radiative heat transfer and convective heat transfer are based on two assumptions. The radiative heat transfer calculations are based on the average inner wall temperature of the incubator. Because the inner surface temperature was only measured at one location, this is probably not the average of the wall temperature. To more accurately define the inner wall temperature, more sensors should be used at different locations. The convective heat transfer calculations strongly depend on the convective heat transfer coefficient. In this research, a literature value ( $h = 5.4 \text{ W/m}^2$  [25]) is used. However, as shown in the CFD results chapter, this value might not be accurate. More knowledge about the correct convective heat transfer coefficient should be gathered in the future.

Finally, from a medical point of view, a high relative humidity inside an incubator can be hazardous due to bacterial growth. Bacterial colonisation occurs faster at higher humidity levels, increasing the risk of infection. Therefore, from a medical point of view, increasing the air temperature to reduce convective heat loss is less dangerous compared to increasing the humidity to reduce evaporative heat loss.

## Chapter 8

# Conclusion and recommendations

The goal of this research was to determine the influence on the climate when opening neonatal incubators. In order to determine these climate effects, two approaches were used. The first approach involved developing a Computational Fluid Dynamics (CFD) model to compute the climate effects. The second approach investigated the climate effects due to incubator opening by means of measurements on real incubators.

The effect of opening incubators on the climate inside the incubator depends on several factors. The main conclusion when opening incubators is that the relative humidity (RH) drops are significantly higher compared to the temperature drops. Because evaporative heat loss has the biggest impact on the total heat loss, the effect of a drop in RH is substantial on an infant. Therefore, monitoring and maintaining a constant RH is necessary.

The effect of opening an incubator on the infant's body temperature has been calculated for different neonates, different incubator climate settings and different opening scenarios. The impact on the infants' body temperature varies strongly with physical and thermophysiological properties such as weight, body surface area and gestational and postnatal age. On top of that, it depends on the incubator climate settings and the way the incubator is opened. Therefore, it is critical to be aware of these parameters to determine the impact of opening an incubator on the neonate's thermal state.

Computational Fluid Dynamics (CFD) has proven to be a useful tool when modelling the climate in incubators. Unfortunately, this research has not been able to simulate an opened incubator. Once a CFD model is developed for the opened incubator, it can be effective to determine the thermal state of the neonate. Compared to measurements, it allows for easier parametric testing to determine the optimal climate settings for the desired neonate. Additionally, CFD can be a helpful tool to test new geometries, materials and technologies, which will save time and money in the design cycle of new incubators.

Future research involving the CFD model could include simulating the opening of an incubator. In order to get better insight in the actual heat balance and body temperature of a neonate, another suggestion would be to determine the effects of clothing and blankets on the heat transfer.

## Chapter 9

# Bibliography

- [1] World Health Organization. <http://www.who.int/mediacentre/factsheets/fs363/en/>.
- [2] Hannah Blencowe, Simon Cousens, Mikkel Z Oestergaard, Doris Chou, Ann-Beth Moller, Rajesh Narwal, Alma Adler, Claudia Vera Garcia, Sarah Rohde, Lale Say, and Joy E Lawn. National, regional, and worldwide estimates of preterm birth rates in the year 2010 with time trends since 1990 for selected countries: a systematic analysis and implications. *The Lancet*, 379(9832):2162–2172, jun 2012.
- [3] P Tourneux, J.-P. Libert, L Ghyselen, A. Leke, S Delanaud, L. Degrugilliers, and V Bach. Heat exchanges and thermoregulation in the neonate. *Archives De Pediatrie*, 16(7):1057–1062, 2009.
- [4] World Health Organization. Thermal Protection of the Newborn: a practical guide, 1997.
- [5] R F Soll. Heat loss prevention in neonates. *Journal of perinatology : official journal of the California Perinatal Association*, 28:S57–S59, 2008.
- [6] Robin L Bissinger. Thermoregulation in Very Low-Birth-Weight Infants During the Golden Hour. *Advances in Neonatal Care*, 10(5):230–238, 2010.
- [7] Trevor P. Mann and R.I.K. Elliott. Neonatal Cold Injury. *The Lancet*, 269(6962):229–234, feb 1957.
- [8] S S Miller, H C Lee, and J B Gould. Hypothermia in very low birth weight infants: distribution, risk factors and outcomes. *Journal of Perinatology*, 31(S1):S49–S56, apr 2011.
- [9] Abbot R Laptook, Walid Salhab, and Brinda Bhaskar. Admission temperature of low birth weight infants: predictors and associated morbidities. *Pediatrics*, 119(3):e643–e649, 2007.
- [10] D Berterottière, A M D’Allest, M Dehan, and C Gaultier. Effects of increase in body temperature on the breathing pattern in premature infants. *Journal of developmental physiology*, 13(6):303–8, jun 1990.
- [11] Paul H. Perlstein, Neil K. Edwards, and James M. Sutherland. Apnea in Premature Infants and Incubator-Air-Temperature Changes. *New England Journal of Medicine*, 282(9):461–466, feb 1970.
- [12] W J Daily, M Klaus, and H B Meyer. Apnea in premature infants: monitoring, incidence, heart rate changes, and an effect of environmental temperature. *Pediatrics*, 43(4):510–8, apr 1969.

- [13] R D White, J A Smith, M M Shepley, and I C U Design Committee to Establish Recommended Standards for Newborn. Recommended standards for newborn ICU design, eighth edition. *Journal of Perinatology*, 33 Suppl 1(S1):S2–16, 2013.
- [14] C Deguines, L. Dégrugilliers, L. Ghyselen, K. Chardon, V. Bach, and P. Tourneux. Impact of nursing care on temperature environment in preterm newborns nursed in closed convective incubators. *Acta Paediatrica, International Journal of Paediatrics*, 102(3):96–101, 2013.
- [15] Shuzo Murakami, Shinsuke Kato, and Jie Zeng. Combined simulation of airflow, radiation and moisture transport for heat release from a human body. *Building and Environment*, 35(6):489–500, 2000.
- [16] Tero T Mäkinen, Désirée Gavhed, Ingvar Holmér, and Hannu Rintamäki. Effects of metabolic rate on thermal responses at different air velocities in 10C. *Comparative Biochemistry and Physiology Part A: Molecular & Integrative Physiology*, 128(4):759–768, apr 2001.
- [17] Dan Nørtoft Sørensen and Lars Køllgaard Voigt. Modelling flow and heat transfer around a seated human body by computational fluid dynamics. *Building and Environment*, 38(6):753–762, 2003.
- [18] Maciej K Ginalski, Andrzej J Nowak, and Luiz C Wrobel. Modelling of heat and mass transfer processes in neonatology. *Biomedical Materials*, 3(3):034113, 2008.
- [19] Joachim Wasner. Heat balance of premature infants. *Lubeck, Germany: Dragwerk AG*, 1994.
- [20] Nursan Dede Çinar and Tuncay Muge Filiz. Neonatal thermoregulation. *Journal of Neonatal Nursing*, 12(2):69–74, 2006.
- [21] Bouchra Agourram, Véronique Bach, Pierre Tourneux, Gérard Krim, Stéphane Delanaud, and Jean-Pierre Libert. Why wrapping premature neonates to prevent hypothermia can predispose to overheating. *Journal of applied physiology (Bethesda, Md. : 1985)*, 108:1674–1681, 2010.
- [22] Sadik Kakaç and Yaman Yener. *Heat conduction*. Washington, DC (United States); Taylor Francis, 3rd edition, 1993.
- [23] Theodore L Bergman, Frank P Incropera, David P DeWitt, and Adrienne S Lavine. *Fundamentals of heat and mass transfer*. John Wiley & Sons, 2011.
- [24] Patrick H Oosthuizen and David Naylor. *An introduction to convective heat transfer analysis*. McGraw-Hill Science, Engineering & Mathematics, 1999.
- [25] A E Wheldon. Energy balance in the newborn baby: use of a manikin to estimate radiant and convective heat loss. *Physics in Medicine and Biology*, 27(2):285–296, 1982.
- [26] William S Janna. *Engineering heat transfer*. CRC Press, 1999.
- [27] A Çengel Yunus and J Ghajar Afshin. Heat and mass transfer. *McGrawHill, New York*, 2007.
- [28] K. Hammarlund and G. Sedin. Transepidermal Water Loss in Newborn Infants. VI. Heat Exchange with Environment in Relation to Gestational Age. *Acta Paediatrica*, 71(2):191–196, mar 1982.

- [29] Robin B Knobel, John E Wimmer, and Don Holbert. Heat loss prevention for preterm infants in the delivery room. *Journal of Perinatology*, 25(5):304–308, 2005.
- [30] Sunita Vohra, Robin S. Roberts, Bo Zhang, Marianne Janes, and Barbara Schmidt. Heat Loss Prevention (HeLP) in the delivery room: A randomized controlled trial of polyethylene occlusive skin wrapping in very preterm infants. *Journal of Pediatrics*, 145(6):750–753, 2004.
- [31] Sunita Vohra, Gilda Frent, Valerie Campbell, Michele Abbott, and Robin Whyte. Effect of polyethylene occlusive skin wrapping on heat loss in very low birth weight infants at delivery: A randomized trial. *The Journal of Pediatrics*, 134(5):547–551, 1999.
- [32] K. Hammarlund, G. E. Nilsson, P. Å. Öberg, and G. Sedin. Transepidermal Water Loss in Newborn Infants: V. Evaporation from the Skin and Heat Exchange during the First Hours of Life. *Acta Paediatrica*, 69(3):385–392, may 1980.
- [33] K Hammarlund and Gunnar Sedin. Transepidermal water loss in newborn infants VII. Relation to postnatal age in very preterm and fullterm appropriate for gestational age infants. *Acta Paediatrica Scand*, 71:369–374, 1982.
- [34] Joachim W Fluhr, Peter Elsner, Enzo Berardesca, and Howard I Maibach. *Bioengineering of the skin: water and the stratum corneum*. CRC press, 2004.
- [35] Sarah Waldron and Ralph MacKinnon. Neonatal thermoregulation. *Infant*, 3(3):101–104, 2007.
- [36] J Agren, G Sjörs, and G Sedin. Transepidermal water loss in infants born at 24 and 25 weeks of gestation. *Acta paediatrica (Oslo, Norway : 1992)*, 87(11):1185–90, 1998.
- [37] A Jain, N Rutter, and P H Cartlidge. Influence of antenatal steroids and sex on maturation of the epidermal barrier in the preterm infant. *Archives of disease in childhood. Fetal and neonatal edition*, 83(2):F112–F116, 2000.
- [38] David R Lide. *CRC handbook of chemistry and physics*, volume 85. CRC press, 2004.
- [39] Robert H Perry and Don W Green. *Perry’s chemical engineers’ handbook*. McGraw-Hill Professional, 1999.
- [40] Nathanaëlle Museux, Virginie Cardot, Véronique Bach, Stéphane Delanaud, Loïc De-grugilliers, Bouchra Agourram, Elmountacer Billah Elabbassi, and Jean-pierre Libert. A reproducible means of assessing the metabolic heat status of preterm neonates. *Medical physics*, 35(1):89–100, 2008.
- [41] Kurt Brück. Temperature Regulation in the Newborn Infant. *Neonatology*, 3(2-3):65–81, jul 1961.
- [42] Edith Boyd and Others. The growth of the surface area of the human body. *The growth of the surface area of the human body.*, page 2008, 1935.
- [43] Yasser Amer Al-Taweel. *A Simulation Model of Infant - Incubator - Feedback System with Humidification and Temperature Control*. PhD thesis, 2006.
- [44] E Sulyok, E Jequier, and L S Prod’Hom. Respiratory contribution to the thermal balance of the newborn infant under various ambient conditions. *Pediatrics*, 51(4):641–650, 1973.
- [45] Maciej K Ginalski, Andrzej J Nowak, and Luiz C Wrobel. A combined study of heat and mass transfer in an infant incubator with an overhead screen. *Medical Engineering and Physics*, 29(5):531–541, 2007.



- [46] COMSOL Multiphysics® v. 5.2a. [www.comsol.com](http://www.comsol.com). COMSOL AB, Stockholm, Sweden.
- [47] COMSOL Multiphysics®. <https://www.comsol.com/multiphysics/finite-element-method>.
- [48] COMSOL Multiphysics®. <https://www.comsol.com/blogs/which-turbulence-model-should-choose-cfd-application/>.
- [49] B.E. Launder and D.B. Spalding. The numerical computation of turbulent flows. *Computer Methods in Applied Mechanics and Engineering*, 3(2):269–289, mar 1974.
- [50] P Bradshaw. Turbulent Secondary Flows. *Annual Review of Fluid Mechanics*, 19(1):53–74, jan 1987.
- [51] COMSOL Multiphysics®. <https://www.comsol.com/blogs/keeping-track-of-element-order-in-multiphysics-models/>.
- [52] COMSOL Multiphysics®. <https://www.comsol.com/blogs/meshing-your-geometry-various-element-types/>.
- [53] David C Wilcox and Others. *Turbulence modeling for CFD*, volume 2. DCW industries La Canada, CA, 1998.
- [54] COMSOL Multiphysics®. *CFD Module User's Guide*. 5.2a edition, 2016.
- [55] COMSOL Multiphysics®. <https://www.comsol.com/blogs/solutions-linear-systems-equations-direct-iterative-solvers/>.
- [56] Dräger. Caleo ® Couveuse Software 2.n Gebruiksaanwijzing. 2006.
- [57] Yunus A Cengel. Heat transfer - A practical approach. *International edition*. Published by McGraw-Hill, 1998.
- [58] Arkema. Plexiglas optical & transmission characteristics.
- [59] COMSOL Multiphysics®. *Heat Transfer Module User's Guide*. 5.2a edition, 2016.
- [60] Robin B Knobel. Fetal and neonatal thermal physiology. *Newborn and Infant Nursing Reviews*, 14(2):45–49, 2014.
- [61] Simone Teuwen. Contradictory thermal requirements in the Neonatal Intensive Care Unit: exploring middle grounds, 2016.
- [62] TNO. Groeidiagramman prematuren.
- [63] CCLG - Chemotherapy Standardisation Group 2008. Estimation of Body-Surface Area in Infants and Children.
- [64] O.A. Alduchov and R.E. Eskridge. Improved Magnus' form approximation of saturation vapor pressure. Technical report, Oak Ridge Operations, Oak Ridge, TN, nov 1997.

## Appendix A

# Calculating relative humidity from concentration and visa versa

The equation to calculate the concentration,  $c$  (mol/m<sup>3</sup>), from the relative humidity is given by the ideal gas law:

$$c = \frac{p}{R \cdot T} \quad (\text{A.1})$$

where  $p$  is the pressure (Pa),  $R$  is the gas constant (8.31 J/K/mol) and  $T$  is the temperature (K). Equation A.1 can be rewritten using equation 2.11 and yields

$$c = \frac{\text{RH} \cdot p^*}{R \cdot T}. \quad (\text{A.2})$$

In equation A.2, RH is the relative humidity and  $p^*$  is the saturation water vapor pressure of air (Pa). The saturation vapour pressure depends on the air temperature. It is calculated using the experimentally derived August-Roche-Magnus formula [64]:

$$p^* = 6109.4 \cdot \exp\left(\frac{17.625 \cdot T}{T + 243.04}\right), \quad (\text{A.3})$$

in which  $p^*$  is the saturation pressure (Pa) and  $T$  the temperature (°C).

## Appendix B

# Detailed product specifications of measurement equipment

The following pages provide official documentation of the measurement equipment used for the incubator measurements.

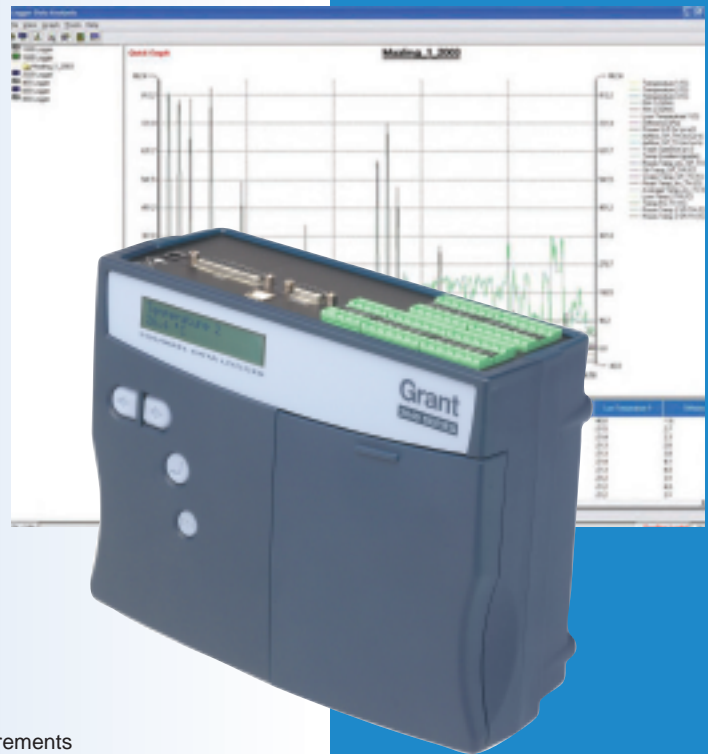
Information for respectively the Grant Data Logger, air temperature and humidity and surface temperature devices is shown.

# Squirrel 2040 DATA LOGGERS

*Squirrel 2040 series, the new generation data logger from Grant Instruments, combines higher channel count with the same high performance, comprehensive features and universal inputs of the smaller 2020 in a neat compact and portable instrument. Using multiple analog to digital convertors, twin processors and removable memory options positions the 2040 series as the ideal data logger for industrial, scientific research and quality assurance applications. The 2040 provides standalone data acquisition and metering that together with a suite of comprehensive software and functional design make the 2040 the "all in one box" first choice.*

## Key Features

- 32 universal analog inputs for voltage, current or resistance measurements plus 2 high voltage, 4 pulse and 8 digital event/state inputs
- Analog inputs can be used with thermistor, thermocouple and RTD temperature sensors and 4-20mA instruments
- User selectable logging rates of up to 100Hz on a single channel
- 16Mb of internal memory for approximately 1 to 2 million readings
- Download of internal data to removable MMC (Multi Media Card) memory
- Easy to use removable connector system
- Sensor power and relay outputs for use with external devices
- Comprehensive access to information using the 2 line, 40 character LCD and button panel
- Readings can be scaled and viewed in realtime on a PC or on the local LCD
- Calculated channels derived from real channels using basic math's functions e.g. channel 1 x channel 2
- USB and RS232 communication ports
- Non volatile flash memory - data retention is virtually indefinite
- Multiple 24 bit analog to digital convertors (ADC) for precision measurements
- Portable, battery operated or mains powered



Free  
Software  
&  
Technical  
Helpline

## Communications:

USB and RS232 serial ports are standard with external options for Ethernet, Landline and GSM communications enabling global access and system integration of the 2040.

## Multiple setups stored in internal and external memory:

A setup is the instruction that tells the 2040 how it will operate. Up to six preconfigured setups, together with the setup in current use, are held in the internal memory. In addition a further 25 setups can be loaded from the external memory. Switching between setups is extremely easy and fast using the convenient LCD display and button panel, avoiding the need to connect to a PC, thereby reducing time and effort to switch between different data logging applications.

## Comprehensive configuration:

SquirrelView configuration, download and data export software permits full control and use of the 2040 data logger. The convenient LCD display and button panel enable metering and logging in true portable operation.

## Concurrent sampling:

2040 multiple ADCs allows true concurrent sampling and logging. For instance one channel can sample at a rate of 100Hz whilst retaining different sample speeds on other channels, making the 2040 ideal for measuring parameters that change at different rates such as temperature and pressure.

## Software

### SquirrelView:

Easy to use setup and download software

### SquirrelView Plus:

SquirrelView with on-line and historical graphing

# Squirrel 2040

## DATA LOGGERS



### System Specification

Input channels:					ADDITIONAL CHANNELS			
2040 TYPE	ANALOG INPUT CHANNEL OPTIONS				PULSE	EVENT/DIGITAL	HIGH VOLTAGE	INTERNAL CHANNELS
	ADCs	DIFFERENTIAL	SINGLE ENDED	3 OR 4 WIRE				
2F16	x 2	16	32	0	(2 x fast - 64kHz) & (2 x slow -100Hz)	8 State inputs or 1 x 8 bit Binary	2	2 Temperature
4F16	x 4	16	32	8	(2 x fast - 64kHz) & (2 x slow -100Hz)	8 State inputs or 1 x 8 bit Binary	2	2 Temperature

**Standard ranges for temperature channels:**  
Each channel can be individually set to any of the ranges listed below. Pt100 to IEC751 and JIS1604 and Pt1000 to IEC751.

INPUT TYPE	RANGES °C	RANGES °F	INPUT TYPE	RANGES °C	RANGES °F
Thermistor Y & U:	-50 to150	-58 to 302	Thermocouple K:	-200 to 1372	-328 to 2501
Thermistor S:	-30 to150	-22 to 302	Thermocouple T:	-200 to 400	-328 to 752
			Thermocouple J:	-200 to 1200	-328 to 2192
Pt100/Pt1000 *	-200 to 850	-328 to1562	Thermocouple N:	-200 to 1300	-328 to 2372
* 2 wire only on 2F16, 3 or 4 wire on 4F16			Thermocouple R & S:	-50 to 1768	-58 to 3214

**Standard ranges for d.c. voltage/current and resistance channels:**  
Each voltage/current channel can be any of the voltage or current ranges below. Mixed differential and single ended configurations are permitted.  
Note: current ranges use differential input channels.

VOLTAGE RANGE	VOLTAGE RANGE	HIGH VOLTAGE RANGE	CURRENT RANGE (EXT.10Ω SHUNT)	RESISTANCE RANGE 2 WIRE	RESISTANCE RANGE 3 AND 4 WIRE (4F16 VERSION)
-0.075 to 0.075V	-0.6 to 2.4V	4.0 to 20.0V	-30.0 to 30.0mA	0.0 to 1250.0 Ω	0.0 to 500.0 Ω
-0.15 to 0.15V	-3.0 to 3.0V	4.0 to 40.0V	4 to 20mA	0.0 to 5000.0 Ω	0.0 to 4000.0 Ω
-0.3 to 0.3V	-6.0 to 6.0V	4.0 to 60.0V		0.0 to 20000.0 Ω	
-0.6 to 0.6V	-6.0 to 12.0V			0.0 to 300000.0 Ω	
-0.6 to 1.2V	-6.0 to 25.0V				

**ANALOG INPUTS**  
**Accuracy:** (at 25°C) voltage and resistance ± (0.05% readings + 0.025% range)  
**Common mode rejection:** 100dB  
**Input impedance:** > 1MΩ  
**Linearity:** 0.0015%  
**Series mode line rejection:** 50/60Hz 100dB

**ANALOG-DIGITAL CONVERSION**  
**Type:** Sigma-Delta  
**Resolution:** 24bit  
**Sampling rate:** up to 10, 20\* or 100\* readings per second per ADC

**ALARM OUTPUTS**  
4 x open drain FET (18V 0.1A)

**POWER OUTPUT FOR EXTERNAL DEVICE**  
Regulated 5 VDC at 50mA or logger supply voltage at 100mA

**TIME AND DATE**  
In built clock in 3 formats

**SCALING DATA**  
Displays readings in preferred engineering units.

**MEMORY**  
**Internal:** 16Mb (Up to 1,800,000 readings)  
**External:** Up to 64Mb - removable MMC (For transferring internal memory and storing setups only)

\*With mains rejection off

**CALCULATED CHANNELS**  
Up to 16 virtual channels derived from physical input channels

**RESOLUTION**  
Up to 6 significant digits

**PROGRAMMING/LOGGER SETUP**  
SquirrelView or SquirrelView Plus software

**COMMUNICATION**  
**Standard:** RS232 (Auto bauding to 115k baud) USB 1.1 and 2.0 compatible  
**External options:** Ethernet, GSM and PSTN Modems

**POWER SUPPLY**  
**Internal:** 6 x AA Alkaline batteries  
**External:** 10-18VDC  
Reverse polarity and over-voltage protected

**POWER CONSUMPTION @ 9V**  
**Sleep mode:** < 600µA  
**Logging:** 40-120mA

**DIMENSIONS AND WEIGHT**  
**Dimensions:** W235 x D175 x H92mm  
**Weight:** Approx 1.5kgs  
**Enclosure material:** ABS

**MEMORY MODES (internal only)**  
Stop when full or overwrite

**DISPLAY AND KEYPAD**  
2 line x 40 character LCD display  
Battery state and external power indicator  
Keypad lock  
**Navigate to:**  
Arm/disarm/pause/continue  
Meter any channel or alarm  
Select from up to 6 x pre-stored setups  
Status/diagnostics/memory/time and date  
Download to MMC

**OPERATING ENVIRONMENT**  
-30°C to +65°C  
Humidity: 90% at 40°C non condensing

**ACCESSORIES**  
**MPU 12V:** Universal (97-263V AC) power supply  
**LC76:** DC lead  
**SQ20RB12-6:** External rechargeable battery (12V, 6Ah)  
**SB102:** 25 way digital I/O connector  
**CS202:** Current shunt kit (8 x 10Ω 0.125W)  
**PEL4:** Rugged weather proof enclosure  
**CAL2040:** Test and Calibration certificates  
**SQ20A802:** External GSM communications kit  
**SQ20A801:** External Ethernet adaptor kit  
**MMC64:** Multi Media Card  
(Please see price list for additional accessories)

**Please note:** SQ2040 is supplied with software, manual, USB cable, wall bracket and batteries.

Due to our policy of continuous improvements, specifications may change without prior notice. Grant believe that all information declared is correct at the time of issue. No liability is accepted for errors and omissions.



**Grant Instruments**  
**(Cambridge) Ltd**  
Shepreth  
Cambridgeshire  
SG8 6GB England

Tel: +44 (0) 1763 260811  
Fax: +44 (0) 1763 262410  
www.grant.co.uk  
loggersales@grant.co.uk

Printed in England-2040/0405UK/V2

### Software

**SquirrelView - supplied with 2040**  
2040 logger setup, download and data export to Excel or CSV application for Windows 98, 2000 and XP. Features include metering and support for Modem, Ethernet and GSM communications.

**SquirrelView Plus**  
As SquirrelView with additional features including on-line or historical graphing of data with manual and automatic scaling of graphs. Readings can be listed in tabular format with timestamps and statistics.

**Warranty:** Equipment manufactured by Grant Instruments is warranted against faulty materials or workmanship for three years. For repairs carried out under warranty, no charge is made for labour, materials or return carriage.

**CE mark:** The Grant 2040 data acquisition system bears a CE mark and meets relevant European directives.

**Quality Statement:** Grant Instruments operates a Quality Management System complying with ISO9001:2000.

It is Grant's policy to supply customers with products which are fit for their intended purpose, safe in use, perform reliably to published specification and are backed by a fast and efficient customer support service.

**Manufactured and designed in Cambridge, England.**

## TECHNICAL DATA

## HUMITTER® 50U, HUMITTER® 50Y/YX

### RELATIVE HUMIDITY

Measurement range (for which accuracy is specified)	10...90 %RH
Operating range	0...100 %RH
Accuracy	see Figure 1
Temperature dependence	see Figure 2
Sensor	INTERCAP® Humidity Sensor, part no. 15778

### TEMPERATURE

#### Y-model - active output

Measurement range	-10...+60 °C
Accuracy	see Figure 3
Sensor	Pt 1000 IEC 751 Class B

#### YX-model - passive output

2-wire connection wire resistance	2 x 0.08 Ω
Sensor	Pt 1000 IEC 751 Class B

### GENERAL

Output signal	0...1 V, $R_L > 100 \text{ k}\Omega$ (equals 0...100 %RH and -40...+60 °C, i.e. 10 mV equals 1 %RH or 1 °C), other voltage outputs and 4...20 mA output available with external electronics
Power supply	7...28 VDC
Current consumption	2 mA typical
Operating temperature range	-10...+60 °C
Storage temperature range	-40...+60 °C
Operating humidity range	0...100 %RH
Sensor protection	membrane filter part no. 17039
option	plastic grid part no. 17038
Housing material	chromed ABS plastic
Housing classification	IP65

Complies with EMC standard: EN61326-1:1997 + Am1:1998, Generic Environment.

INTERCAP® and HUMITTER® are registered trademarks of Vaisala. Specifications are subject to change without prior notice.

© Vaisala Oyj



Dimensions in mm

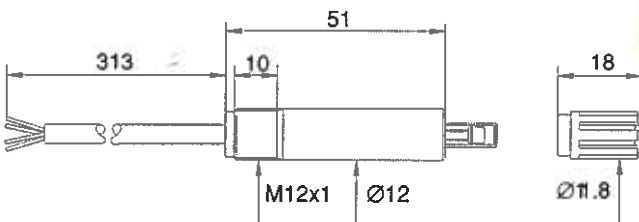


Fig. 1 Accuracy of humidity measurement

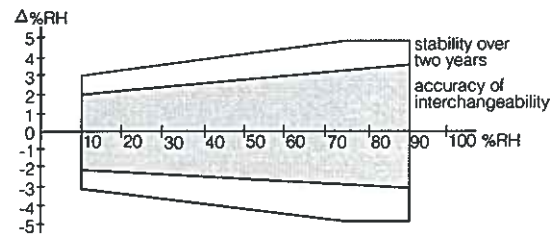


Fig. 2 Temperature dependence

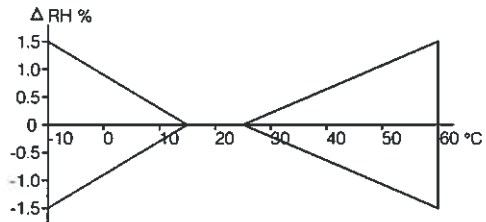
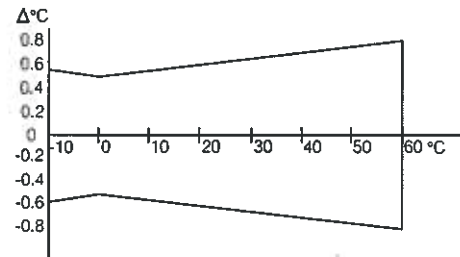
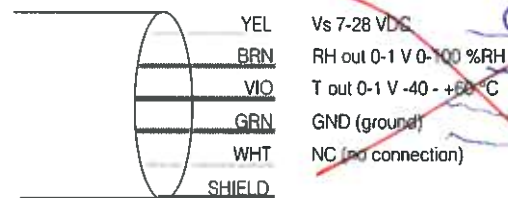


Fig. 3 Accuracy of temperature measurement



Cable connections



*Geel*  
*Bruin*  
*groen*  
*wit*

In the HUMITTER® 50YX, the resistive temperature signal is available via the violet and white wires.

*Geel = Power.*  
*Groen = NTC 2K U-Type.*  
*Bruin = RV 0-1V*  
*wit = GND*



Vaisala Oyj  
P.O. Box 26  
FIN-00421 Helsinki  
FINLAND

Phone (+358-9) 894 91  
Fax (+358-9) 894 9305

industrialsales@vaisala.com  
www.vaisala.com

## SURFACE TEMPERATURE

Sensor mounted on either copper or stainless steel base.  
 Typical applications include radiators, pipes, pumps, motors...

PROBE CODE

**EU** copper base

**EUS** st.st. base



length 18mm, max width 8.5mm

SENSOR	CODE	CABLE CODE	CONNECTOR
Thermistor	U, UU	VS, VL, F	0, 1, 2

## SENSOR TYPES

### Thermistors

Thermistors are metal oxide sensors which provide a larger electrical signal for a given temperature change than any other temperature sensor and, combined with fast response time, are the preferred sensor over operating range -50 to 150°C. The high resistance of thermistor sensors minimises the effect of cable resistance, allowing long cable lengths to be used without causing significant errors. Small size thermistors (code S and SU) are available which are suitable for use in miniature, catheter, and hypodermic needle probes.

CODE	MAX TEMP(°C)	RESISTANCE(@ 25°C)	ACCURACY (@ 0°C to 70°C)
<b>U</b>	150	2K Ohms	±0.2°C

# PRECISION INTERCHANGEABLE NTC THERMISTORS

## standard, precision & ultra precision

Thermistors with interchangeable curves ( $\varnothing$  2,4 mm) are highly accurate, stable devices, designed especially for temperature sensing and control applications. They are particularly suited for uses where there precision interchangeability eliminates the necessity for costly individual circuit calibration. Special types with isolated connections

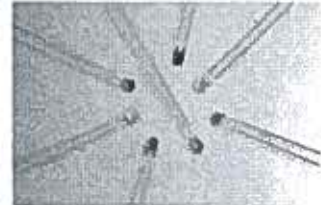
### Features

- High accuracy
- Fast thermal response
- Long life
- R/T Curve-matched
- Epoxy encapsulated
- High stability
- Small size

NTC 0,05°C

### Options

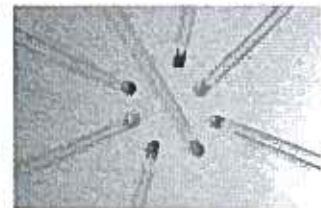
- Special lead materials and lengths
- Special encapsulants or probe housings
- Non-standard resistance values and tolerances



Standard



Precision



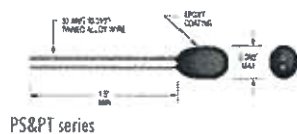
Ultra Precision

### SPECIFICATIONS

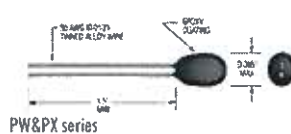
Accuracy
Thermal time constant
Dissipation constant
Maximum power rating
Interchangeability tolerance
Operating temperature
Storage and operation temp. for best long term stability
Dimensions sensor
Dimensions connections

### Ultra precision

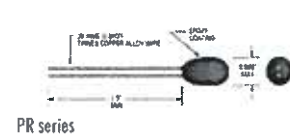
PR series
0.05°C
1 sec. max. in a well stirred oil bath 10 sec. max. in still air
1 mW/°C
30 mW at 25°C derated to 1 mW at 125°C
±0.05°C from 0..50°C
-55°C..+80°C
-55°C..+50°C
Ø 2,4 mm
L=38 mm, Ø 0,25 mm



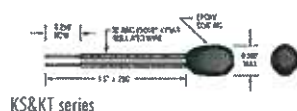
PS&PT series



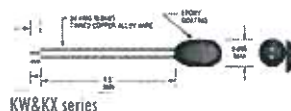
PW&PX series



PR series



KSR&KT series



KW&KX series



## Appendix C

# Detailed description of measurement locations

The position of the measurement equipment described in section 4.4.2 is described in more detail in the table presented below.

**Table C.1** – Detailed description of the measurement locations.

<b>Position</b>	<b>Description</b>	<b>Physical Parameters</b>
1. Location of neonate	In the center of the incubator, at a height of 0.10m	Air Temperature Relative Humidity Air Velocity
2. Next to incubator sensor	0.05m at the left of the incubator's T and RH sensor	Air Temperature Relative Humidity
3. Outside and inside of incubator hood	In the center of the hood, on top of the hood and on the inside of the hood	Surface Temperature
4. Inside of porthole	On the inside on the middle of the porthole furthest away from the incubator sensor	Surface Temperature

## Appendix D

# Mesh refinement analysis

This appendix goes into more depth about the mesh analysis. Because the wall lift-off (m) and wall lift-off in viscous units plots in section 5.1 showed adequate results, the flow profiles between the two meshes have not been compared. On top of that, since the temperature and relative humidity distribution are mainly influenced by the flow profile, they are more insightful to plot because they provide information on the adequateness of the mesh on the flow profile as well. Two result plots of the temperature and relative humidity have been compared between the normal-sized mesh and the fine-sized mesh. They are presented in the Figures below. Small differences are observed. The average temperature air temperature differs  $\pm 0.004$  °C after five minutes. The average relative humidity at several points around the neonate differ  $\pm 0.2\%$ . Because differences are small, the normal-sized mesh is used in the simulations. This also reduces computation time ( $\pm 8$  hours vs  $\pm 24$  hours).

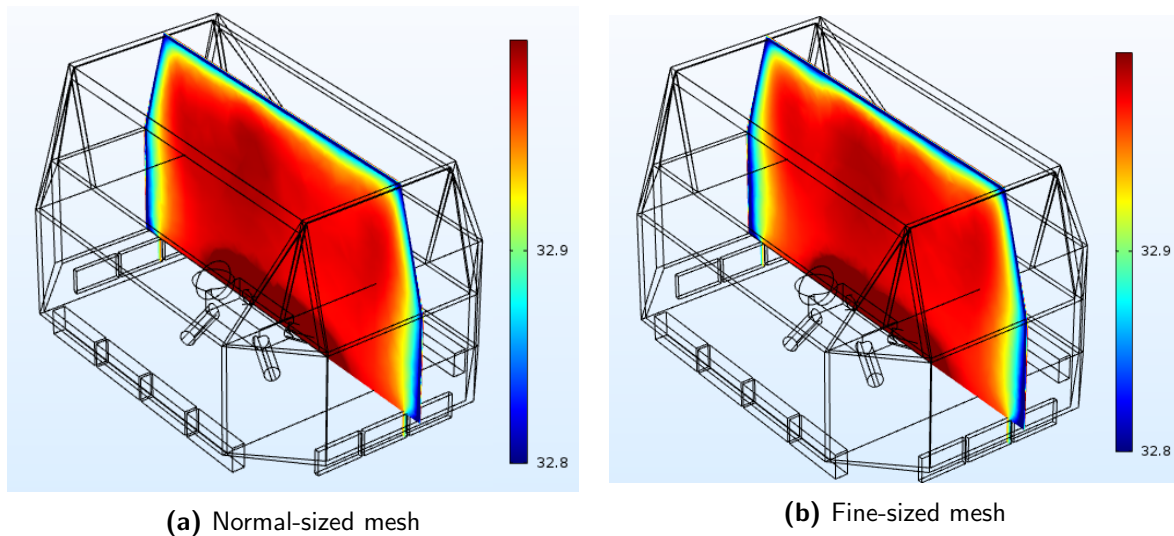
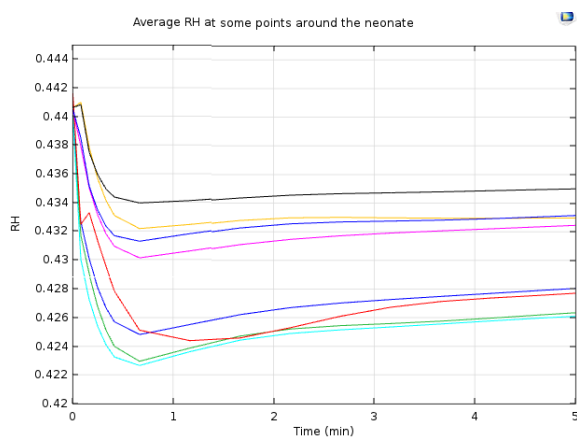
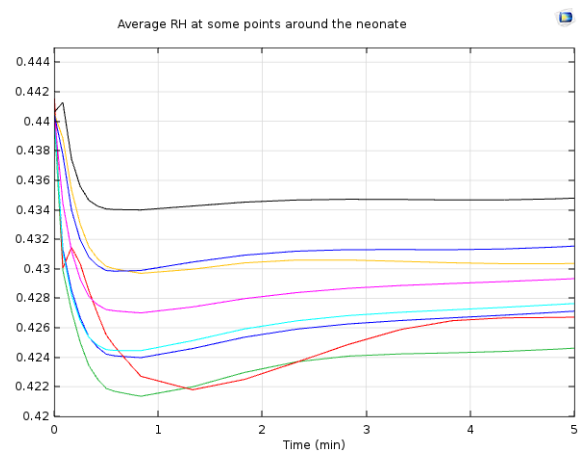


**Figure D.1** – Temperature slice plots (°C) at t=5min. Figure D.1a shows the results for the normal-sized mesh. Figure D.1b represents the results for the fine-sized mesh. No notable differences are observed.



(a) Normal-sized mesh



(b) Fine-sized mesh

**Figure D.2** – Relative humidity at different points around the neonate. Figure D.2a shows the results for a the normal-sized mesh. Figure D.2b represents the results for a=the fine-sized mesh. Small differences of  $\pm 0.2\%$  are observed.

# Appendix E

## Simulation graphs

### E.1 Scenario 1: Incubator setpoint 33°C-45% RH

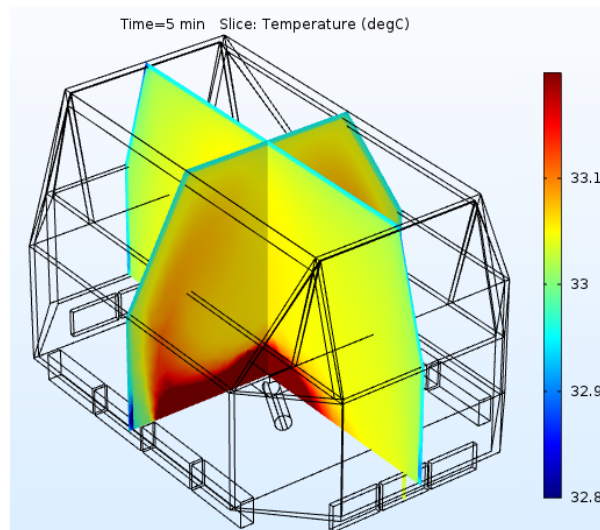


Figure E.1 – Temperature slice plot at t=5 min.

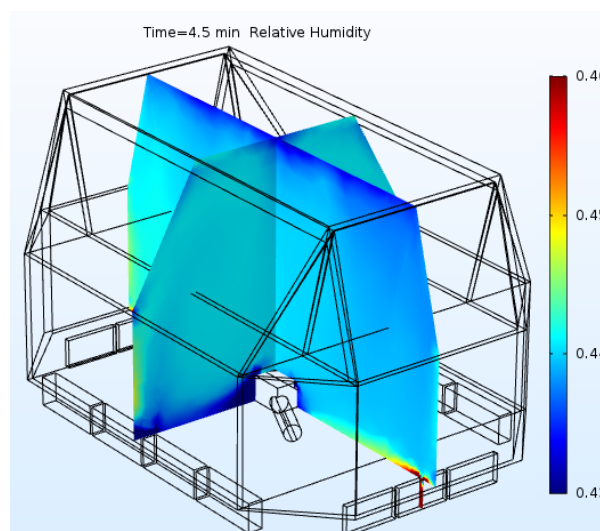
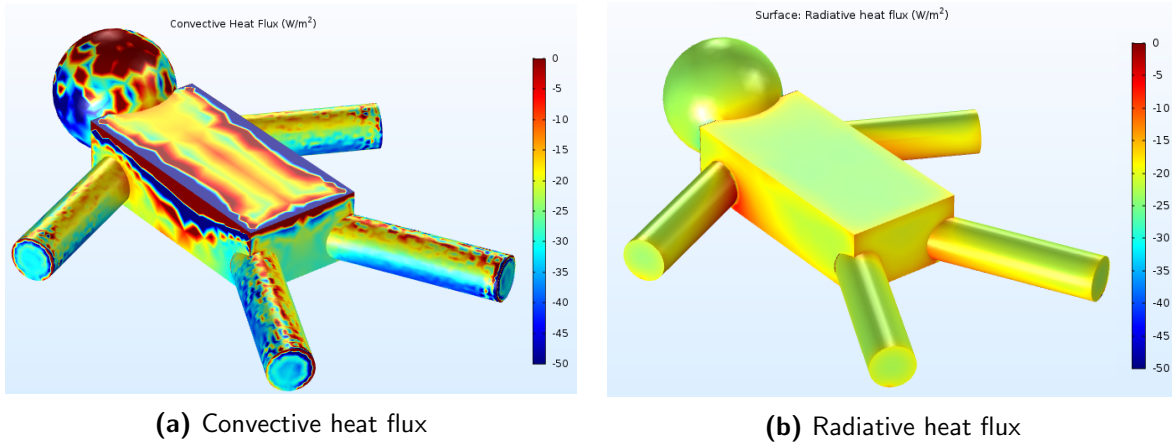
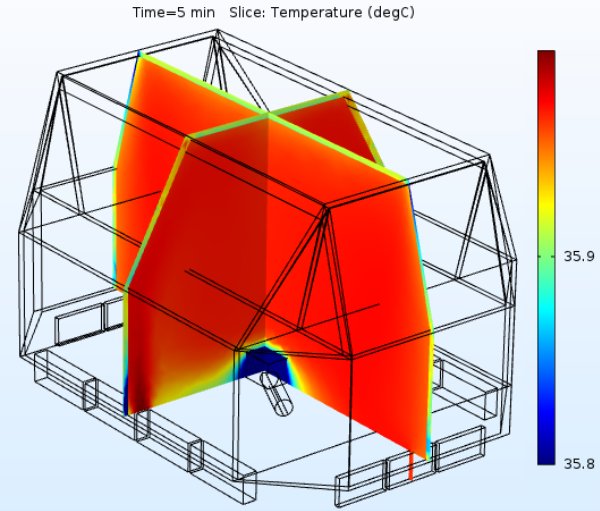


Figure E.2 – RH slice plot at t=4.5 min.



**Figure E.3** – Time-averaged convective (a) and radiative (b) heat flux surface plots for scenario 1: incubator setpoint 33°C - 45% RH.

**E.2 Scenario 2: Incubator setpoint 36°C-70% RH**



**Figure E.4** – Temperature slice plot at t=5 min.

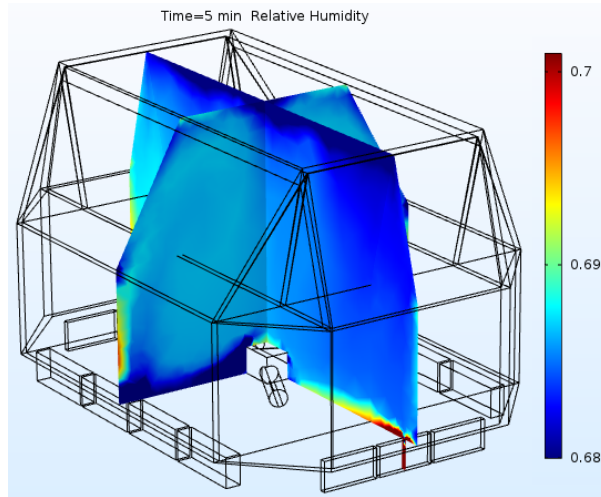
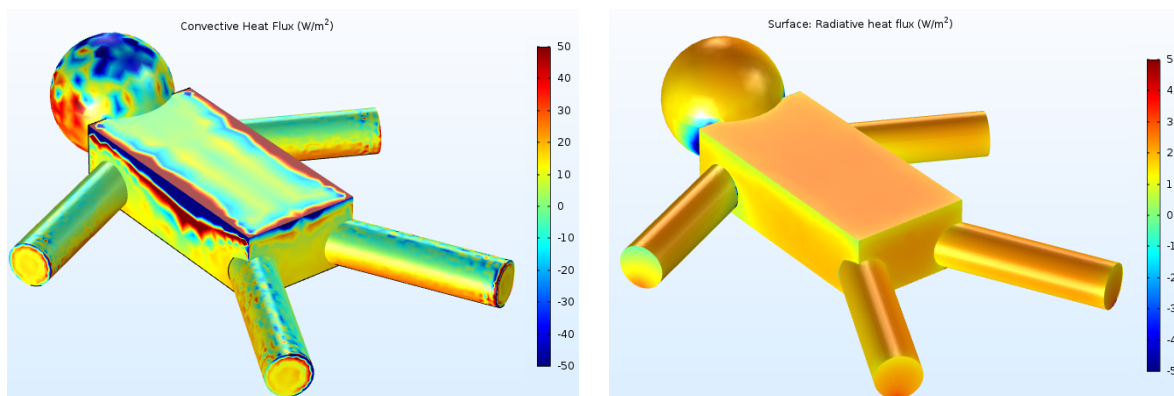


**Figure E.5** – RH slice plot at t=5 min.



**(a)** Convective heat flux

**(b)** Radiative heat flux

**Figure E.6** – Time-averaged convective (a) and radiative (b) heat flux surface plots

# Appendix F

## All measurement results Dräger Caleo™

All incubator measurements done on the Dräger Caleo™ are shown in this appendix. The first section addresses all air and relative humidity measurements while the second section addresses the surface temperature measurements. The time at which the incubator was closed is indicated by a vertical black dashed line.

### F.1 Climate chamber setpoint: 25°C-45% RH

#### F.1.1 Air temperature and relative humidity

Incubator setpoint 34°C-50% RH

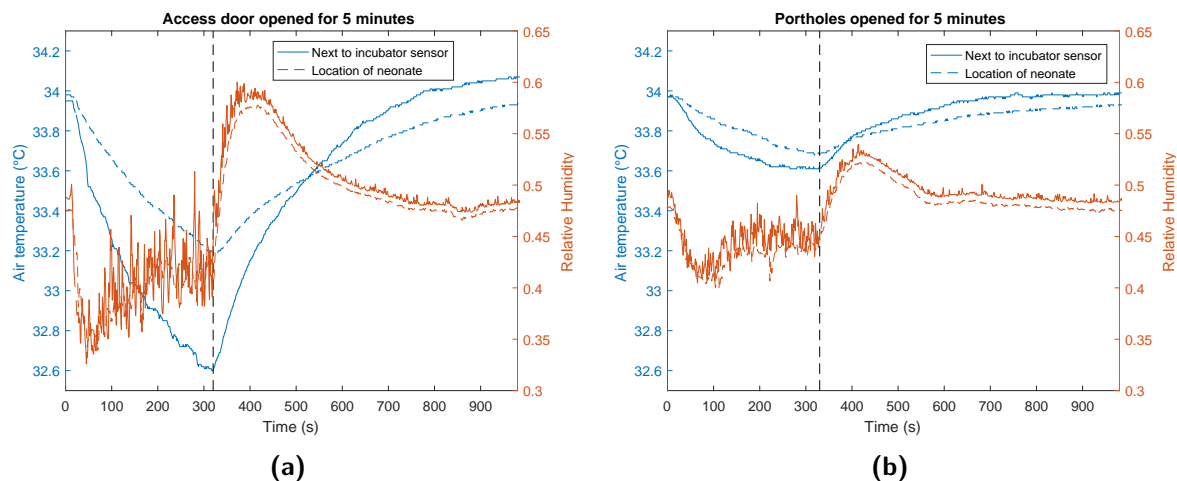


Figure F.1

### Incubator setpoint 36°C-70% RH

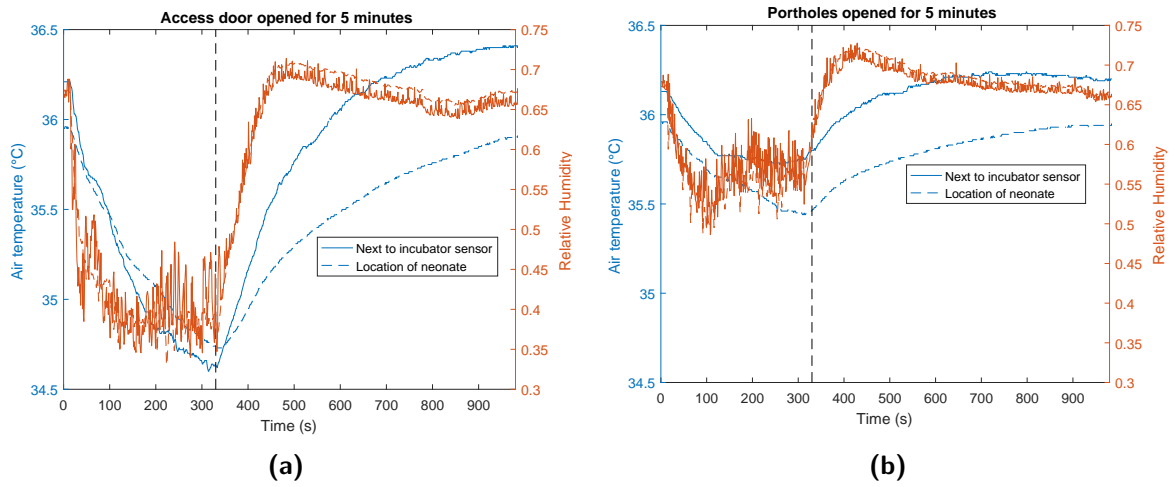


Figure F.2

### Incubator setpoint 38°C-99% RH

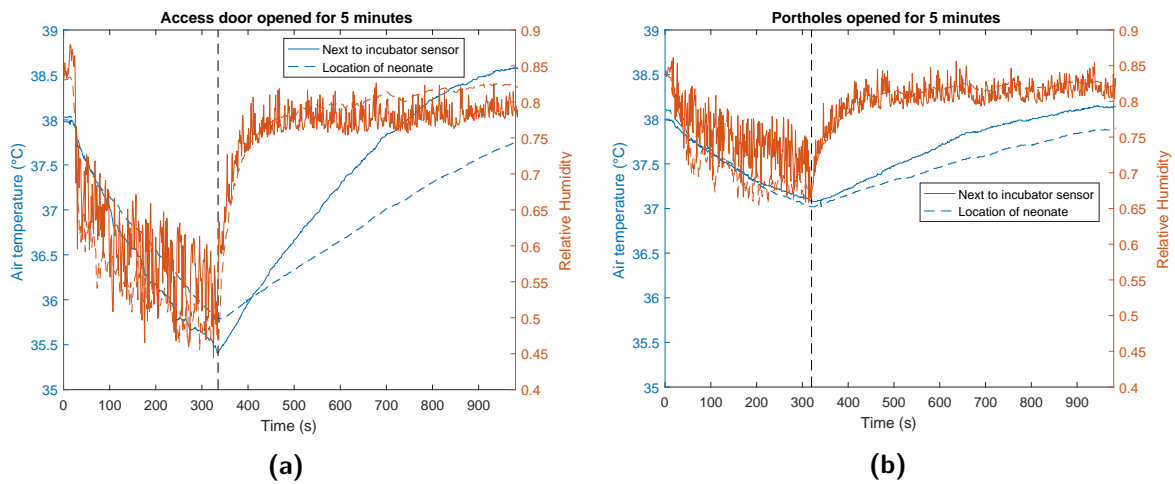


Figure F.3



### F.1.2 Surface temperature

Incubator setpoint 34°C-50% RH

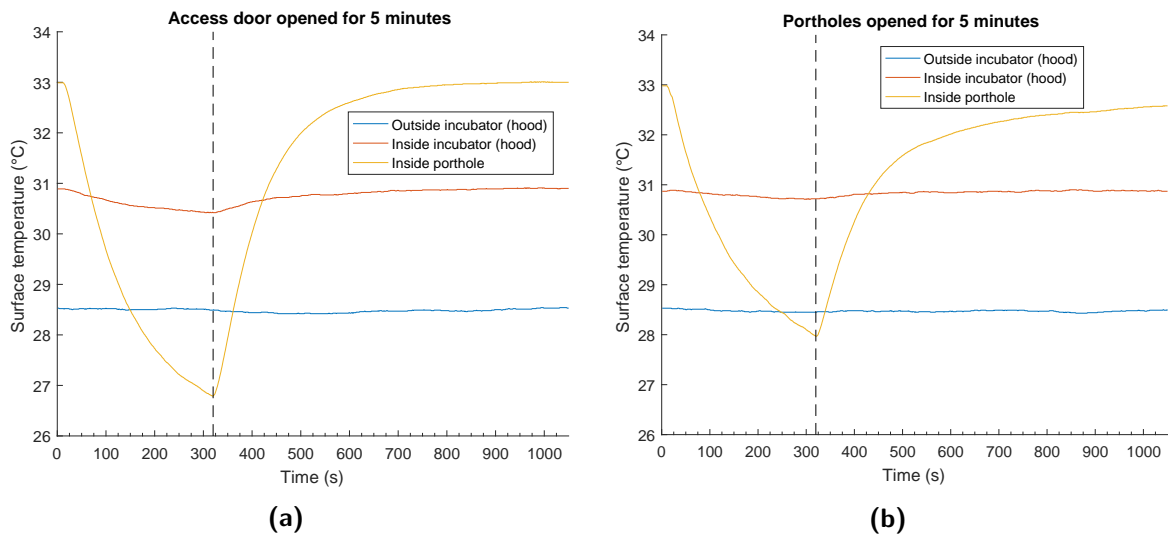


Figure F.4

### Incubator setpoint 36°C-70% RH

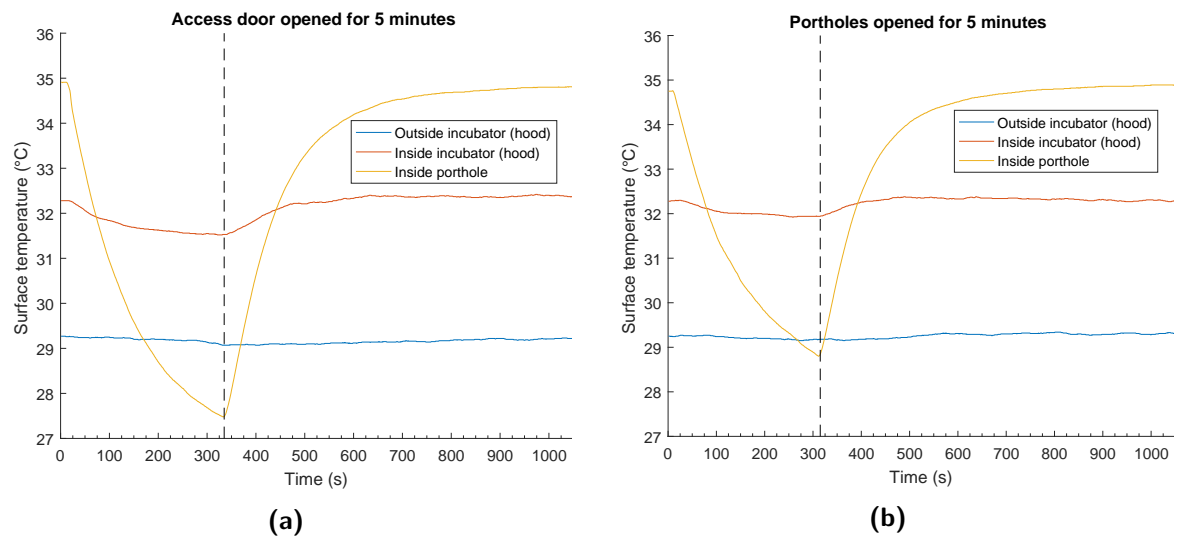


Figure F.5

# Incubator setpoint 38°C-99% RH

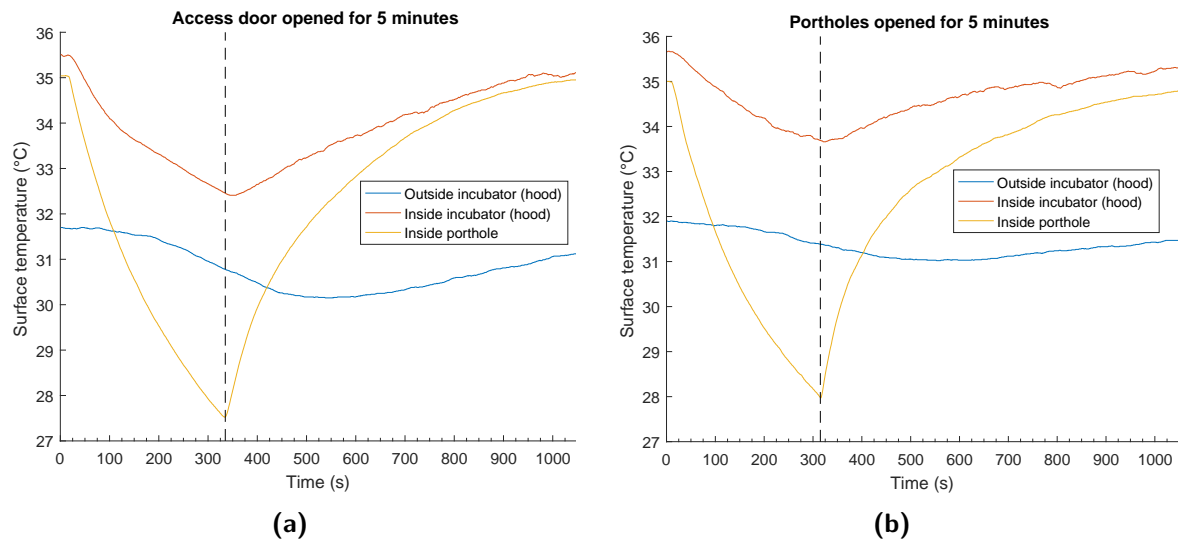


Figure F.6

## F.2 Incubator setpoint: 36°C-70% RH

### F.2.1 Air temperature and relative humidity

Climate chamber setpoint 21°C-45% RH

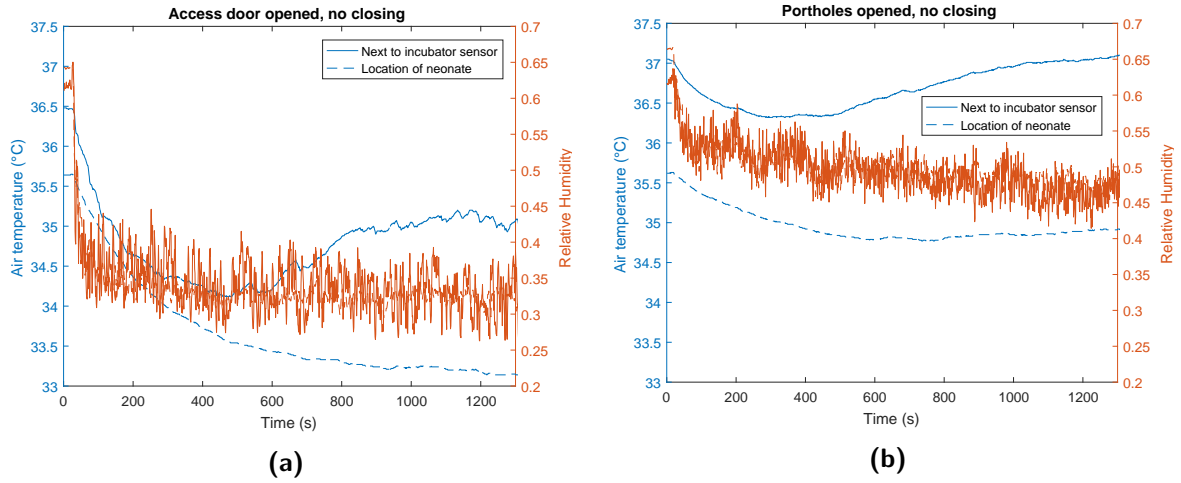


Figure F.7

Climate chamber setpoint 21°C-60% RH

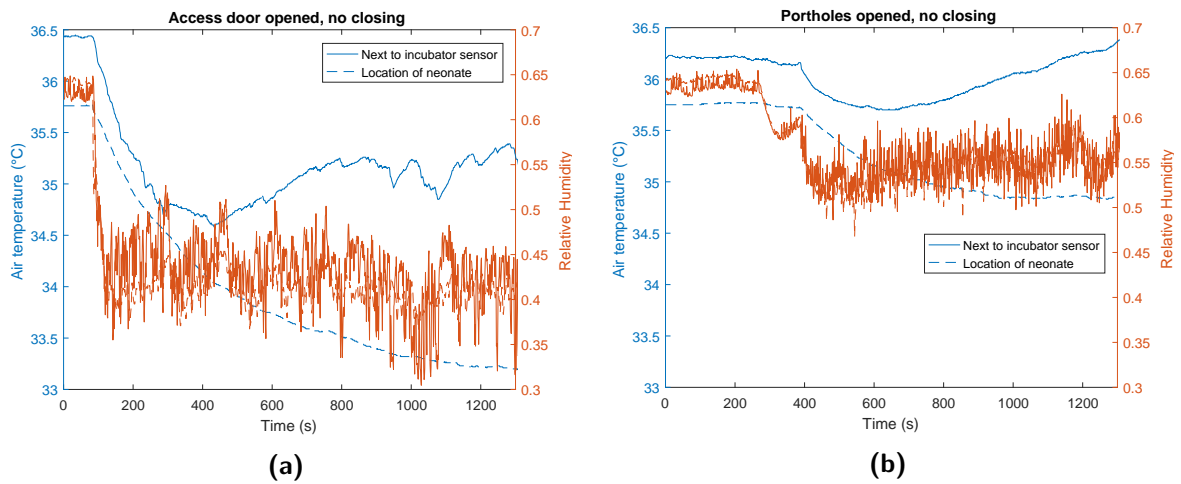


Figure F.8

## F.2.2 Surface temperature

Climate chamber setpoint 21°C-45% RH

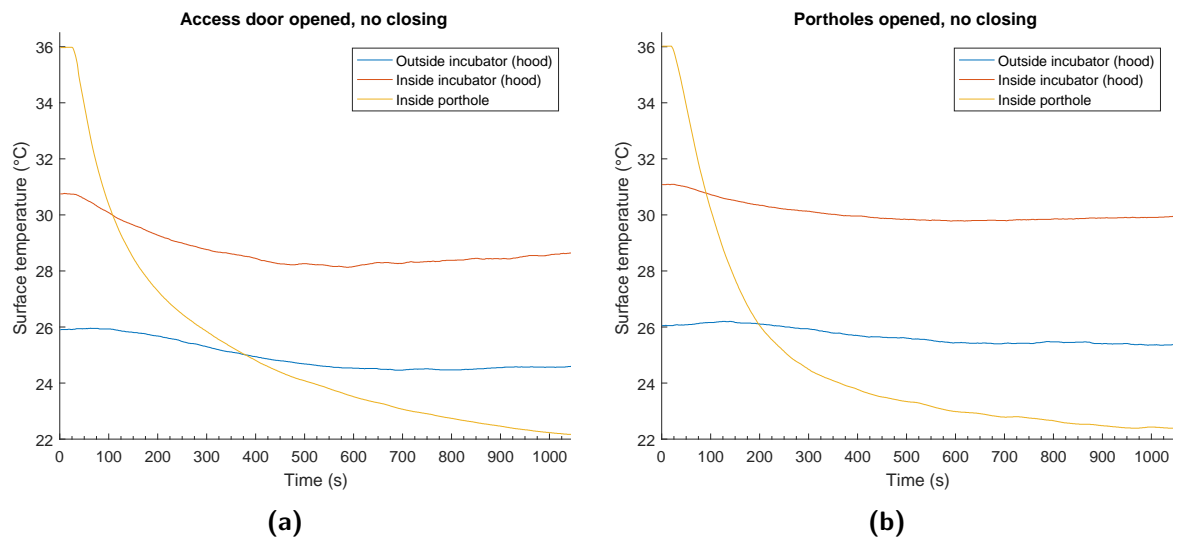


Figure F.9

Climate chamber setpoint 21°C-60% RH

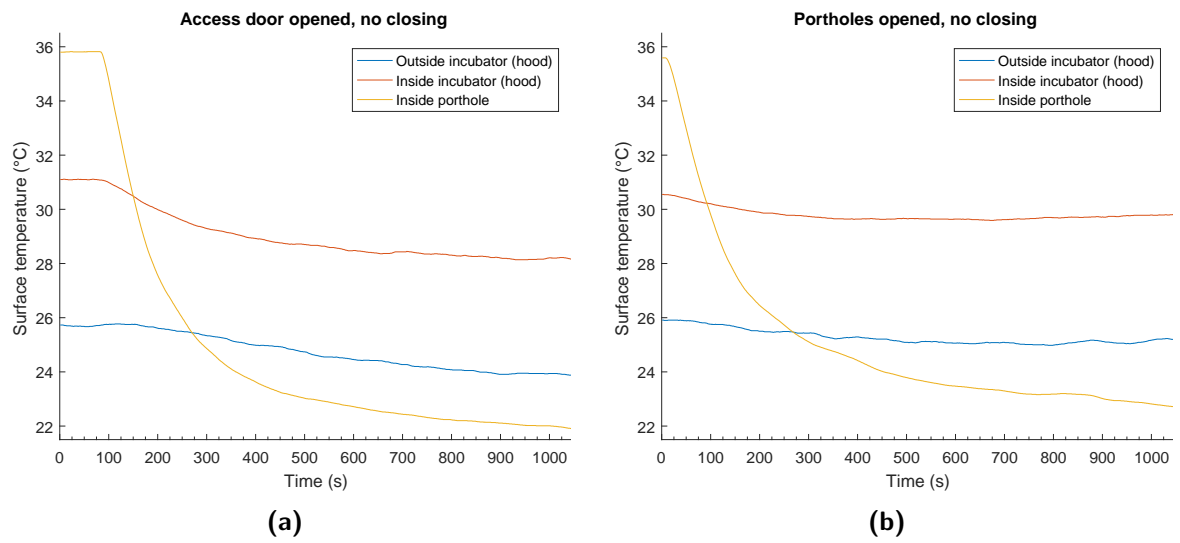


Figure F.10

## Appendix G

# All measurement results GE Giraffe Carestation

All incubator measurements done on the GE Giraffe Carestation are shown in this appendix. The first section addresses all air and relative humidity measurements while the second section addresses the surface temperature measurements. The time at which the incubator was closed is indicated by a dashed vertical black line.

### G.1 Air temperature and relative humidity

Setpoint 28°C-70% RH

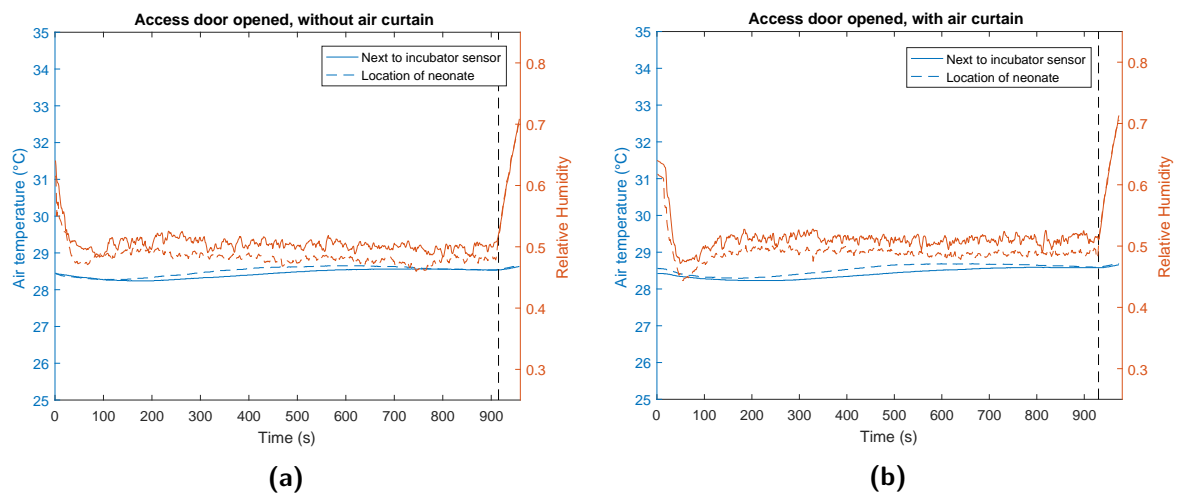
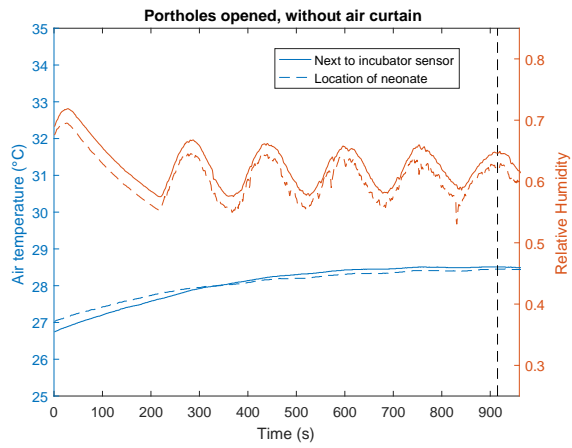
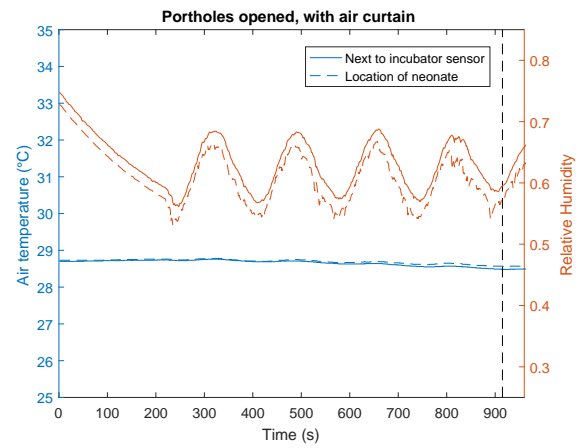


Figure G.1



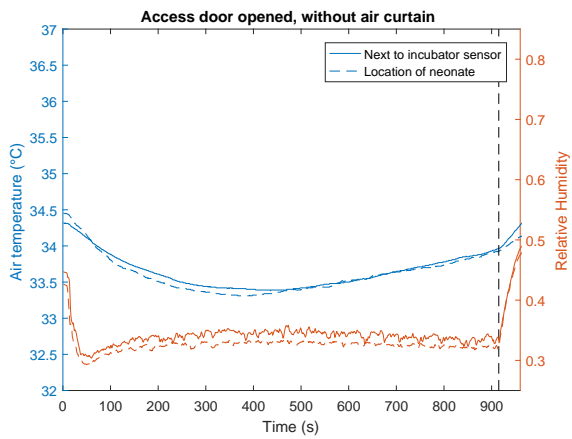
(a)



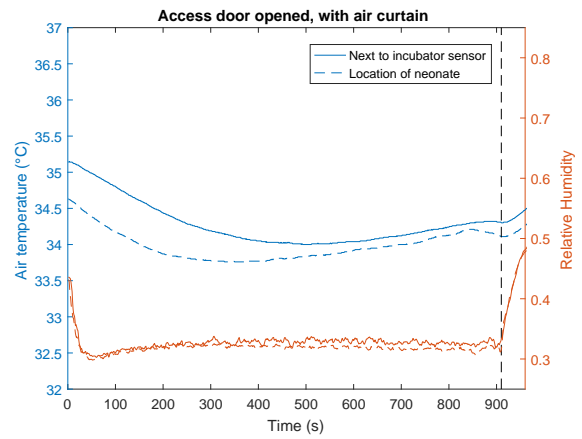
(b)

Figure G.2

Setpoint 34°C-50% RH

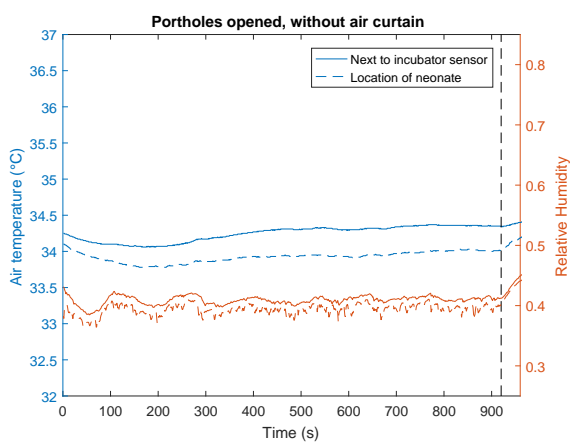


(a)

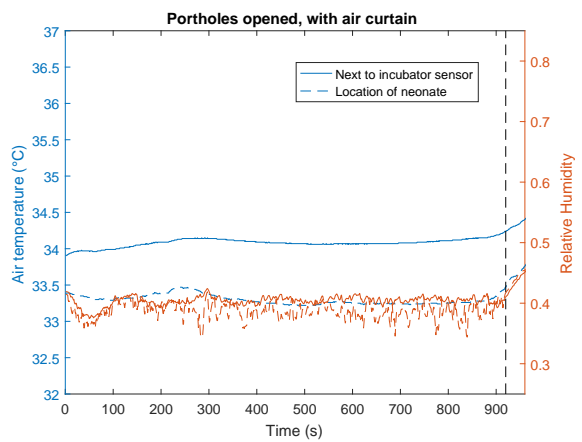


(b)

Figure G.3



(a)



(b)

Figure G.4

## Setpoint 34°C-70% RH

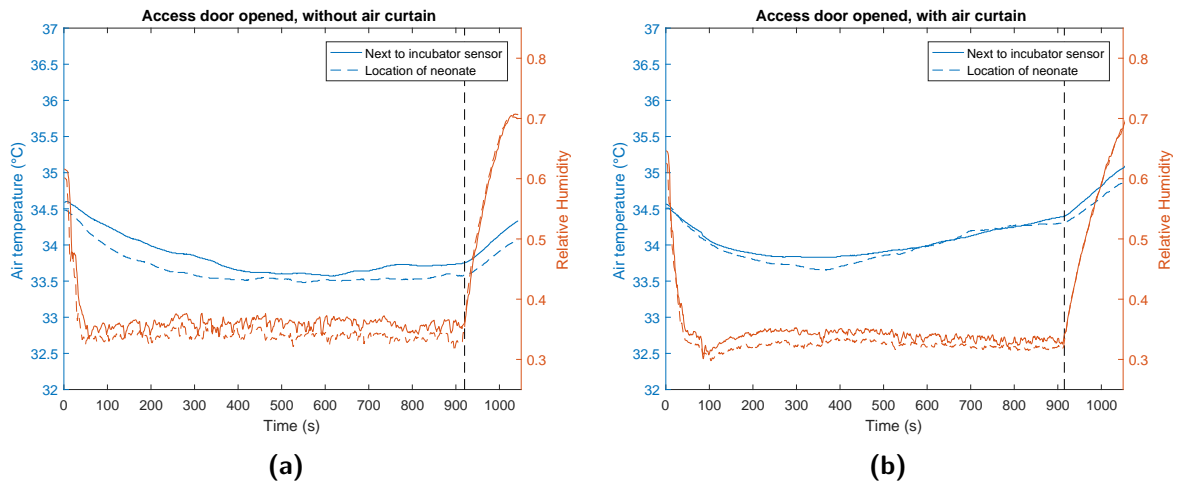


Figure G.5

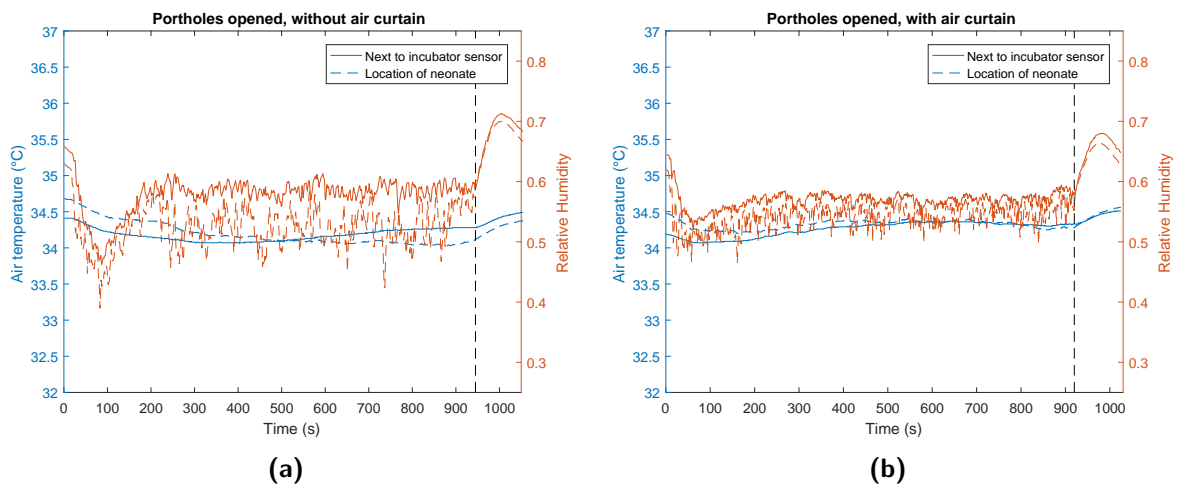


Figure G.6

# Setpoint 34°C-99% RH

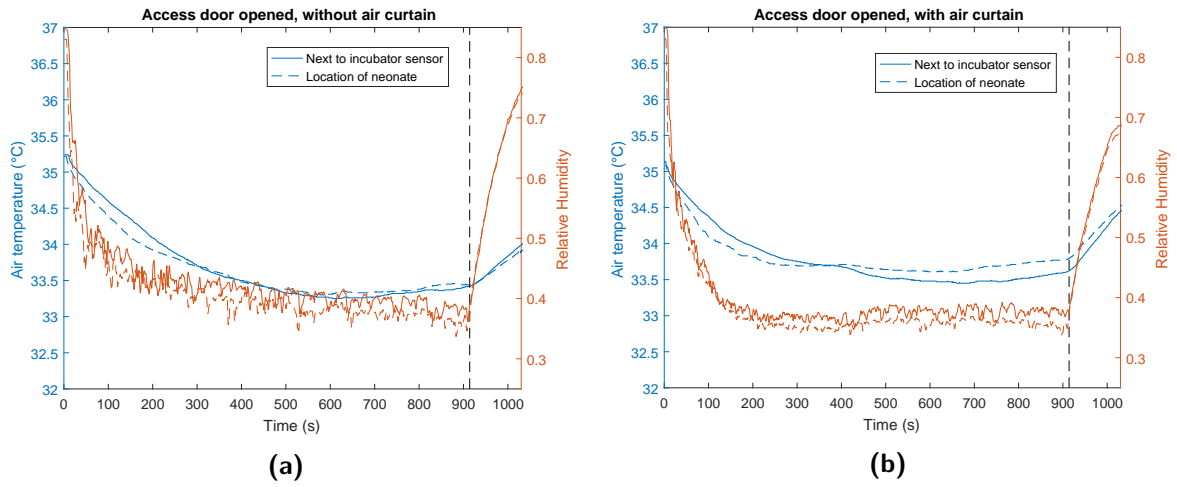


Figure G.7

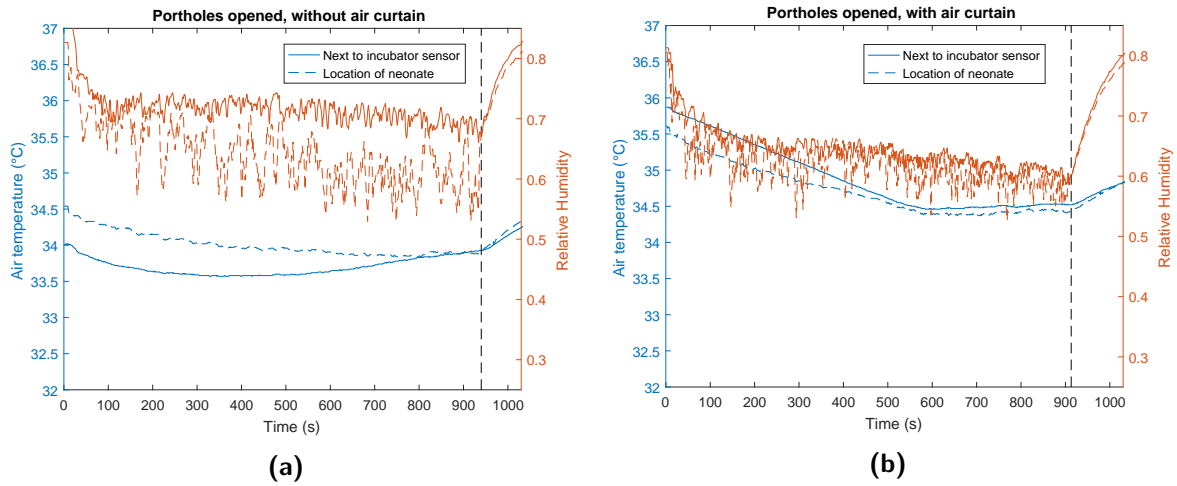


Figure G.8



# Setpoint 36°C-70% RH

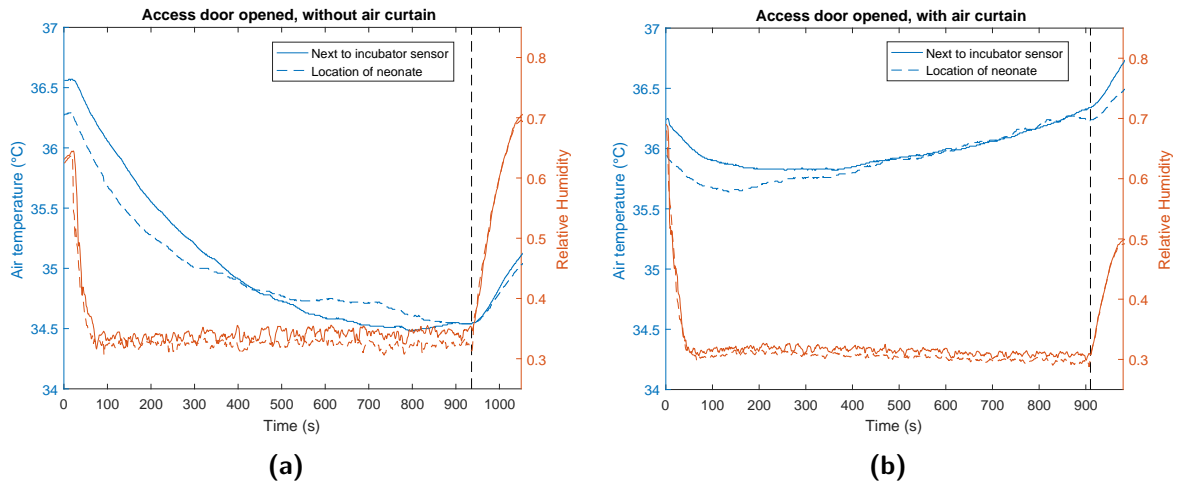


Figure G.9

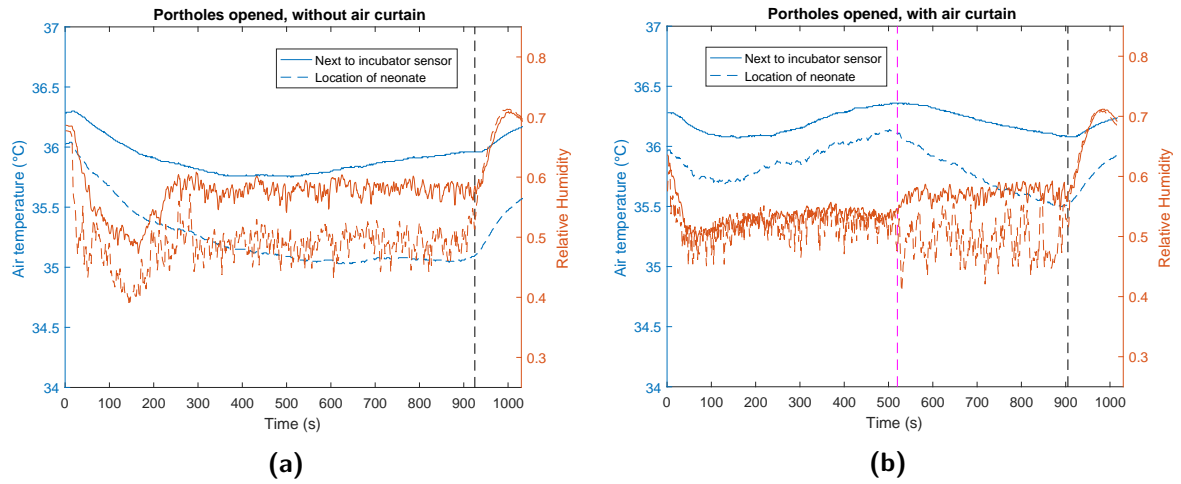


Figure G.10

# Setpoint 38°C-50% RH

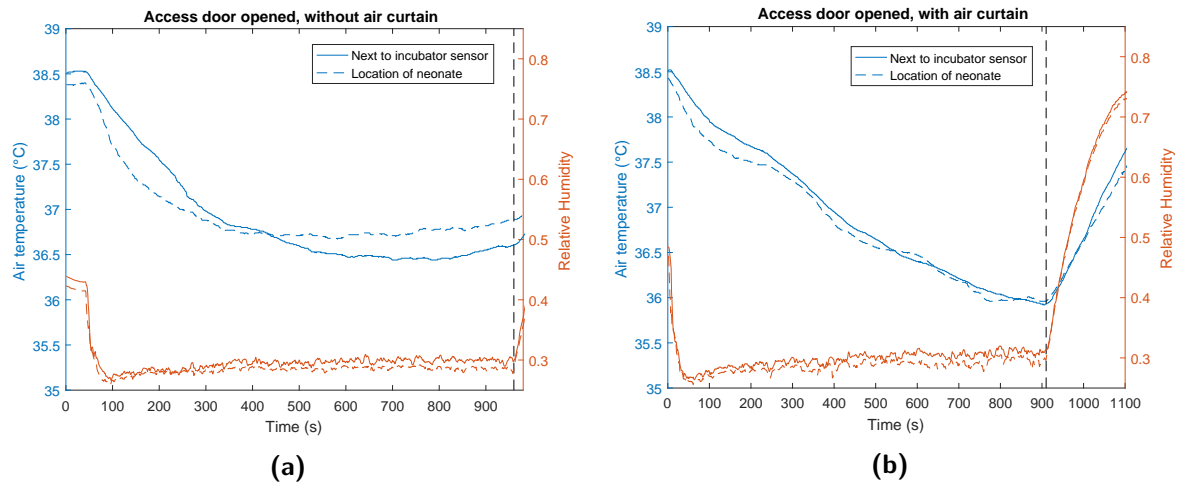


Figure G.11

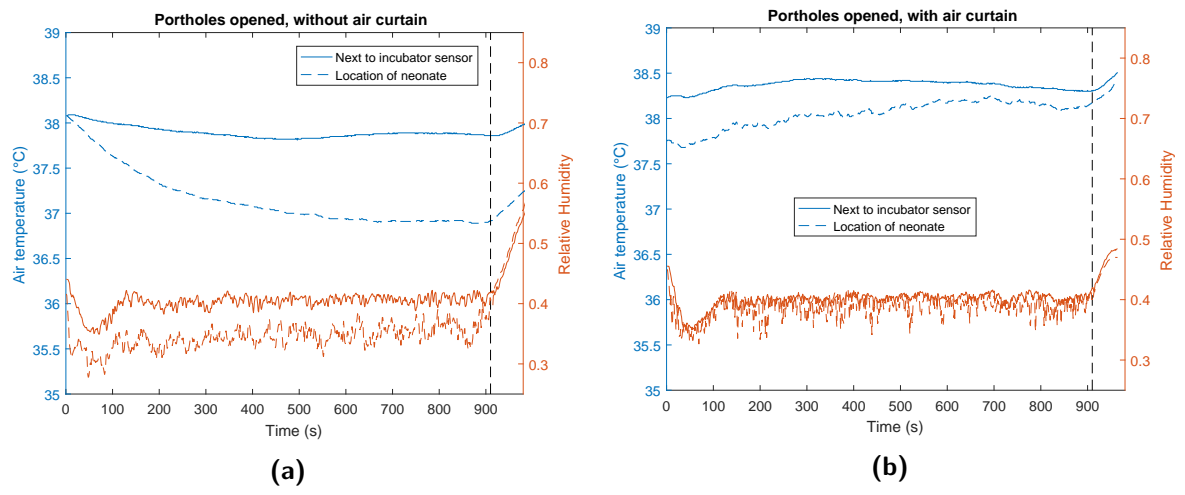


Figure G.12

# Setpoint 38°C-99% RH

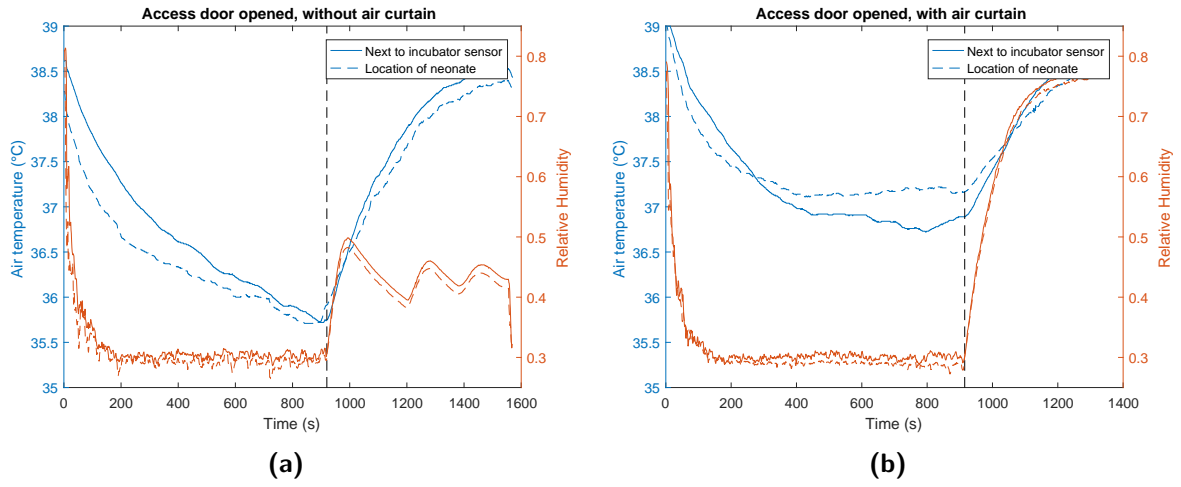


Figure G.13

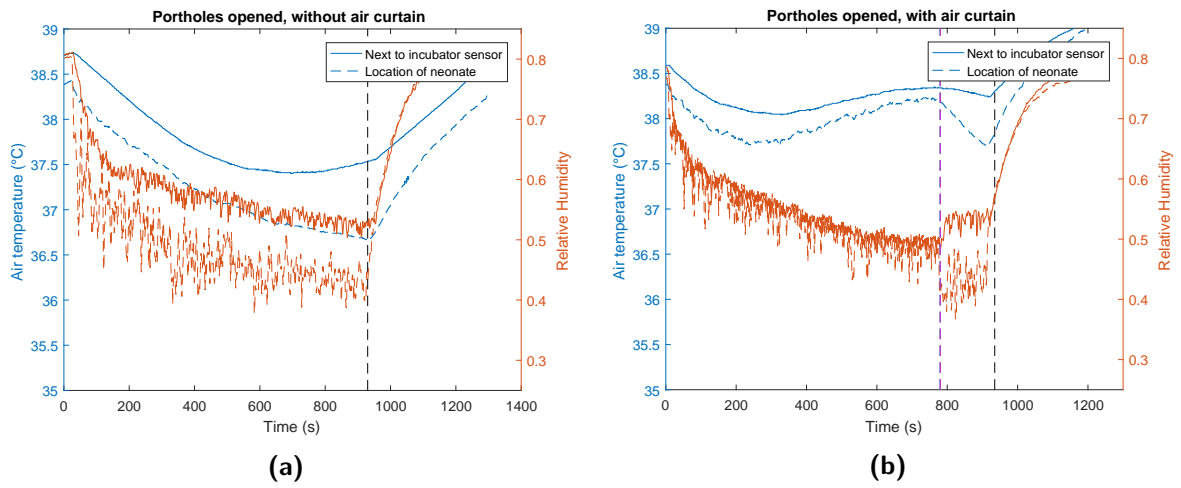


Figure G.14

## G.2 Surface temperature

Setpoint 28°C-70% RH

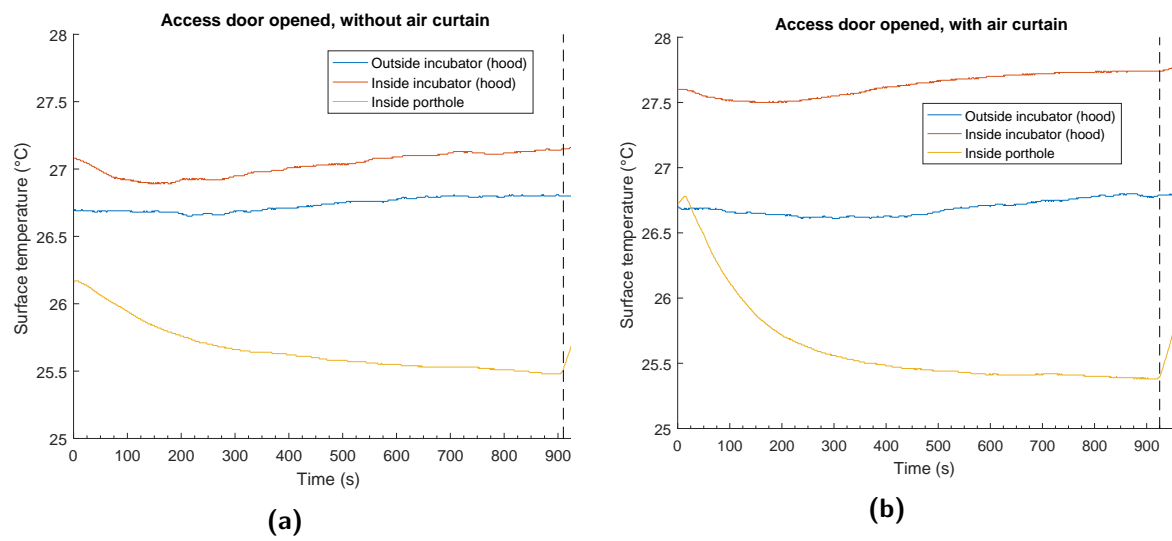


Figure G.15

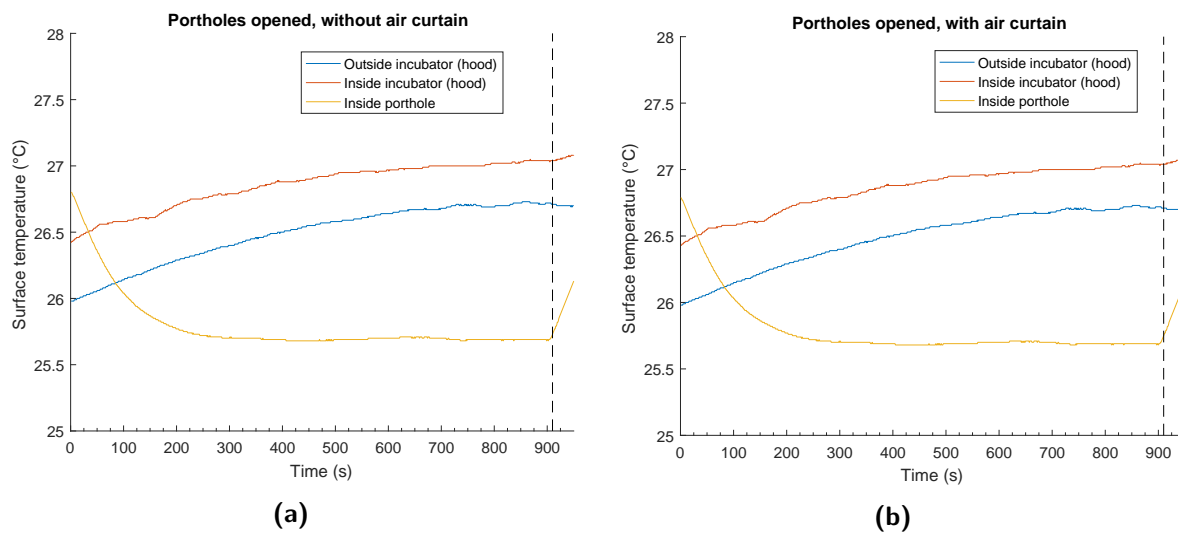


Figure G.16

Setpoint 34°C-50% RH

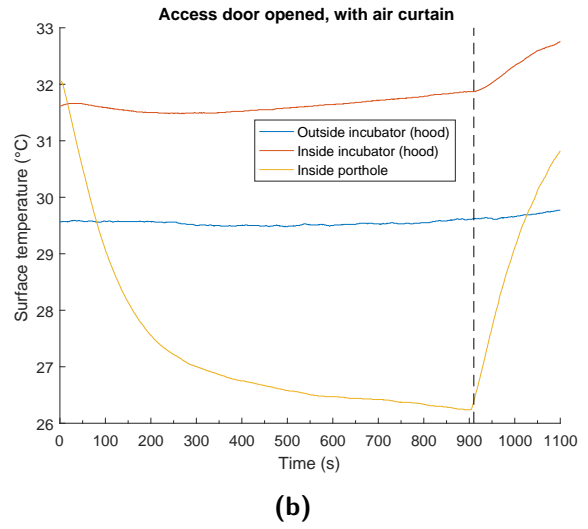
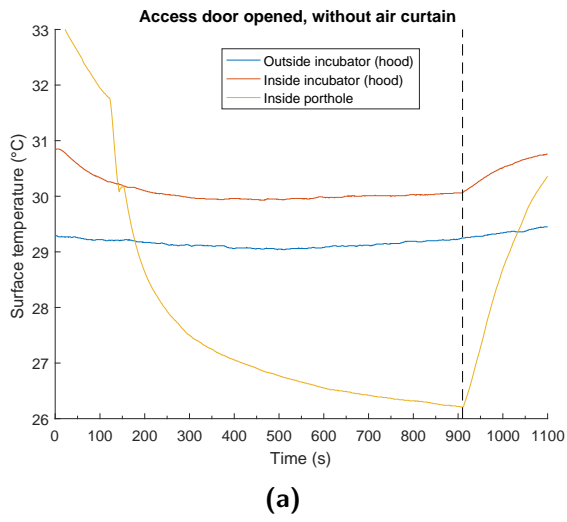


Figure G.17

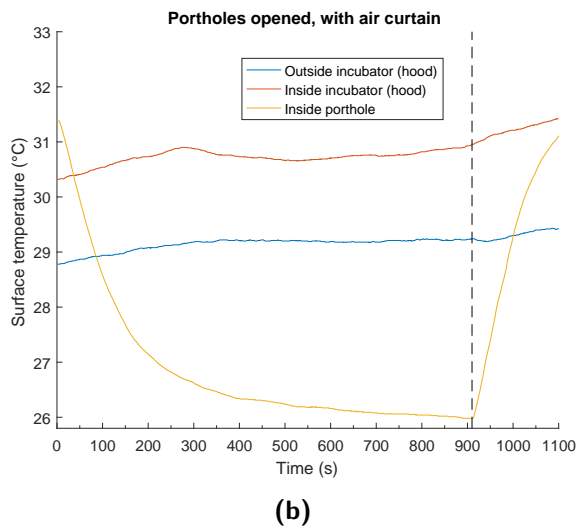
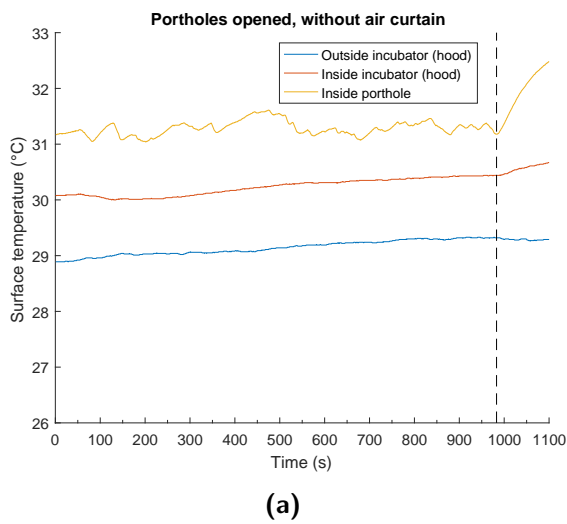


Figure G.18

# Setpoint 34°C-70% RH

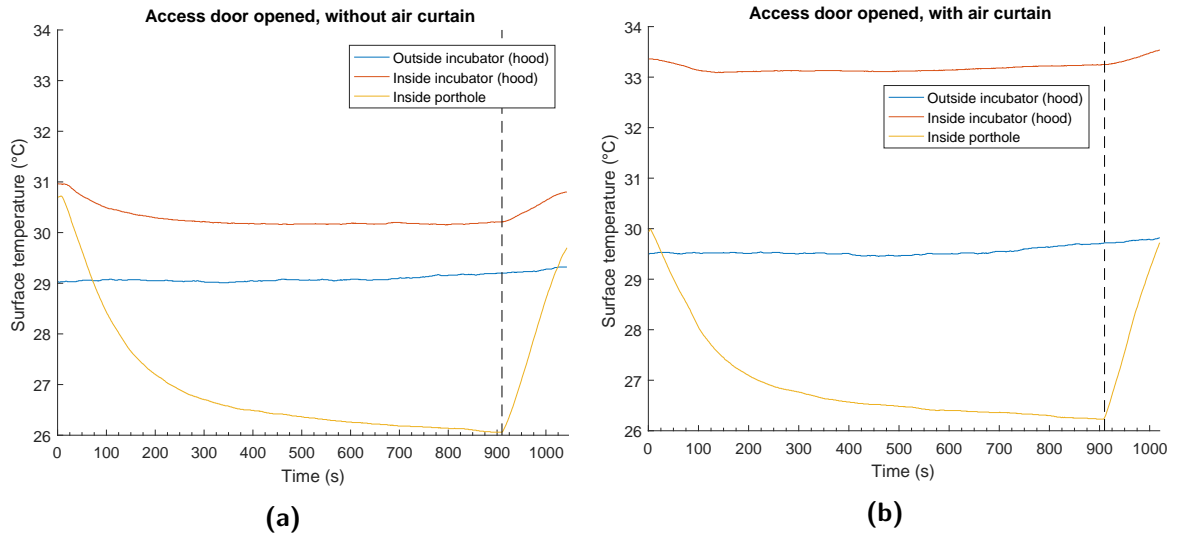


Figure G.19

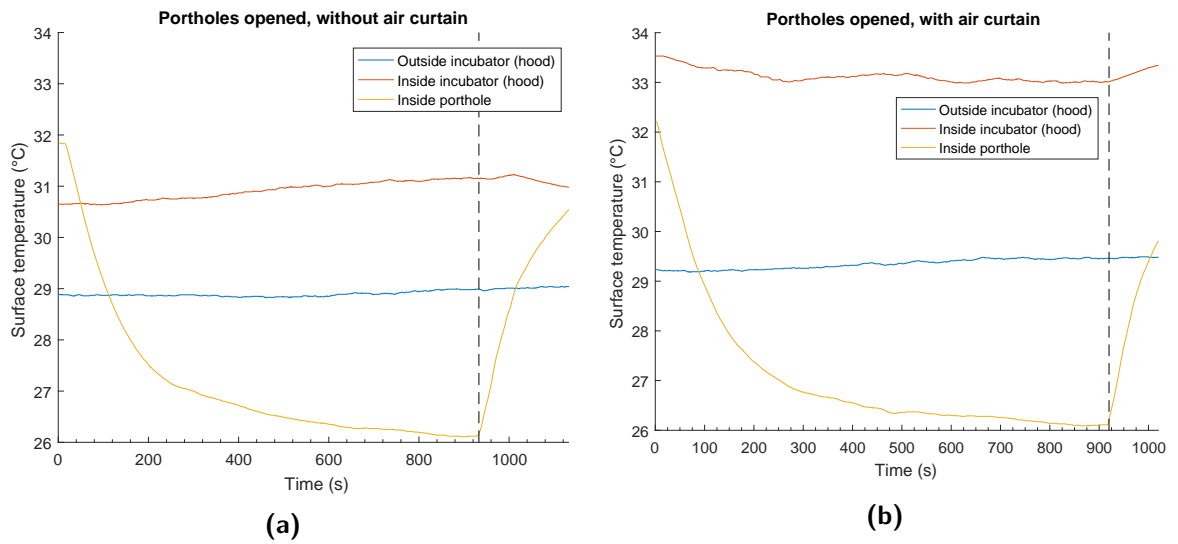
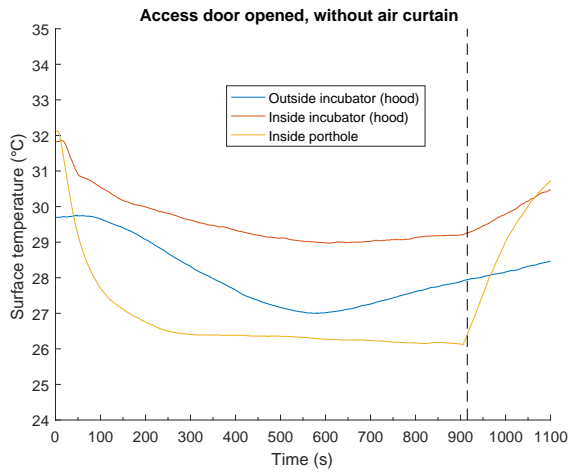
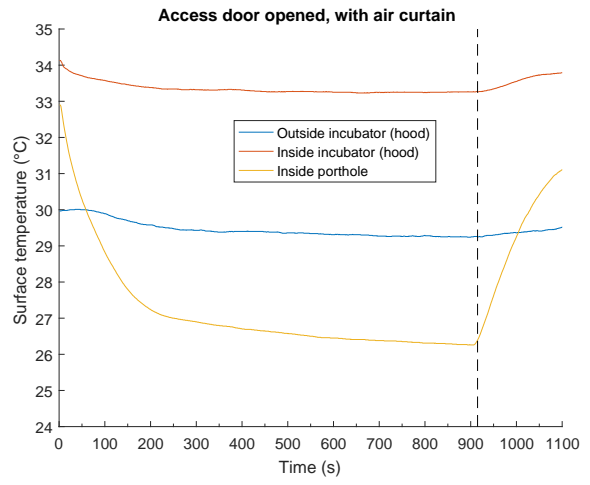


Figure G.20

Setpoint 34°C-99% RH

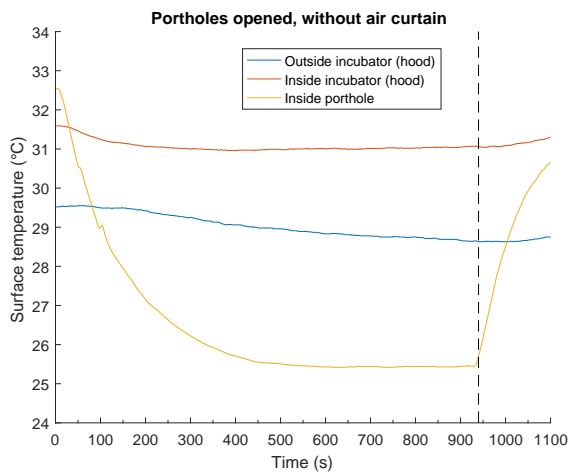


(a)

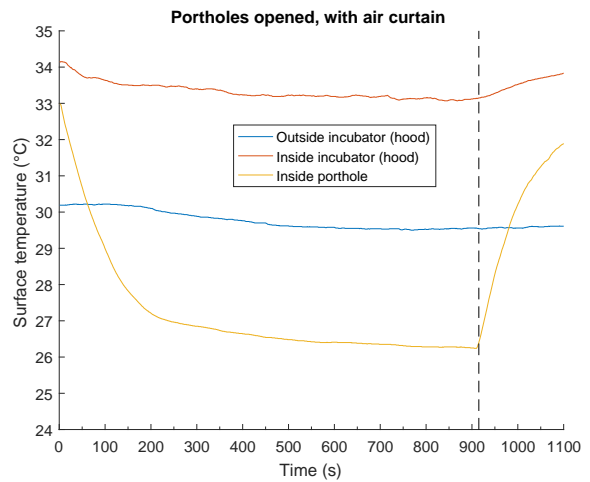


(b)

Figure G.21



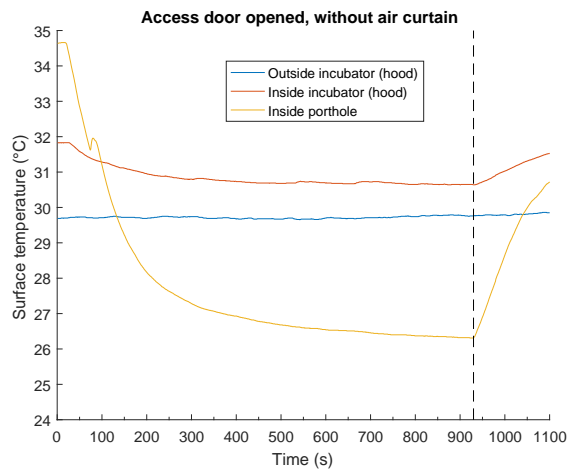
(a)



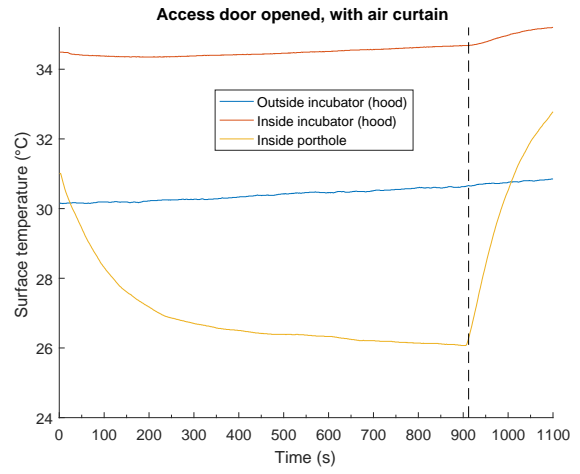
(b)

Figure G.22

Setpoint 36°C-70% RH

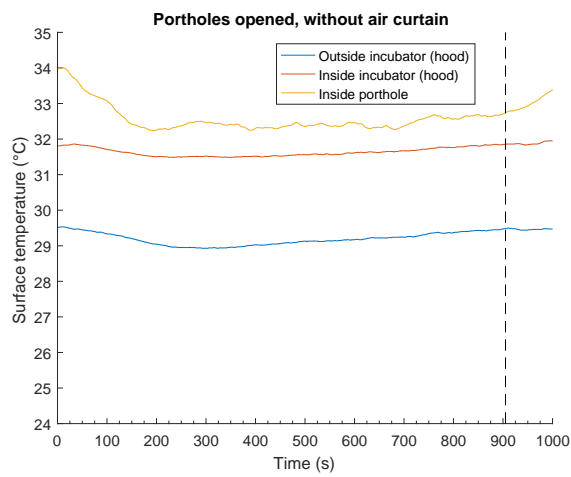


(a)

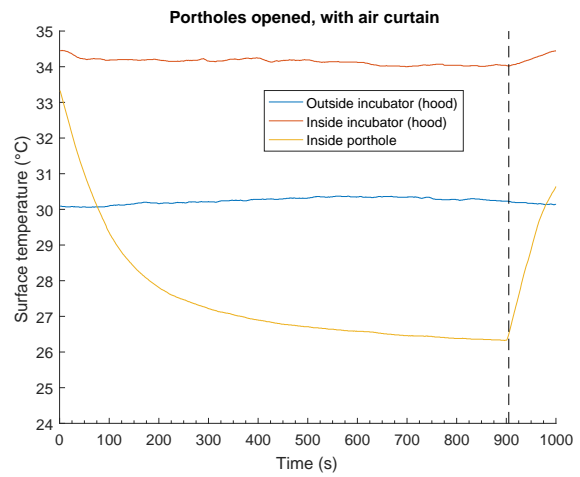


(b)

Figure G.23



(a)



(b)

Figure G.24



# Setpoint 38°C-50% RH

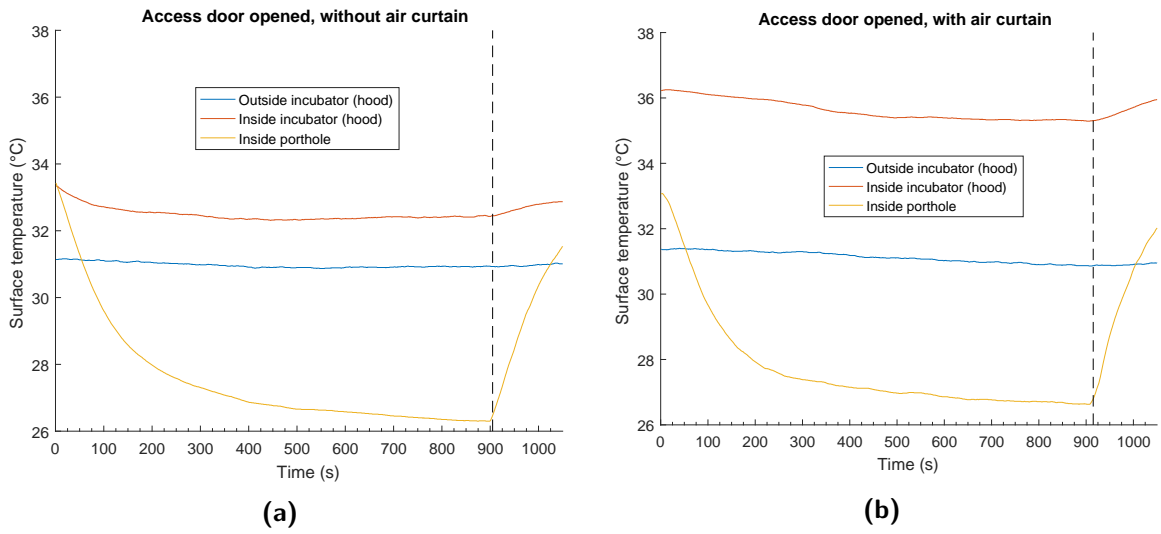


Figure G.25

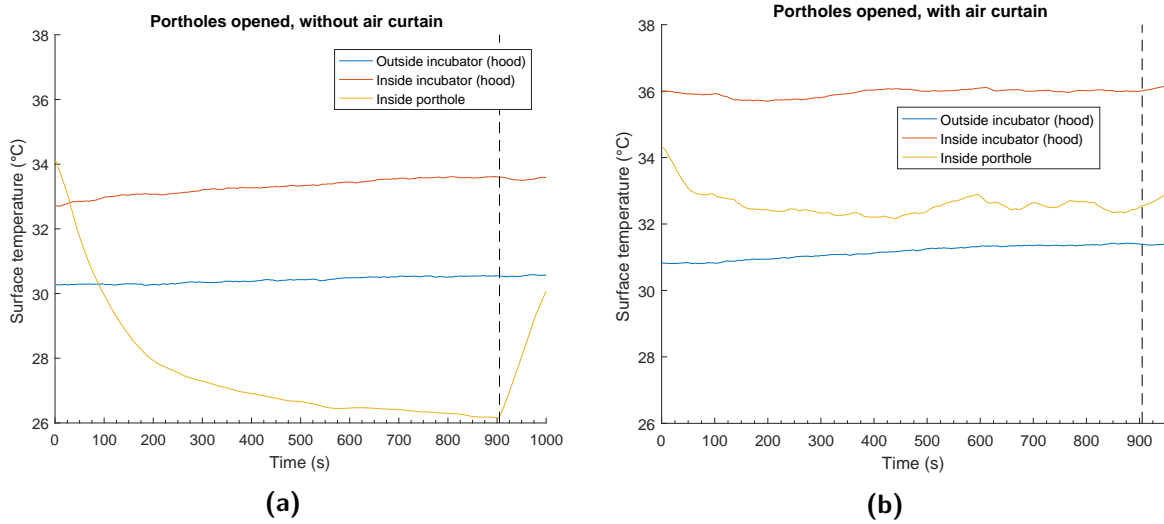


Figure G.26

# Setpoint 38°C-99% RH

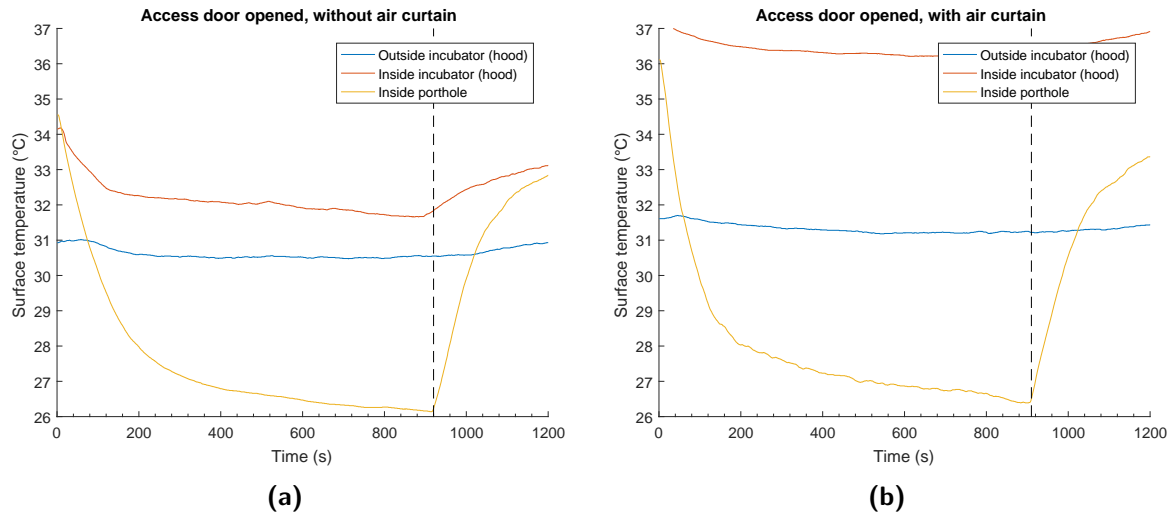


Figure G.27

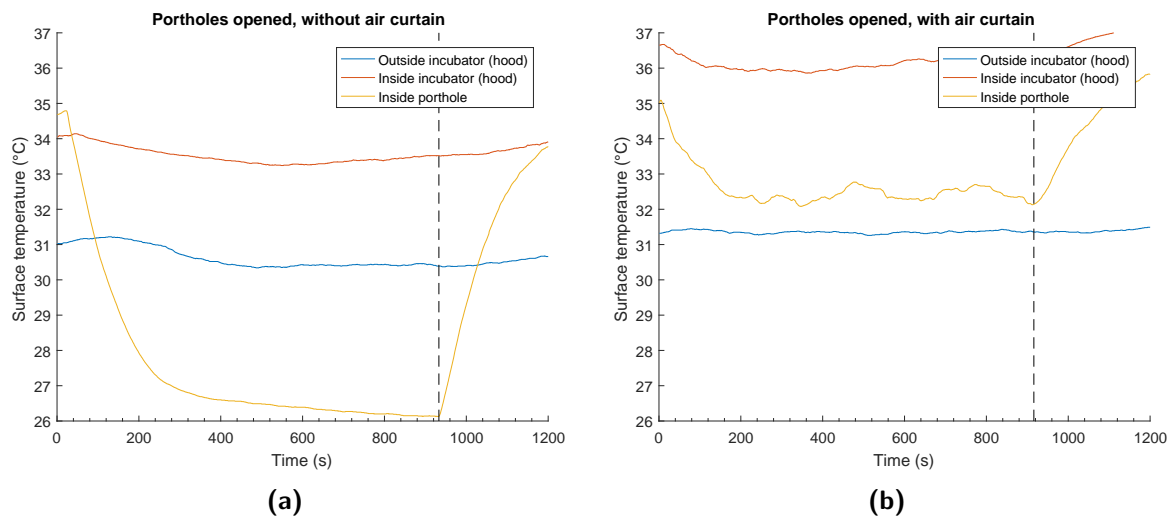
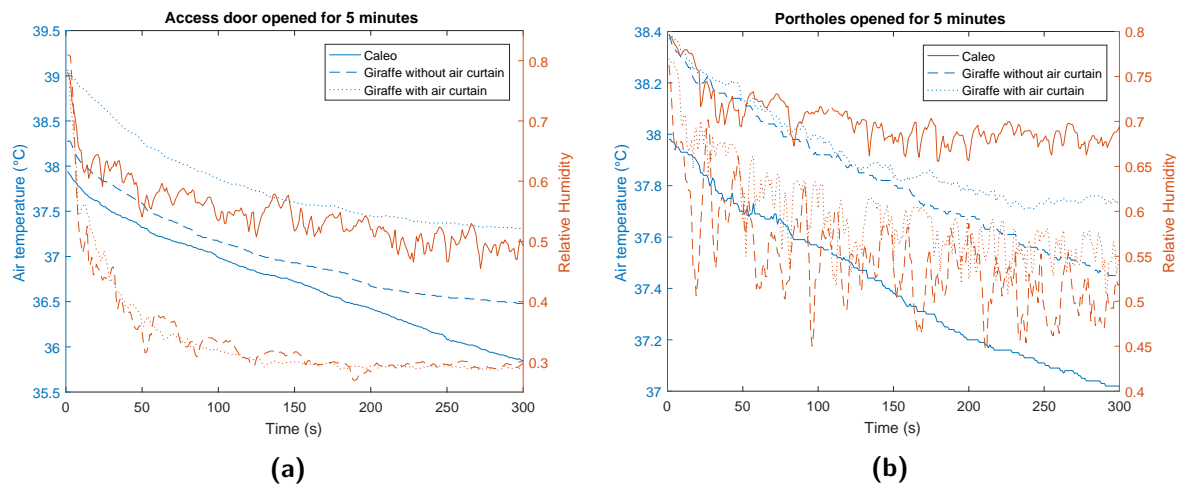


Figure G.28

## Appendix H

# Comparison Dräger Caleo<sup>TM</sup> and GE Giraffe Carestation

Incubator settings 38°C-99%RH



**Figure H.1** – Comparison between the Dräger Caleo<sup>TM</sup> and the GE Giraffe carestation. The air temperature and relative humidity at the location of the neonate are presented. Figure (a) shows the results of opening the access door for 5 minutes and Figure (b) shows the results of opening the portholes for five minutes.

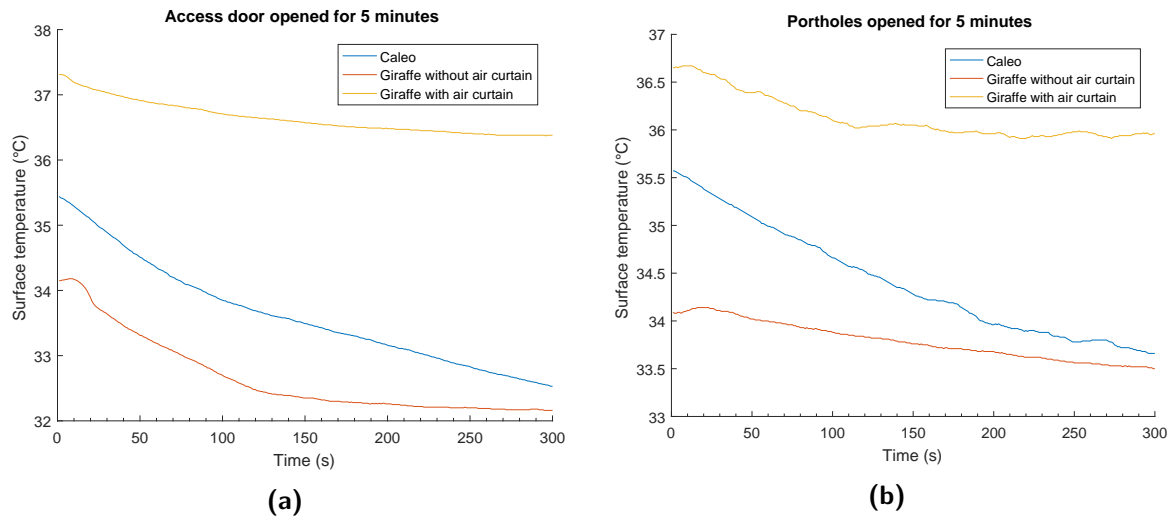


**Figure H.2** – Comparison between the Dräger Caleo™ and the GE Giraffe carestation. The surface temperature on the inside of the incubator hood is presented. Figure (a) shows the results of opening the access door for 5 minutes and Figure (b) shows the results of opening the portholes for five minutes.

### Incubator settings 34°C-50%RH

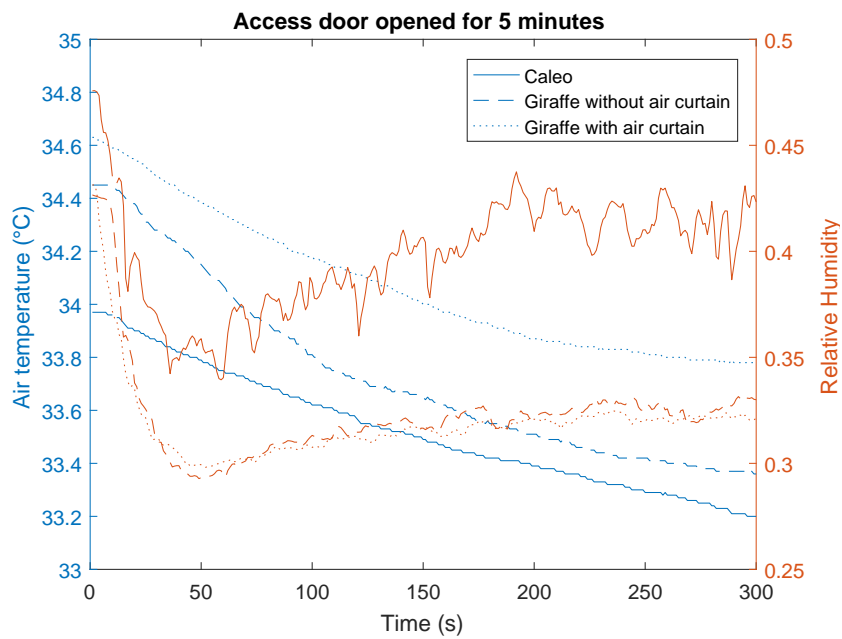


**Figure H.3** – Comparison between the Dräger Caleo™ and the GE Giraffe carestation. The air temperature and relative humidity at the location of the neonate are presented.

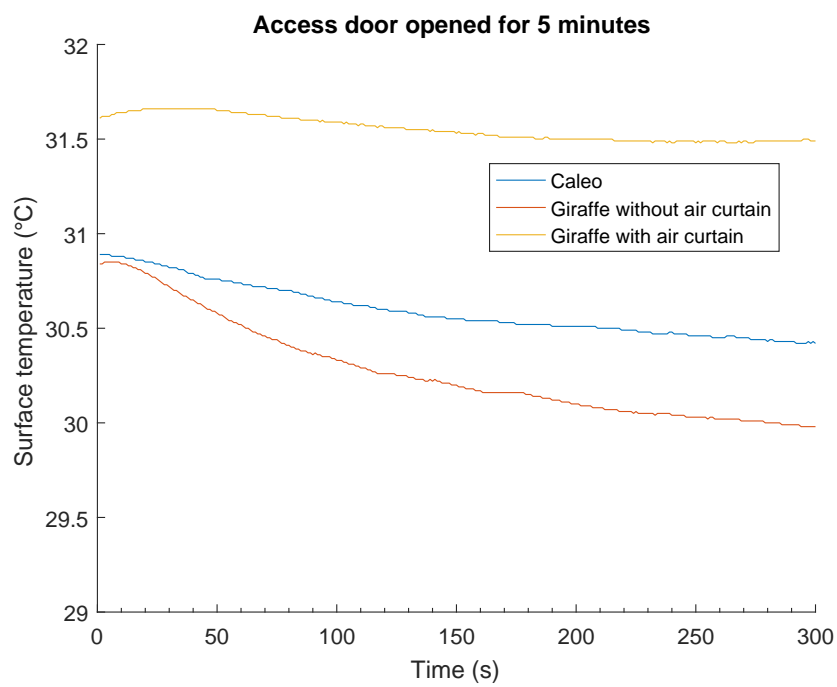


**Figure H.4** – Comparison between the Dräger Caleo<sup>TM</sup> and the GE Giraffe carestation. The surface temperature on the outside of the incubator hood is presented.

## Appendix I

# Typical incubator opening scenarios: the effect on the neonate's body temperature, a guideline for NICU personnel

The results of opening the incubator on the neonate's body temperature are presented in the Table below. The neonate's physical and thermophysiological properties have been extracted from Table 7.2. The results of the incubator measurements on the GE Giraffe have been used to determine the climate changes when the incubator is opened. The Giraffe is chosen since it is the incubator used within our own NICU department. The body temperature change is given in °C/min.

**Table 1.1** – Impact of opening an incubator on the neonate’s body temperature. The body temperature drop is given in °C/min. The impact of several opening scenarios at different incubator has been calculated for six neonates who’s gestational age and postnatal age differ.

Temperature drop, °C/min	Neonate’s age	28-1	28-5	30-1	30-5	32-1	32-5
	(GA(weeks) -PA(days))						
Incubator settings: 34°C-50%RH	Opening portholes, without air curtain	-0.006	-0.005	-0.005	-0.005	-0.004	-0.004
	Opening portholes, with air curtain	-0.004	-0.003	-0.003	-0.003	-0.003	-0.002
	Opening access door, without air curtain	-0.028	-0.023	-0.024	-0.023	-0.020	-0.021
	Opening access door, without air curtain	-0.020	-0.016	-0.016	-0.015	-0.013	-0.013
Incubator settings: 34°C-70%RH	Opening portholes, without air curtain	-0.027	-0.020	-0.020	-0.018	-0.015	-0.015
	Opening portholes, with air curtain	-0.020	-0.015	-0.015	-0.014	-0.012	-0.012
	Opening access door, without air curtain	-0.040	-0.031	-0.031	-0.030	-0.025	-0.025
	Opening access door, without air curtain	-0.039	-0.029	-0.029	-0.027	-0.023	-0.023
Incubator settings: 36°C-70%RH	Opening portholes, without air curtain	-0.036	-0.027	-0.028	-0.026	-0.022	-0.022
	Opening portholes, with air curtain	-0.022	-0.017	-0.017	-0.016	-0.014	-0.013
	Opening access door, without air curtain	-0.051	-0.041	-0.042	-0.040	-0.035	-0.035
	Opening access door, without air curtain	-0.039	-0.027	-0.027	-0.024	-0.020	-0.020